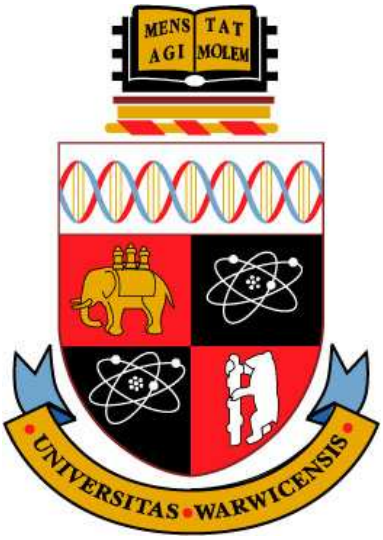

Thermoelectric Properties of Disordered Systems

by

Alexander Croy

Thesis

Submitted to the University of Warwick

for the degree of

Master of Science by Research

Physics

September 2005

THE UNIVERSITY OF WARWICK

Contents

List of Figures

List of Tables

Acknowledgments

At first, I would like to thank my supervisor Dr. Römer for his support throughout my time here in Warwick, but also back in Chemnitz. I am also much obliged for the encouragement of Prof. Schreiber who supported me throughout my last years in Chemnitz. Special thanks go to my colleague and house-mate Chris, who was always listening to my ideas and did not hesitate to tell me when I was wrong. Furthermore, I would like to thank my family; my father, my uncle and my aunt without whom the stay abroad were not possible and Ilona who was always very patient with me. Finally, I appreciate the hospitality of the Centre for Scientific Computing, in particular of Christine, Matt and Grok.

Declarations

I hereby declare that this thesis represents my own work and to the best of my knowledge it contains no materials previously published or written by another person, nor material which to a substantial extent has been accepted for the award of any other degree at The University of Warwick or any other educational institution, except where the acknowledgement is made in the thesis. Any contribution made to the research by others, with whom I have worked at The University of Warwick or elsewhere, is explicitly acknowledged in the thesis.

Parts of the thesis have been submitted for publication:
Croy, Alexander and Römer, Rudolf A. Scaling at the Energy-driven Metal-Insulator Transition and the Thermoelectric Power. phys. stat. sol (c). 2005. ArXiv: cond-mat/0509405

Abstract

The electronic properties of disordered systems at the Anderson metal-insulator transition (MIT) have been the subject of intense study for several decades. Thermoelectric properties at the MIT, such as thermopower and thermal conductivity, however, have been relatively neglected. Using the recursive Green's function method (RGFM) we calculate the average and the typical conductance for the case of completely coherent transport of cubic 3D disordered systems with semi-infinite metallic leads attached at both ends. We investigate the influence of the leads on the energy driven MIT. We find that the numerical results are consistent with the one-parameter scaling theory, in particular, we find that at $T = 0$ the d.c. conductivity close to the mobility edge is well described by the power-law. Finally, we study the case of incoherent transport and compare numerical results obtained from the RGFM and an approach based on the Landauer-Büttiker formalism.

Symbols and Abbreviations

a lattice spacing

d spatial dimension

L system size, length

M system size, width

N number of sites, strips or slices

T temperature

k_{B} Boltzmann's constant

$\mathcal{E}$ electric field

L_{ij} kinetic coefficients

σ d.c. conductivity (in transport direction)

S thermopower (Seebeck coefficient)

κ thermal conductivity

L_0 Lorenz number

$\mathfrak{g}$ conductance in Ω^{-1}, also $\mathfrak{g}_2$ and $\mathfrak{g}_4$ for 2- and 4-terminal conductance

g dimensionless conductance, also g_2 and g_4 for 2- and 4-terminal conductance

$\mathcal{H}$ Hamiltonian in an abstract vector space

$\mathcal{G}$ Green's function in an abstract vector space

H_{ij} matrix element of $\mathcal{H}$ in position basis

$G^{\pm}_{ij}$ matrix element of $\mathcal{G}^{\pm}$ in position basis

$\mathbf{H}_{mn}$ sub-matrix of H_{ij}

$\mathbf{G}_{ij}^{\pm}$ sub-matrix G_{ij}

$\Sigma^{\pm}$ self-energy due to the leads

ℓ mean free path

ℓ_{Φ} phase-relaxation length

μ chemical potential

Π Peltier coefficient

ρ density of states (DOS)

$z^{\pm}$ complex energy

λ de Broglie wave length

γ imaginary part of the complex energy z

ν universal critical exponent

W disorder strength

W_{c} critical disorder

E energy

E_{c} mobility edge

ξ localisation length

$\mathcal{F}$ scaling function

Chapter 1

Introduction

Traditionally, condensed matter physics has focused on the investigation of perfect crystals. However, real materials usually contain impurities, dislocations or other defects, which distort the crystal. If the deviations from the perfect crystalline structure are large enough, one speaks of *disordered systems*. In recent years such systems have aroused new interest in the field of *mesoscopic physics*. This was driven by the observation that transport can be completely coherent in systems of macroscopic size and therefore a quantum mechanical description is inevitable.

The Anderson model [1] is widely used to investigate the phenomenon of localisation in disordered materials and transport properties in mesoscopic devices in general. Especially the occurrence of a quantum phase transition driven by disorder from an insulating phase, where all states are localised, to a metallic phase with extended states, has lead to extensive analytical and numerical investigations of the critical properties of this metal-insulator transition (MIT) [2, 3]. But while electronic properties of disordered systems at the MIT have been the subject of intense study for several decades, thermoelectric properties, such as thermopower and thermal conductivity, however, have not been investigated to the same extent. Usually, the calculation of these properties aims at either the deeply insulating or deeply metallic regime. The investigation of the

behaviour close to the MIT on the other hand relies on certain assumptions such as the one-parameter scaling hypothesis [4, 5].

This scaling theory plays a crucial role in understanding the MIT [6]. It is based on an ansatz interpolating between metallic and insulating regimes [7]. So far, scaling has been demonstrated to an astonishing degree of accuracy by numerical studies of the Anderson model [8]. However, most studies focused on scaling of the localisation length and the conductance at the disorder-driven MIT in the vicinity of the band centre [8–10]. In order to calculate the temperature behaviour of the thermoelectric properties one moreover needs the explicit energy dependence of the d.c. conductivity close to the energy transition [5]. Assuming a power-law form for the d.c. conductivity, as it is expected from the one-parameter scaling theory, Villagonzalo et al. [5] have used the Chester-Thellung-Kubo-Greenwood formalism to calculate the temperature dependence of the thermoelectric properties numerically. They showed that all thermoelectric quantities follow single-parameter scaling laws, but found an unphysical dynamic exponent [11].

In this thesis we will investigate whether the assumptions made in previous studies can be recovered in numerical calculations, and in particular if the energy dependence of the d.c. conductivity follows a power-law. Therefore we will use the recursive Green's function method [12, 13] to calculate the conductance of a disordered system for fixed disorder strength at $T = 0$. Applying the finite size scaling analysis we will compute the critical exponent and the mobility edge at the energy transition.

Finally, in order to study how deviations from the one-parameter scaling theory can be caused by physical processes we will focus on incoherent transport. Therefore, we will show how dephasing processes can be modelled within an approach based on the Landauer-Büttiker formalism [14, 15]. At last, we will compare numerical results for the conductance obtained from this approach to calculations using the Kubo formula for the same setup.

Chapter 2

Thermoelectric Transport Properties

Transport properties describe the ability of a material to transport energy, entropy, heat or electric charge. Two familiar examples are the electric and the thermal conductivity in case of electric charge and heat transport, respectively. If both transport types are present, new effects can be observed. And as a result *thermoelectric* transport properties, such as thermopower and the Peltier coefficient have been defined. The investigation of transport properties is not only important for the understanding of the physics behind these transport processes, but is also relevant for technological applications especially in modern microelectronics.

In this Chapter the two most important thermoelectric effects for this work, the Seebeck and the Peltier effect, will be explained and the respective transport properties will be introduced. By using kinetic transport theory all transport quantities will be expressed in terms of the *kinetic coefficients*. Finally with the Chester-Thellung-Kubo-Greenwood (CTKG) formalism, a method of calculating these coefficients and thus all thermoelectric properties will be given.

2.1 Thermoelectric Effects in Solids

Intimately connected with transport mechanisms and properties is the question of the type of carriers involved. While charge is almost solely carried by electrons or holes, heat can also be transported by phonons, magnons or other quasi-particles. Although the latter can constitute a significant contribution to the behaviour of transport properties, such as the phonon-drag to thermopower, we assume in the following that the temperature is low enough to neglect these effects. Experimentally, respective measurements are therefore usually done below $1\mathrm{K}$ [16].

2.1.1 Electric and Thermal Conductivity

If there are mobile charge carriers available, the presence of an external electric field $\mathcal{E}$ will result in an electric current through the sample. For a sufficiently small electric field $\mathcal{E}$ the electric current density $\mathbf{j}_e$ is directly proportional to the field, which is subsumed in *Ohm's law*,

$$\mathbf{j}_e(\mathbf{r}) = \boldsymbol{\sigma}\, \mathcal{E}(\mathbf{r}) \; . \tag{2.1}$$

The tensor $\boldsymbol{\sigma}$ is the *electric d.c. conductivity*, which describes the response, i.e. the flow of carriers, to the external field. It therefore reflects the ability of the material to conduct electric current. In the case of an isotropic material, e.g. with a simple-cubic symmetry, and in absence of a magnetic field the conductivity tensor becomes proportional to the unit tensor $(\boldsymbol{\sigma})_{ij} = \sigma\delta_{ij}$.

In a similar way a constant temperature gradient ∇T leads to a "thermal flow" of carriers and thus to a thermal current density $\mathbf{j}_q$. If the gradient is small, Fourier's law relates $\mathbf{j}_q$ to ∇T [17],

$$\mathbf{j}_q = -\kappa\, \nabla T \; , \tag{2.2}$$

where κ is the *thermal conductivity*, which characterises the ability to conduct heat. The change of heat dQ in some small fixed region of the solid, where the temperature can

be assumed to be constant, is just T times the change of entropy $\mathcal{S}$, $dQ = Td\mathcal{S}$. Hence the thermal current density is related to the entropy current density in the following way,

$$\mathbf{j}_q = T\mathbf{j}_{\mathcal{S}} \,. \tag{2.3}$$

Notice that this is no longer valid if one goes beyond the linear theory [17].

2.1.2 Law of Wiedemann-Franz and Lorenz Number

In the case of an electric *and* a thermal current, the phenomenological law of Wiedemann and Franz states that for metals the quotient of κ and σ is directly proportional to the temperature T. The proportionality constant is the so-called *Lorenz number*

$$L_0 = \frac{e^2}{k_{\mathrm{B}}^2}\frac{\kappa}{\sigma T} \,, \tag{2.4}$$

where e is the electron charge and k_{B} is Boltzmann's constant. For metals, it takes the universal value $\pi^2/3$ [17, 18].

2.1.3 Seebeck, Peltier and Thomson Effect

Now, if the circuit is open ($\mathbf{j}_e = 0$), the heat current density $\mathbf{j}_q$ will eventually lead to an accumulation of electrons at the cold end and a depletion at the hot end of the conductor. Consequently, this sets up a *thermoelectric field* $\mathcal{E}$, which opposes the thermal flow of the electrons (see Fig. 2.2). This so-called **Seebeck effect** was discovered in 1821 by the physicist Thomas Johann Seebeck. For small ∇T one obtains for the field,

$$\mathcal{E} = S\,\nabla T \,, \tag{2.5}$$

which defines the *thermopower* (or *Seebeck coefficient*) S. In general the thermopower is due to two different effects: the diffusion of the electrons and the so-called "phonon-drag" [19]. Notice that in some cases there may also be a "magnon-drag" [19]. The phonon-drag rests upon a momentum transfer from the phonons to the electrons as a result of collisions. In metals the diffusive S is found to be proportional to $-T$ [17], where

the sign is determined by the charge of the thermal conductors, which are electrons in the case of metals. In semiconductors the diffusive thermopower shows a different behaviour. Here S diverges for $T \to 0$ with $1/T$. The sign of S indicates whether the current is carried predominantly by holes or electrons [19].

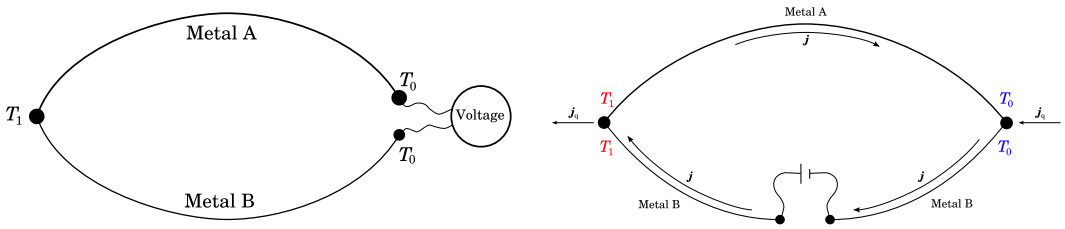

(a) Seebeck effect (b) Peltier effect

Figure 2.1: (a) The Seebeck effect. The difference of the temperatures in the two metals yields a difference in the thermopower and hence a voltage can be measured. To obtain the thermopower of one metal only, the other metal has to be superconducting [17]. (b) The Peltier effect. Driving a current in a bimetallic circuit leads to a thermal current.

The **Peltier effect** is the counterpart of the Seebeck effect. If an electric current is driven trough a bimetallic circuit at a uniform temperature, there will be a release of heat at one of the junctions and absorption at the other one (see Fig. 2.1). This can be understood from the fact, that in an electric circuit at constant temperature an electric current is accompanied by a thermal current $\mathbf{j}_q$, which is directly proportional to the electric current $\mathbf{j}_e$ [17],

$$\mathbf{j}_q = \Pi \mathbf{j}_e \, . \tag{2.6}$$

The material specific constant Π is called *Peltier coefficient*, which is connected to the thermopower S by the relation

$$\Pi = TS \, , \tag{2.7}$$

which was first deduced by Lord Kelvin and can be rigorously derived using the kinetic coefficients (cf. Section 2.2). The Combination of Equations (2.6) and (2.7) and using

the relation of the thermal current density $\mathbf{j}_q$ to the entropy current density $\mathbf{j}_s$ (2.3) gives

$$\mathbf{j}_q = T\mathbf{j}_s = \Pi\mathbf{j}_e = TS\mathbf{j}_e \qquad \Longrightarrow \qquad \mathbf{j}_s = S\mathbf{j}_e \ . \tag{2.8}$$

Thus, the thermopower is just the entropy per unit charge transported by the electric flow of carriers.

There is yet another thermoelectric effect, namely the **Thomson effect**. Here the change of heating is related to presence of a electric current and a fixed temperature gradient in a homogeneous conductor. The change rate is completely determined by the values of σ, κ and S for a given temperature gradient and electric current density [17],

$$\frac{dq}{dt} = \frac{1}{\sigma}\mathbf{j}_e^2 + \frac{d\kappa}{dT}(\boldsymbol{\nabla})^2 - T\frac{dS}{dT}(\boldsymbol{\nabla}) \cdot \mathbf{j}_e \ .$$

2.1.4 Applications and Figure of Merit

The technological importance of the Peltier effect lies in the possibility to use it for "thermoelectric cooling". The sample to be cooled is placed at one of the junctions and a large heat bath is placed at the other junction. Then a current is driven in the circuit in such a way that the heat from the sample is absorbed and transferred into the heat bath. Such thermoelectric cooling systems are used for example to cool heat sensitive electronic components such as computer chips and to stabilise the operating temperature of some CCD detectors in digital cameras [20]. The Seebeck effect also has a broad range of applications. For example thermocouples, which are basically junctions of two dissimilar metals, are widely used for temperature sensing. But there are also thermo-generators, which use heat sources to generate sufficient electric current to drive electronic devices. Such systems have been used for instance in space probes [20].

The efficiency of a thermoelectric device depends obviously on the thermoelectric properties σ, κ and S. To achieve high voltages the material must have a large thermopower S. In order to reduce thermal noise it has to have a high electric conductivity

σ and a low thermal conductivity κ to decrease thermal losses. To quantify the efficiency of a thermoelectric material usually the *dimensionless figure of merit* ZT is used, which is defined as follows [21],

$$ZT = \frac{TS^2\sigma}{\kappa} = \frac{e^2}{k_{\mathrm{B}}^2}\frac{S^2}{L_0} \, . \tag{2.9}$$

The quantity Z is known as the figure of merit. A higher value of ZT yields a better performance as a thermoelectric material.

2.2 Thermoelectric Properties and Kinetic Coefficients

In summary, thermoelectric properties describe the response of a system to the presence of an external electric field $\mathcal{E}$ *and* a temperature gradient ∇T. Dependences of the resulting electric and thermal currents on the electric field and the temperature gradient up to linear order are [22]

$$\mathbf{j}_e = \frac{1}{|e|}\left(|e|\, L_{11}\mathcal{E} - L_{12}\frac{\nabla T}{T}\right) \, , \tag{2.10}$$

$$\mathbf{j}_q = \frac{1}{|e|}\left(|e|\, L_{21}\mathcal{E} - L_{22}\frac{\nabla T}{T}\right) \, . \tag{2.11}$$

This defines the quantities L_{ij} $(i,j = 1,2)$ which are called *kinetic coefficients*. Now, all thermoelectric properties can be expressed in terms of the L_{ij}. Using Ohm's law (2.1) in Equation (2.10) for $T = \mathrm{const.}$, one obtains immediately

$$\sigma = L_{11} \, . \tag{2.12}$$

Upon combining Fourier's law (2.2) and Equation (2.11) under the condition of zero electric current, the thermal conductivity in terms of the kinetic coefficients becomes

$$\kappa = \frac{L_{22}L_{11} - L_{21}L_{12}}{|e|^2 T L_{11}} \, . \tag{2.13}$$

Similarly, using the same condition, Equation (2.10) yields for the thermopower,

$$S = \frac{L_{12}}{|e|TL_{11}} \, . \tag{2.14}$$

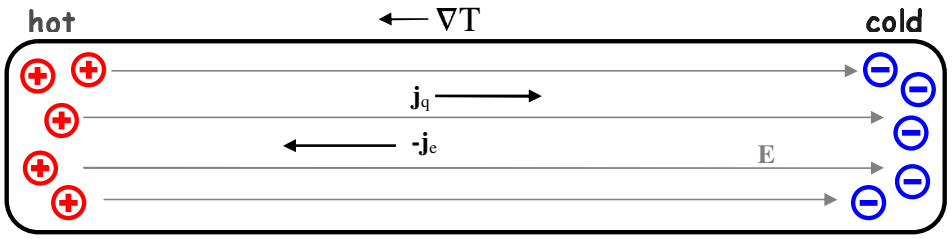

Figure 2.2: If $\nabla T \neq 0$, the heat current density $\mathbf{j}_q$ will eventually lead to an accumulation of electrons at the cold end and a depletion at the hot end of the conductor. The resulting current density $-\mathbf{j}_e$ is opposed to this process.

From the definition of the Lorenz number (2.4) it follows that

$$L_0 = \frac{e^2}{k_\mathrm{B}^2}\frac{\kappa}{\sigma T} = \frac{L_{22}L_{11} - L_{21}L_{12}}{(k_\mathrm{B}T L_{11})^2} \,. \tag{2.15}$$

Additionally, in the absence of a magnetic field, the Onsager relation states that $L_{21} = L_{12}$ [22].

Moreover, by setting $T = \mathrm{const.}$ in Equations (2.10) and (2.11) one can calculate the Peltier coefficient with the definition (2.6),

$$\Pi = \frac{L_{12}}{|e|L_{11}} = TS \,. \tag{2.16}$$

This result proves the Kelvin relation (2.7).

2.3 Chester-Thellung-Kubo-Greenwood Formalism

From Section 2.2 it is obvious, that the kinetic coefficients L_{ij} are the key to calculating thermoelectric transport properties. One can for example compute the coefficients L_{ij} in the context of the relaxation-time approximation [17], which is, however, rather unsatisfying since the explicit form of the relaxation-time $\tau(E,T)$ is often unknown. Therefore a microscopic approach would be preferred.

A well-established formalism is due to Kubo [23] and Greenwood [24] who derived an expression for the d.c. conductivity within linear response theory. Their results can be

summarised in the following way,

$$\sigma(T, E_{\mathrm{F}}) = \int_{-\infty}^{\infty} \sigma(E) \left[-\frac{\partial f(E, \mu, T)}{\partial E} \right] dE \ , \tag{2.17}$$

where $\mu(T)$ is the chemical potential and $f(E, \mu, T)$ is the Fermi function

$$f(E, \mu, T) = \frac{1}{\exp\left(\frac{E-\mu}{k_{\mathrm{B}}T}\right) + 1} \ . \tag{2.18}$$

For the energy dependence of the conductivity $\sigma(E)$ they obtained

$$\sigma(E) = 2\pi \sum_{m,n} \left| \langle m | \hat{j}_e | n \rangle \right|^2 \delta(E - E_n) \delta(E - E_m) \ . \tag{2.19}$$

Here $\hat{j}_e$ is the electric current operator, and $|n\rangle$ and E_n are the eigenstates and eigenenergies, respectively, of the Hamiltonian under consideration. Additionally Kubo, Yokota and Nakajiama [25] showed that the kinetic coefficients L_{ij} for systems in thermal equilibrium are the current-current correlation functions [26]

$$L_{ij} \propto \langle \mathbf{j}_i \, \mathbf{j}_j \rangle \quad (i, j = 1, 2) \ , \tag{2.20}$$

with $\mathbf{j}_1 = \mathbf{j}_e$ and $\mathbf{j}_2 = \mathbf{j}_q$ denoting the electric current and thermal current density, respectively. Assuming elastic scattering of independent electrons by static impurities or by lattice vibrations one can obtain the kinetic coefficients from Equation (2.20) by the Chester-Thellung-Kubo-Greenwood formulation [18, 23, 24], which yields the expression

$$L_{ij}(T) = (-1)^{i+j} \int_{-\infty}^{\infty} A(E)[E - \mu(T)]^{(i+j-2)} \left[-\frac{\partial f(E, \mu, T)}{\partial E} \right] dE \ , (i, j = 1, 2) \ , \tag{2.21}$$

where $A(E)$ contains all the system-specific features and $\mu(T)$ is the chemical potential. Since we know from Equation (2.12) that $L_{11} = \sigma$ we can identify $A(E) = L_{11}(T = 0)$ with the energy dependent d.c. conductivity $\sigma(E)$.

Chapter 3

Disordered and Mesoscopic Systems

Traditionally, condensed matter physics has been focused on the investigation of perfect crystals. However, real materials usually contain impurities, dislocations or other defects, which distort the crystal. If the deviations from the perfect crystalline structure are large enough, one may also speak of *disordered systems*. One of the most striking features of such systems is the occurrence of localised wave functions and therefore the possibility of a vanishing conductivity for $T \to 0$ without an energy gap as in band-like insulators. Since the pioneering work of P.W. Anderson in 1958 [1], where he explained this behaviour, the Anderson model has become a paradigm for disordered systems and attracted a lot of interest. Furthermore, it is often used in numerical calculations of transport properties and we will use it as a starting point for our calculations as well.

The observation that for sufficiently low temperatures the transport in small, but macroscopic devices or samples is completely coherent and therefore these systems may show quantum effects such as localisation, has lead to the definition of *mesoscopic systems* (from Greek *mesos* = middle). Moreover, the experimental and technological progress

makes it possible to fabricate and manipulate these devices with increasing precision.

In this Chapter we will present a brief introduction to the vast field of mesoscopic systems. Especially the role of characteristic length scales for electronic transport will be pointed out. Finally, the Anderson model of localisation will be explained and the consequences of the one-parameter scaling theory will be discussed.

3.1 Mesoscopic Systems

In solid state physics one is usually faced with systems of macroscopic size, which exhibit classical behaviour such as Ohm's law for the conductance and can usually be treated with classical theories. On the other hand, there are devices of microscopic size, which consist of only a few atoms or molecules. Such systems are governed by the laws of quantum mechanics. Here the wave-like nature of the electrons plays an important role and is responsible for many interesting phenomena such as discrete spectra and interference patterns. Consequently, the question arises at which size the classical description breaks down and quantum phenomena become prominent. It turns out that a system shows classical behaviour if its dimensions are much larger than each of the following characteristic length scales, (1) the de Broglie wave length ($\Leftrightarrow$ kinetic energy), (2) the mean free path ($\Leftrightarrow$ momentum-relaxation), and (3) the phase-relaxation length ($\Leftrightarrow$ phase-relaxation). Notice that this length scale is intimately connected with the wave-like nature of the electrons, namely the phase of the wave-function. This unexpected size dependence has lead to the definition of the so-called *mesoscopic systems*, which are systems of macroscopic size but whose properties show quantum effects, i.e. they are systems *between* the microscopic and macroscopic regime. In order to realise such a behaviour, one of the characteristic lengths has to become large compared to the others. This will be discussed in the next Section. In a sense mesoscopic systems are "really like a large molecule" [27], but also show new and interesting phenomena like *universal*

conductance fluctuations (UCF) and *localisation*, which will be discussed in Chapter 3.2. Additionally these systems are usually coupled to much larger systems, which also results in significant new behaviour (cf. Chapter 7).

3.1.1 Characteristic Length Scales

The **de Broglie wave length** λ is connected with the kinetic energy of a particle and is defined as

$$\lambda = \frac{2\pi}{k} \,, \tag{3.1}$$

where k is the wave number. For a free electron $k = \sqrt{2m_e E}$ with E being the (kinetic) energy and m_e is the mass of the electron.

The **mean free path** ℓ on the other hand is related to the change of the momentum of an electron moving through the sample [28]. This change is caused by collisions with impurities, phonons, other electrons or defects in general, which are inevitable in any real system. The time before the initial momentum of the electron is destroyed is the so-called *momentum-relaxation time* τ_m. The distance which an electron can travel during the time τ_m and hence the mean free path is given by

$$\ell = v_t \tau_m \,. \tag{3.2}$$

Here $v_t = \hbar k_t / m$ is the typical velocity. Because the transport at low temperatures is dominated by electrons close to Fermi surface, v_t is often replaced by the Fermi velocity v_F. Comparing the mean free path ℓ with the characteristic dimension L of the sample one can distinguish between *diffusive* and *ballistic* transport, characterised by $l \ll L$ and $l \geq L$, respectively [28]. In the former case the electron motion consist of a series of short trajectories in random directions, whereas in the latter case the momentum does not change while the electron is moving through the system. Additionally one might also define a *quasi-ballistic* transport regime, if for example in 2D $l \ll L_x$ and $l \geq L_y$.

The third characteristic length scale is the **phase-relaxation length** l_Φ, which is a consequence of the quantum mechanical description of the electrons and their coupling to the environment [27]. One can also define a *phase-relaxation time* τ_Φ, which is just the time before the initial phase of the wave function is changed. It turns out that for static impurities

$$\tau_\Phi \longrightarrow \infty \,,$$

because in this case the phase-relationship between different paths is fixed by the impurity distribution [28]. Contrary to this dynamic scatterers, like phonons, or impurities with an internal degree of freedom, do not lead to static interference [28] and therefore τ_Φ is finite. It turns out that $\tau_\Phi < \infty$ holds in general for systems with a broken time reversal symmetry [29].

For the definition of the phase-relaxation length ℓ_Φ one has to distinguish between ballistic and diffusive regime. If $\tau_\Phi \leq \tau_m$, the momentum does not change during the time τ_Φ and therefore ℓ_Φ may be defined as $\ell_\Phi = v_t \tau_\Phi$. For $\tau_\Phi \gg \tau_m$, on the other hand, the motion becomes non-ballistic and the distance travelled by the electron during the time τ_Φ is given by the root mean square distance of a random movement [28]. This leads to the following expression [28]

$$\ell_\Phi = \sqrt{D\tau_\Phi} \,. \tag{3.3}$$

Here the constant D denotes the *diffusion coefficient*.

The phase-relaxation time τ_Φ turns out to be strongly temperature dependent and in many cases on can write [27]

$$\tau_\Phi \propto T^{-p} \qquad (p > 0) \,. \tag{3.4}$$

The exponent p and the constant of proportionality are determined by the respective scattering process. For electron-electron scattering for example $p = 2$ and for electron-phonon interaction $p = 3$ under some limitations [29]. Consequently, at low temperatures

electron-electron interactions are more important for dephasing than electron-phonon scattering.

3.1.2 Weak Localisation

The fact that the electronic transport in mesoscopic systems might be coherent over the whole sample makes it necessary to use a full quantum mechanical description, which is provided for example by the Kubo-Greenwood formula (2.19). For analytical calculations it is convenient to rewrite Equation (2.19) in terms of *advanced and retarded Green's functions* $\mathcal{G}^-$ and $\mathcal{G}^+$, respectively. In the limit $k_F\ell \gg 1$, i.e. in the case of the Fermi wave length $\lambda_F = 2\pi/k_F$ being much smaller than the mean free path ℓ, the d.c. conductivity at $T = 0$ including a factor of two for the spin degree of freedom is then given by [29]

$$\sigma(E) = \frac{\hbar e^2}{\pi\Omega}\left(\frac{\hbar}{m}\right)^2 \sum_{k_x k_x'} k_x k_x' \langle k|\mathcal{G}^+|k'\rangle\langle k'|\mathcal{G}^-|k\rangle \ . \tag{3.5}$$

Here m is the electron mass and Ω is the Volume of the system under consideration. The quantity $i\hbar\langle k|\mathcal{G}^+(E)|k'\rangle$ can be interpreted as the *probability amplitude* $A(\mathbf{k}' \to \mathbf{k})$ that an electron with Energy E is scattered from state $\mathbf{k}'$ to $\mathbf{k}$ [29]. Assuming isotropy the conductivity may therefore be written as

$$\sigma(E) = \frac{e^2}{\pi\hbar}\left(\frac{\hbar}{m}\right)^2 \frac{1}{3\Omega} \sum_{kk'} \mathbf{k}\cdot\mathbf{k}' \ |A(\mathbf{k} \to \mathbf{k}')|^2 \ , \tag{3.6}$$

and is consequently an average of $\mathbf{k}\cdot\mathbf{k}'$ over all scattering processes with initial momentum $\mathbf{k}$ and final momentum $\mathbf{k}'$. Such a process may consist of several individual scattering events with probability amplitudes A_i. The total probability $|A(\mathbf{k} \to \mathbf{k}')|^2$ is thus

$$|A(\mathbf{k} \to \mathbf{k}')|^2 = \left|\sum_i A_i\right|^2 = \sum_{ij} A_i A_j^* \ . \tag{3.7}$$

The values of the individual amplitudes A_i are determined by the actual impurity configuration, and therefore terms with $i \neq j$ are cancelled out on taking the average $\langle|A|^2\rangle$. As a first approximation only terms with $i = j$ will survive. This basically gives the classical

limit, $\langle |A|^2 \rangle \approx |\langle A \rangle|^2$, since all the interference terms $A_i A_j^*$ are missing. One can show that in this case Equation (3.5) gives the semiclassical Boltzmann-Drude formula [29]

$$\sigma_{\mathrm{BD}} = \frac{ne^2\tau}{m} \,, \tag{3.8}$$

where n is the electron density and τ being the lifetime of a momentum state[1]. The latter may be given by a parallel combination of the phase relaxation time τ_Φ and the momentum-relaxation time τ_m [28],

$$\frac{1}{\tau} = \frac{1}{\tau_\Phi} + \frac{1}{\tau_m} \,. \tag{3.9}$$

The terms with $i = j$ are, however, not the only contribution to $\langle |A|^2 \rangle$. If the sequence of scattering events $\{j\}$ is exactly the time reverse of those in $\{i\}$, the finial momentum will be $-\mathbf{k}$ instead of $\mathbf{k}$. Hence, such a reversed sequence describes a backscattering process with a momentum transfer of $2k_F$. The product $\mathbf{k} \cdot \mathbf{k}'$ will be negative and therefore reduces the d.c. conductivity compared to the value σ_{BD}. If one considers the probability of being scattered back into the state $\mathbf{k}$, one finds [28]

$$|A(\mathbf{k} \to \mathbf{k})|^2 = |A(\mathbf{k} \to \mathbf{k}') + A_R(\mathbf{k}' \to \mathbf{k})|^2 \,, \tag{3.10}$$

where A_R is the amplitude of the time reversed process. In absence of a magnetic field $A = A_R$ [28] and hence

$$|A(\mathbf{k} \to \mathbf{k})|^2 = 4|A(\mathbf{k} \to \mathbf{k}')|^2 \tag{3.11}$$

instead of

$$|A|^2 + |A_R|^2 = 2|A(\mathbf{k} \to \mathbf{k}')|^2 \tag{3.12}$$

in the classical case. The "quantum probability" for exact backscattering is therefore enhanced compared to the classical probability, which leads to a *quantum correction* to the conductivity. This is the so-called *weak localisation correction*. It can be shown that for $d = 3$ and $\ell_\Phi \gg L$ the first order correction leads to [7]

$$\sigma(L) = \sigma_0 - \frac{e^2}{\hbar\pi^3}\left(\frac{1}{\ell} - \frac{1}{L}\right) \,, \tag{3.13}$$

[1] It turns out that for isotropic scatterers this is identical to the collision time. For anisotropic scatterers, however, one has to include correction terms to the conductivity [28].

where L is the typical size of the system. Notice that in the case $\ell \ll \ell_\Phi < L$, i.e. when phase breaking processes dominate and the phase-relaxation length is the relevant length scale, one gets [7]

$$\sigma(T) = \sigma_0 + \frac{e^2}{\hbar\pi^3}\frac{1}{\ell_\Phi(T)} = \sigma_0 + \frac{e^2}{\hbar\pi^3}\frac{1}{A}T^{p/2} \,, \tag{3.14}$$

where Equations (3.3) and (3.4) were used. The conductivity will therefore decrease with decreasing temperature, which is not expected for metals [7, 27].

3.1.3 Conductivity and Conductance

A further consequence of the quantum mechanical formulation, in particular of the wave-like nature of the electrons, is the fact that the local character of Ohm's law (2.1) is no longer valid. Instead one has to use a generalisation [29], which has the form

$$\mathbf{j}_e(\mathbf{r}) = \int d^3\mathbf{r}'\sigma(\mathbf{r},\mathbf{r}')\mathcal{E}(\mathbf{r}') \,, \tag{3.15}$$

and is nonlocal on a scale of order ℓ_Φ [29]. A further complication arises because the local electric field $\mathcal{E}(\mathbf{r})$ in Equation (3.15) depends on the precise position of the impurities in the sample and might therefore show strong spatial fluctuations.

In experiments, however, $\sigma(\mathbf{r},\mathbf{r}')$ is not directly accessible and usually the *global* conductance $\mathfrak{g}$, which is a property of the whole sample, is measured. Such experiments are often performed in a multiprobe geometry, where the sample is connected to several perfect metallic leads guiding the electrons to the scattering region [27]. This is also the setup we will use for our calculations of transport properties (cf. Section 4).

Assuming such a multiprobe geometry one can establish a connection between the conductance and the nonlocal conductivity, which also solves the problem of the strongly fluctuating electric field. For $\mathcal{B} = 0$ and because of current conservation the nonlocal conductivity obeys [29]

$$\nabla\sigma(\mathbf{r},\mathbf{r}') = \nabla'\sigma(\mathbf{r},\mathbf{r}') = 0 \,. \tag{3.16}$$

The local electric field $\mathcal{E}(\mathbf{r})$ can be obtained from the electrostatic potential $V(\mathbf{r})$ in the sample via

$$\mathcal{E}(\mathbf{r}) = -\nabla V(\mathbf{r}) \; . \tag{3.17}$$

If the sample is surrounded by an insulator, no current can flow out at the insulating boundaries and the normal component of $\sigma(\mathbf{r}, \mathbf{r}')$ must vanish. Partial integration of Equation (3.15) leads to

$$\mathbf{j}_e(\mathbf{r}) = -\int\limits_{\text{leads}} d\mathbf{S}' \sigma(\mathbf{r}, \mathbf{r}') V(\mathbf{r}') \; , \tag{3.18}$$

where the integration is restricted to the surface of the leads. Hence the current density depends only on the potential *in* the leads and not on the precise field in the sample. Therefore, $V(\mathbf{r})$ can be replaced by *any* potential $V'(\mathbf{r})$ having the same asymptotic values in the leads as the original potential [29]. A convenient choice for V' would be for example a locally linear function, which results in a constant electric field.

If there are $n = 1, \ldots, N_L$ leads with respective potentials V_n attached to the sample the integral in Equation (3.18) becomes

$$\mathbf{j}_e(\mathbf{r}) = -\sum_{n=1}^{N_L} V_n \int\limits_{S_n} d\mathbf{S}' \sigma(\mathbf{r}, \mathbf{r}') \; . \tag{3.19}$$

Integration over the cross section of lead m finally gives the current

$$I_m = -\sum_{n=1}^{N_L} V_n \int\limits_{S_m} d\mathbf{S} \int\limits_{S_n} d\mathbf{S}' \sigma(\mathbf{r}, \mathbf{r}') = \sum_{n=1}^{N_L} \mathfrak{g}_{mn} V_n \tag{3.20}$$

in terms of the potentials V_n and the *conductance coefficients* $\mathfrak{g}_{mn}$. Local current conservation, $\nabla \mathbf{j}_e = 0$, implies [29]

$$\sum_m I_m = 0 \quad \forall V_n \quad \Longrightarrow \quad \sum_m \mathfrak{g}_{mn} = 0 \; . \tag{3.21}$$

For the usual case of a 2-probe geometry one gets the familiar expression

$$I = \mathfrak{g}(V_2 - V_1) = \frac{1}{R} \triangle V \; . \tag{3.22}$$

One can also obtain the *macroscopic* conductivity σ for a system of size $M^{d-1} \times L$

$$\mathfrak{g} = \frac{I}{\triangle V} = \frac{jW^{d-1}}{\mathcal{E}L} = \sigma \frac{M^{d-1}}{L} \ . \tag{3.23}$$

The conductance coefficients $\mathfrak{g}_{mn}$ can be related to quantum mechanical transmission probabilities [28]. Such a relation is given by the Landauer-Büttiker formalism, which will be discussed in Section 4.1.

3.2 Anderson Model of Localisation

3.2.1 Anderson Metal-Insulator Transition

The Anderson model [1,2] is widely used to investigate the phenomenon of localisation in disordered materials. It is based upon a tight binding Hamiltonian in site representation

$$\mathcal{H} = \sum_i \varepsilon_i |i\rangle\langle i| + \sum_{i \neq j} t_{ij} \, |i\rangle\langle j| \ , \tag{3.24}$$

where $|i\rangle$ is a localized state at site i and t_{ij} are the hopping parameter, which are usually restricted to nearest neighbours. The on-site potentials ε_i are random numbers, chosen according to some distribution $P(\varepsilon)$ with zero mean and variance s^2. In what follows we take $P(\varepsilon)$ to be a box distribution over the interval $[-W/2, W/2]$, where W determines the strength of the disorder in the system. Other distributions have also been considered [2, 3, 30].

For strong enough disorder, $W > W_{\mathrm{c}}(0)$, all states are exponentially localized and the respective wave function $\Psi(\mathbf{r})$ is proportional to $\exp(-|\mathbf{r} - \mathbf{r}_0|/\xi)$. Thus, Ψ is confined to a region of some finite size, which may be described by the so-called localisation length ξ. In this language extended states are characterised by $\xi \longrightarrow \infty$. The localisation length is an additional characteristic length scale. Comparing ξ with the size L of the system one can distinguish between *strong* and *weak localisation*, for $\xi \ll L$ and $L < \xi$, respectively. Notice that for finite phase-relaxation length the effective system size is determined by ℓ_Φ.

It turns out that the value of the critical disorder strength W_c depends on the distribution function $P(\varepsilon)$ and the dimension d of the system. In absence of a magnetic field and for $d < 3$ all states are localized [2], i.e. $W_c = 0$ [6,7]. For systems with $d = 3$ the value of W_c additionally depends on the Fermi energy E and the curve $W_c(E)$ separates localized states, $W > W_c(E)$, form extended states, $W < W_c(E)$, in the phase diagram. If instead of E the disorder strength is fixed, there will be a critical Energy $E_c(W)$ and states with $|E| < E_c$ are extended and those with $|E| > E_c$ localized. The separation of localized and extended states is illustrated in Fig. 3.1, which shows a schematic density of states of a 3D Anderson model. In addition to the band edges of an ordered system, the mobility edges $\pm|E_c|$ are shown. Since for $T = 0$ localized states cannot carry any

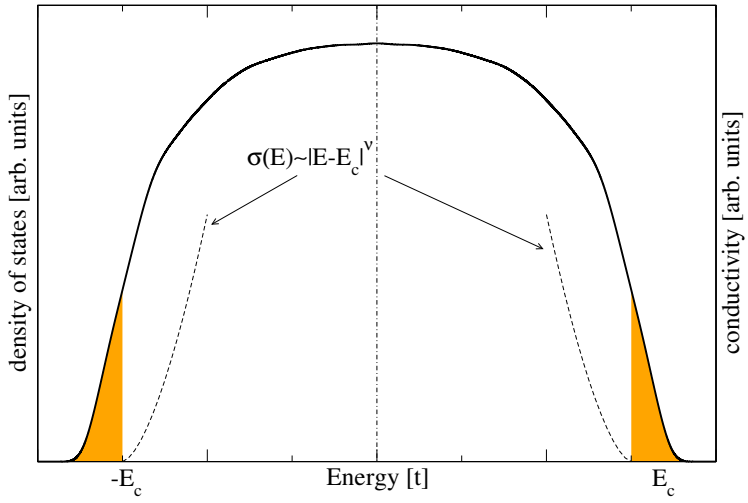

Figure 3.1: Typical density of states of a 3D Anderson model. The states in the coloured regions are localized and extended otherwise. The mobility edges are indicated at $\pm E_c$. Also shown is the power-law behaviour of $\sigma(E)$ according to Equation (3.28).

electric current, the system shows insulating behaviour, i.e. the electric conductivity σ vanishes for $|E| > E_c$ or $W > W_c$. Otherwise the system is metallic. Therefore, the transition at the critical point is called a *disorder driven metal-insulator transition (MIT)* or Anderson MIT.

[2] Strictly speaking, this is only true if $\mathcal{H}$ belongs to the Gaussian Orthogonal Ensemble [31].

3.2.2 One-parameter Scaling Theory

In general, it is extremely complicated to obtain analytical results of transport properties for the Anderson model of localisation. For example, only in the case of $d = 1$ rigorous proofs of strong localisation for all energies and disorder strengths have been given [32]. Moreover, the explicit energy and disorder dependence of the localisation length has been derived [33, 34]. For the 2D and 3D case no such general proofs exist. Only recently a perturbative analytical calculation of the localisation length in 2D has been given [35]. Therefore, numerical computations are very important for the investigation of MIT [2, 3]. The *one-parameter scaling theory*, on the other hand, is based on an extrapolation between the metallic and the insulating regime in the Anderson model [6, 7]. The key-point is the definition of the so-called β-function as the logarithmic derivative of the dimensionless conductance g,

$$\beta = \frac{d \ln g}{d \ln L} \,, \tag{3.25}$$

for a d-dimensional hypercube of size L. The basic assumption of the one-parameter scaling theory is that β depends only on g and not explicitly on the system size, disorder strength or Fermi energy. Deep in the metallic regime g behaves according to Ohm's law (3.23) and hence

$$g(L) \propto L^{d-2} \quad \Longrightarrow \quad \beta(g) \longrightarrow d - 2 \,, \tag{3.26}$$

while in the insulating regime

$$g(L) \propto \exp(-L/\xi) \quad \Longrightarrow \quad \beta(g) \longrightarrow \ln g + \text{const.} \,. \tag{3.27}$$

Notice that this implies the following behaviour for g in the thermodynamic limit $L \longrightarrow \infty$:

$$\text{metallic: } g \longrightarrow \infty \,, \qquad \text{insulating: } g \longrightarrow 0 \,.$$

Assuming a smooth monotonically increasing function $\beta(g)$ one obtains the following picture [7], which is schematically shown in Fig. 3.2. Only for $\beta > 0$ the conductance increases with increasing system size. Therefore, $\beta > 0$ indicates metallic behaviour,

while for $\beta < 0$ the conductance decreases with increasing L, which denotes insulating behaviour. For $d = 1$, β is always negative and hence all states are localized in the thermodynamic limit. On the other hand for $d = 3$ the function β has a zero, which corresponds to the MIT. At this point g becomes independent of the system size (cf. Section 4.4). In the marginal case $d = 2$ the one-parameter scaling theory cannot decide if all states are eventually localized in the thermodynamic limit. For the interesting case

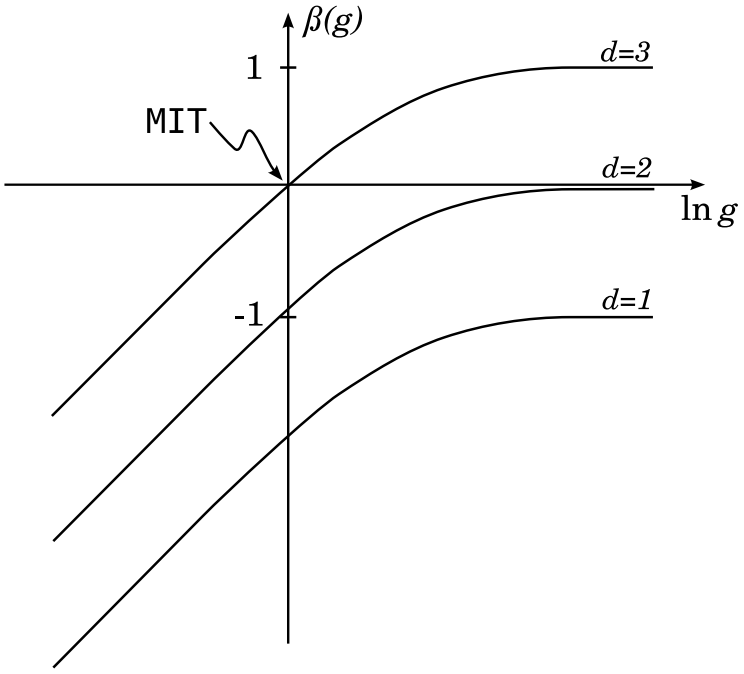

Figure 3.2: The β-function $\beta(g)$ vs $\ln g$ (schematic). The zero of $\beta(g)$ indicates the MIT.

of the MIT for $d = 3$ it was found that the behaviour of σ is given by a power law at the critical point [2],

$$\sigma(E) = \begin{cases} \sigma_0 \left|1 - \frac{E}{E_c}\right|^{\nu} & |E| < E_c \\ 0, & |E| > E_c \end{cases} \tag{3.28}$$

with ν being the universal critical exponent of the phase transition and σ_0 is a constant. The value of ν has been computed numerically from various methods [2] and was also

derived from experiments [36]. The results range from 1 to 1.6, depending on the distribution $P(\varepsilon)$ used and the computational method [3] used.

Moreover, Wegner [37] was able to show that for non-interacting electrons the d.c. conductivity σ obeys a general scaling form close to the MIT,

$$\sigma(\varepsilon, \omega) = b^{2-d}\, \sigma(b^{1/\nu}\varepsilon, b^z \omega)\ . \tag{3.29}$$

Here ε denotes the dimensionless distance from the critical point, ω is an external parameter such as the frequency or the temperature, b is a scaling parameter and z is the dynamical exponent. For non-interacting electrons $z = d$ [38]. Assuming a finite conductivity for $\omega = 0$ and $t > 0$, where $\varepsilon = \left|1 - \frac{E}{E_c}\right|$, one obtains from Equation (3.29)

$$\sigma(\varepsilon, 0) \propto \varepsilon^{\nu(d-2)}.$$

With $d = 3$ this gives Equation (3.28).

Chapter 4

Computation of Coherent Transport Properties in Mesoscopic Systems

The calculation of transport properties always was a central point of condensed matter physics. For the investigation of localisation in disordered systems, coherent transport is of most interest. For this case there are two frequently used approaches to calculate the conductance or conductivity of mesoscopic systems. One approach was proposed by Landauer [39, 40] and further developed amongst others by Büttiker. The second one is based on the Kubo linear response formalism, which connects nonequilibrium processes to fluctuations in equilibrium. Today it is well established that both methods are equivalent in case of coherent transport.

In this chapter we will introduce the recursive Green's function method (RGFM) for the case of completely coherent transport, which finally yields recursion formulæ for the density of states and the conductance. We will also show how to incorporate semi-infinite leads in the RGFM. At last, finite size scaling (FSS) analysis will be explained.

4.1 Elastic Scattering: Landauer-Büttiker Approach and Kubo Formula

In the derivation of the Kubo formula the current is treated as a response of the system to an (external) electric field, which should be sufficiently small to ensure staying in the linear response regime [26, 29]. The obtained d.c. conductivity σ is connected to the energy absorption from the field [27]. However, an isolated finite system, which has a discrete spectrum, cannot absorb energy from this electro-magnetic field [27] and σ is zero. In order to obtain a finite σ the system must be coupled to a large heat bath, which leads eventually to a finite width of the energy levels (cf. Section 7.1). Because a detailed microscopic description is difficult to obtain usually the level broadening is modelled by introducing a small imaginary part γ to the energy. A finite d.c. conductivity is then obtained for γ being larger than the inter-level spacing [27].

For Landauer this way of "circumventing" the problems caused by the finiteness of the system was not satisfying. He considered a model where the sample (disordered region) is connected through ideal wires (leads) to some electron reservoirs with different chemical potentials [39–41]. This setup results in a current being driven through the sample by the potential drop, which very much resembles the experimental situation. Moreover, in this point of view the transport becomes a scattering problem: the incoming electrons are elastically scattered by the random impurities in the sample (at least for $\ell_\Phi \gg L$). Landauer found that the conductance can be obtained from the probability of the electrons travelling through the sample. This *transmission probability* T can in turn be calculated by solving the Schrödinger equation. At first, however, there were two versions of the Landauer formula, which caused some discussions about which one to use [27]. Later the situation was clarified as it turned out that one of the formulæ,

$$\mathfrak{g}_4 = \frac{e^2}{\pi\hbar} g_4 = \frac{e^2}{\pi\hbar} \frac{T}{1-T} \,, \tag{4.1}$$

referred to the conductance of the sample itself, as it would be measured in a four-

terminal measurement (including spin degeneracy). The other formula,

$$\mathfrak{g}_2 = \frac{e^2}{\pi\hbar} g_2 = \frac{e^2}{\pi\hbar} T \,, \tag{4.2}$$

gives the conductance of a two-terminal measurement, which includes a finite contact resistance due to the leads [27]. The different ways of measuring the conductance are illustrated in Fig. 4.1.

Over the years there have been many generalisations of the Landauer approach [27],

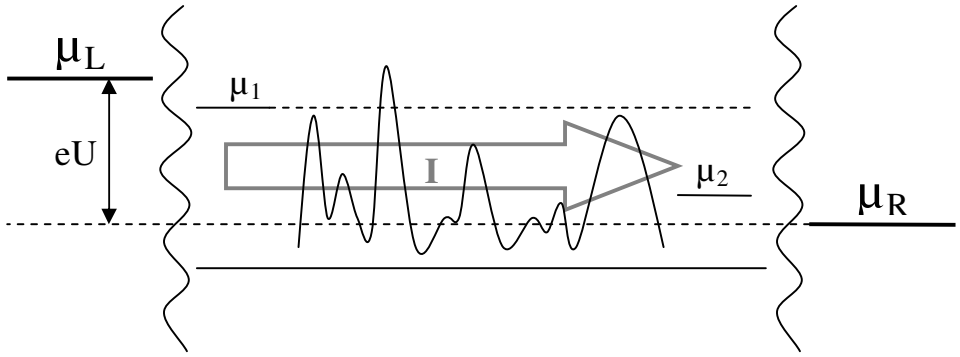

Figure 4.1: Illustration of the difference between 2- and 4-terminal conductance. In a 2-terminal measurement $\mathfrak{g}_2$ is calculated from the current I and the voltage $U = (\mu_L - \mu_R)/e$. In a four-terminal arrangement the potential difference is reduced to $\mu_1 - \mu_2$ due to the contact resistance.

for example to the multichannel case for leads with a finite width, inclusion of inelastic processes (cf. Section 7) and the quantum Hall effect. There have also been various attempts of deriving the Landauer formula from microscopic approaches and in particular it was proven that the (multichannel) Landauer formula can bee derived from the Kubo linear response formalism provided that the leads are taken into account [42].

4.2 Recursive Green's Function Method

An approach to calculate the d.c. conductivity only given the Anderson tight-binding Hamiltonian (3.24) is the recursive Green's function method [12, 13], which yields a

recursion scheme for the d.c. conductivity tensor starting from the Kubo-Greenwood formula. Moreover, this method allows to compute the density of states and the localization length.

4.2.1 Recursion Formulation

A general tight-binding Hamiltonian can be written as

$$\mathcal{H} = \sum_{ij} H_{ij} |i\rangle\langle j| \ , \tag{4.3}$$

where $|i\rangle$ are localized wave-functions at points on an arbitrary dimensional lattice and $\mathcal{H}$ is hermitian. The single particle Green's function $\mathcal{G}^{\pm}(z)$ is defined by the relation [43]

$$(z^{\pm} - \mathcal{H})\mathcal{G}^{\pm} = \mathbb{1} \ , \tag{4.4}$$

where $z = E \pm \imath\gamma$ is called complex energy and the sign of the small imaginary part γ distinguishes between advanced and retarded Green's functions, $\mathcal{G}^{-}(E - \imath 0)$ and $\mathcal{G}^{+}(E + \imath 0)$, respectively [43]. Equivalently, $\mathcal{G}^{\pm}$ can be represented in the basis of the functions $\{|i\rangle\}$. Using Equation (4.3) and (4.4) one obtains

$$(z^{\pm}\delta_{ij} - H_{ij})G^{\pm}_{ij} = \delta_{ij} \ , \tag{4.5}$$

where $G^{\pm}_{ij}$ is the matrix element $\langle i|\mathcal{G}^{\pm}|j\rangle$. Notice that for a hermitian Hamiltonian the advanced Green's function is the hermitian conjugate of the retarded Green's function, i.e. $G^{-}_{ij} = (G^{+}_{ji})^{*}$.

If $\mathcal{H}$ contains only nearest-neighbour hopping, like in the Anderson model of localisation, Equation (4.5) can be simplified using a block matrix notation. This is equivalent to consider the system as being built up of slices or strips for 3D or 2D, respectively, along one lattice direction. In what follows all quantities written in **bold capitals** are matrices acting in the subspace of such a slice or strip[1]. The LHS of

[1] For 2D and 3D these are matrices of size $M \times M$ and $M^2 \times M^2$, respectively, where M is the lateral size (cf. Fig. 4.2).

Equation (4.5) is then given as

$$\begin{pmatrix} \ddots & \ddots & \ddots & 0 & 0 & \cdots \\ 0 & -\mathbf{H}_{ii-1} & (z^{\pm}\mathbf{I}-\mathbf{H}_{ii}) & -\mathbf{H}_{ii+1} & 0 & \cdots \\ \cdots & 0 & -\mathbf{H}_{i+1i} & (z^{\pm}\mathbf{I}-\mathbf{H}_{i+1i+1}) & -\mathbf{H}_{i+1i+2} & 0 \\ \cdots & 0 & 0 & \ddots & \ddots & \ddots \end{pmatrix} \times \begin{pmatrix} \ddots & \vdots & \ddots \\ \cdots & \mathbf{G}^{\pm}_{i-1j} & \cdots \\ \cdots & \mathbf{G}^{\pm}_{ij} & \cdots \\ \cdots & \mathbf{G}^{\pm}_{i+1j} & \cdots \\ \ddots & \vdots & \ddots \end{pmatrix} . \tag{4.6}$$

From the last equation one can easily see that Equation (4.5) is equivalent to

$$(z^{\pm}\mathbf{I}-\mathbf{H}_{ii})\mathbf{G}^{\pm}_{ij} - \mathbf{H}_{ii-1}\mathbf{G}^{\pm}_{i-1j} - \mathbf{H}_{ii+1}\mathbf{G}^{\pm}_{i+1j} = \mathbf{I}\delta_{ij} \ . \tag{4.7}$$

Using the hermiticity of $\mathcal{H}$ we define the hopping matrix $\mathbf{t}_i \equiv \mathbf{H}_{i,i+1}$ (and hence $\mathbf{t}_i^{\dagger} = \mathbf{H}_{i,i-1}$) connecting the ith and the $(i+1)$st slice. Now, we consider adding an additional slice to a system consisting of N slices. The Hamiltonian of this larger system can be written as follows [13]

$$\mathcal{H}^{(N+1)} \longrightarrow \mathbf{H}_{ij} + (\mathbf{t}_N + \mathbf{t}_N^{\dagger}) + \mathbf{H}_{N+1N+1} \quad (i,j \leq N). \tag{4.8}$$

The first and the last terms describe the uncoupled N-slice and the 1-slice system. Using $\mathbf{t}_N$ as an "interaction" the Green's function $\mathbf{G}^{(N+1)}$ of the coupled system can be calculated via Dyson's equation [13, 43],

$$\mathbf{G}^{(N+1)}_{ij} = \mathbf{G}^{(N)}_{ij} + \mathbf{G}^{(N)}_{iN}\mathbf{t}_N\mathbf{G}^{(N+1)}_{Nj} \quad (i,j \leq N). \tag{4.9}$$

In particular

$$\mathbf{G}^{(N+1)}_{N+1N+1} = \left[z^{\pm}\mathbf{I} - \mathbf{H}_{N+1N+1} - \mathbf{t}^{\dagger}_{N}\mathbf{G}^{(N)}_{NN}\mathbf{t}_{N}\right]^{-1} \tag{4.10a}$$

$$\mathbf{G}^{(N+1)}_{ij} = \mathbf{G}^{(N)}_{ij} + \mathbf{G}^{(N)}_{iN}\mathbf{t}_{N}\mathbf{G}^{(N+1)}_{N+1N+1}\mathbf{t}^{\dagger}_{N}\mathbf{G}^{(N)}_{Nj} \quad (i,j \leq N) \tag{4.10b}$$

$$\mathbf{G}^{(N+1)}_{iN+1} = \mathbf{G}^{(N)}_{iN}\mathbf{t}_{N}\mathbf{G}^{(N+1)}_{N+1N+1} \quad (i \leq N) \tag{4.10c}$$

$$\mathbf{G}^{(N+1)}_{N+1j} = \mathbf{G}^{(N+1)}_{N+1N+1}\mathbf{t}^{\dagger}_{N}\mathbf{G}^{(N)}_{Nj} \quad (j \leq N)\,. \tag{4.10d}$$

With Equation (4.10) the Green's function can be obtained iteratively. Additionally, there

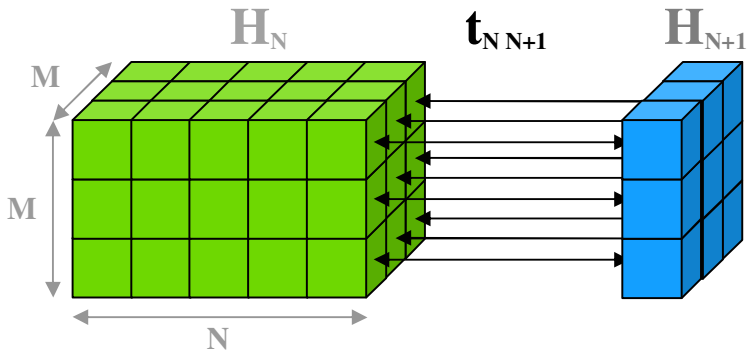

Figure 4.2: Scheme of the recursive Green's function method for a 3D system. The new Green's function $\mathbf{G}^{(N+1)}$ can be calculated from the old Hamiltonian $\mathbf{H}_N$, the new slice Hamiltonian $\mathbf{H}_{N+1}$ and the coupling $\mathbf{t}_N$.

are two kinds of boundary conditions which must be considered: across each slice and at the beginning and the end of the stack. The first kind doesn't present any difficulty and usually fixed or periodic boundary conditions are employed. The second kind of boundary conditions is connected to some subtleties which are addressed in Section 4.3.

4.2.2 Density of States and D.C. Conductivity

Knowing the Green's function of a system one can calculate all properties related to $\mathcal{G}^{\pm}$. Moreover, using Equation 4.10 it is possible to determine them within a recursion scheme. The density of states, for example, in terms of the Green's function is given

by [43]

$$\rho(E) = -\frac{1}{\pi\Omega}\mathrm{Im}\,\mathrm{Tr}\,\mathcal{G}^{+} = -\frac{1}{\pi \mathrm{N} \mathrm{M}^2}\mathrm{Im}\sum_{\mathrm{i}=1}^{\mathrm{N}}\mathrm{Tr}\,\mathbf{G}_{\mathrm{ii}}^{+}\ . \tag{4.11}$$

In Section 3.1.2 it was already mentioned that the d.c. conductivity can be expressed in terms of Green's functions. The expression for σ in Equation (3.5) can be written in a more convenient way,

$$\sigma = \frac{2e^2\hbar}{\pi\Omega m^2}\mathrm{Tr}\,\left[\mathrm{p}\,\mathrm{Im}\,\mathcal{G}^{+}\,\mathrm{p}\,\mathrm{Im}\,\mathcal{G}^{+}\right]\ . \tag{4.12}$$

Using the relation $p = \frac{im}{\hbar}[\mathcal{H}, x]$ one can rewrite Equation (4.12) in position representation

$$\sigma = \frac{e^2 4}{hNM^2}\mathrm{Tr}\,\left\{\gamma^2\sum_{\mathrm{i,j}}^{\mathrm{N}}\mathbf{G}_{\mathrm{ij}}^{+}\,\mathrm{x_j}\,\mathbf{G}_{\mathrm{ji}}^{-}\,\mathrm{x_i} - \imath\frac{\gamma}{2}\sum_{\mathrm{i}}^{\mathrm{N}}(\mathbf{G}_{\mathrm{ii}}^{+} - \mathbf{G}_{\mathrm{ii}}^{-})\,\mathrm{x_i^2}\right\}\ , \tag{4.13}$$

where x_i is the position of the ith slice.

Starting from these relations and using (4.10) one can derive recursion formulæ to calculate the properties for the $(N+1)$-slice system. The results are expressed in terms of the following auxiliary matrices

$$\mathbf{R}_N = \mathbf{G}_{NN}^{+}\ , \tag{4.14a}$$

$$\mathbf{B}_N = \gamma\mathbf{t}_N^{\dagger}\left[\sum_{ij}^{N}\mathbf{G}_{Nj}^{+(N)}x_j(2\gamma\mathbf{G}_{ji}^{-(N)} - \imath\mathbf{I}\delta_{ij})x_i\mathbf{G}_{iN}^{+(N)}\right]\mathbf{t}_N\ , \tag{4.14b}$$

$$\mathbf{C}_N^{+} = \gamma\mathbf{t}_N^{\dagger}\left[\sum_{i=1}^{N}\mathbf{G}_{Ni}^{+(N)}x_i\mathbf{G}_{iN}^{-(N)}\right]\mathbf{t}_N = (\mathbf{C}_N^{+})^{\dagger}\ , \tag{4.14c}$$

$$\mathbf{C}_N^{-} = \gamma\mathbf{t}_N^{\dagger}\left[\sum_{i=1}^{N}\mathbf{G}_{Ni}^{-(N)}x_i\mathbf{G}_{iN}^{+(N)}\right]\mathbf{t}_N = (\mathbf{C}_N^{-})^{\dagger}\ , \tag{4.14d}$$

$$\mathbf{F}_N = \mathbf{t}_N^{\dagger}\left[\sum_{i=1}^{N}\mathbf{G}_{Ni}^{+(N)}\mathbf{G}_{iN}^{+(N)}\right]\mathbf{t}_N\ . \tag{4.14e}$$

The derivation can be simplified assuming the new slice to be at $x_{N+1} = 0$. This leads, however, to corrections for the matrices $\mathbf{B}_N$ and $\mathbf{C}_N^{\pm}$ because the origin of x_i has to

be shifted to the position of the current slice in each iteration step. The substitution $x_i \rightarrow x_i - 1$ leads to the following corrections,

$$\mathbf{B}'_N = \mathbf{B}_N + \imath\mathbf{C}^+_N + \imath\mathbf{C}^-_N + \frac{1}{2}\mathbf{t}^\dagger_N(\mathbf{R}_N - \mathbf{R}^\dagger_N)\mathbf{t}_N \ , \tag{4.15a}$$

$$\mathbf{C}'^{\pm}_N = \mathbf{C}^\pm_N - \imath\frac{1}{2}\mathbf{t}^\dagger_N(\mathbf{R}_N - \mathbf{R}^\dagger_N)\mathbf{t}_N \ . \tag{4.15b}$$

Here we used the identity

$$\gamma\sum_{i=1}^{N}\mathbf{G}^+_{Ni}\mathbf{G}^-_{iN} = \imath\frac{1}{2}(\mathbf{G}^+_{NN} - \mathbf{G}^-_{NN}) = \imath\frac{1}{2}(\mathbf{R}_N - \mathbf{R}^\dagger_N) = -\mathrm{Im}\,\mathbf{R}_\mathrm{N} \ . \tag{4.16}$$

The derivation of the recursion relations is given in Appendix B, it yields the following expressions

$$s^{(N+1)}_\rho = s^{(N)}_\rho + \mathrm{Tr}\left\{\mathbf{R}_{\mathrm{N}+1}(\mathbf{F}_\mathrm{N} + \mathbf{I})\right\} \ , \tag{4.17a}$$

$$s^{(N+1)}_\sigma = s^{(N)}_\sigma + \mathrm{Tr}\left\{\mathrm{Re}\,(\mathbf{B}_\mathrm{N}\mathbf{R}_{\mathrm{N}+1}) + \mathbf{C}^+_\mathrm{N}\mathbf{R}^\dagger_{\mathrm{N}+1}\mathbf{C}^-_\mathrm{N}\mathbf{R}_{\mathrm{N}+1}\right\} \ , \tag{4.17b}$$

$$\mathbf{R}_{N+1} = \left[z^\pm\mathbf{I} - \mathbf{H}_{N+1N+1} - \mathbf{t}^\dagger_N\mathbf{R}_N\mathbf{t}_N\right]^{-1} \ , \tag{4.17c}$$

$$\mathbf{B}_{N+1} = \mathbf{t}^\dagger_{N+1}\mathbf{R}_{N+1}\left[\mathbf{B}_N + 2\mathbf{C}^+_N\mathbf{R}^\dagger_{N+1}\mathbf{C}^-_N\right]\mathbf{R}_{N+1}\mathbf{t}_{N+1} \ , \tag{4.17d}$$

$$\mathbf{C}^+_{N+1} = \mathbf{t}^\dagger_{N+1}\mathbf{R}_{N+1}\mathbf{C}^+_N\mathbf{R}^\dagger_{N+1}\mathbf{t}_{N+1} \ , \tag{4.17e}$$

$$\mathbf{C}^-_{N+1} = \mathbf{t}^\dagger_{N+1}\mathbf{R}^\dagger_{N+1}\mathbf{C}^-_N\mathbf{R}_{N+1}\mathbf{t}_{N+1} \ , \tag{4.17f}$$

$$\mathbf{F}_{N+1} = \mathbf{t}^\dagger_{N+1}\mathbf{R}_{N+1}(\mathbf{F}_N + \mathbf{I})\mathbf{R}_{N+1}\mathbf{t}_{N+1} \ . \tag{4.17g}$$

The density of states and the d.c. conductivity are then given as follows,

$$\rho^{(N+1)}(E) = -\frac{1}{\pi(N+1)M^2}s^{(N+1)}_\rho \ , \tag{4.18}$$

$$\sigma^{(N+1)}(E) = \frac{e^2}{h}\frac{4}{(N+1)M^2}\ s^{(N+1)}_\sigma \ . \tag{4.19}$$

It is also possible to calculate the localisation length $\xi(E)$, which is connected to the matrix $\mathbf{G}^+_{1N+1}$,

$$\frac{1}{\xi(E)} = -\lim_{\gamma\rightarrow 0}\lim_{N\rightarrow\infty}\frac{1}{2N}\ln\left|\mathrm{Tr}\,\mathbf{G}^+_{1\mathrm{N}}(\mathrm{E})\right|^2 \ . \tag{4.20}$$

The recursion relation for $\xi^{(N+1)}(E)$ is

$$\frac{1}{\xi^{(N+1)}(E)} = -\frac{1}{N+1} s_\xi^{(N+1)} , \tag{4.21a}$$

$$s_\xi^{(N+1)} = s_\xi^{(N)} + \ln \left| \mathrm{Tr}\, \mathbf{G}^{(\mathrm{N+1})+}_{\mathrm{N+1N+1}} \right| . \tag{4.21b}$$

4.3 Semi-infinite Leads

Although the imaginary part γ of the complex energy z can be interpreted as an inverse lifetime (see Section 7), one would rather like to set $\gamma = 0$. This is only valid after taking the thermodynamic limit, i.e. for an infinite system [13]. This procedure eventually leads to a description of elastic scattering. In order to make the system effectively infinite, one attaches semi-infinite, metallic leads to both ends of the system. It was shown [44] that in this case the formalism given above using the Kubo-Greenwood formula is equivalent to the Landauer-Büttiker formulation. Here we will show how the leads can be incorporated into the recursion scheme given above. We will also review expressions for the Green's function of purely 1D leads and leads with a finite cross section. The influence of the leads on transport properties will be discussed in Section 5.2.

Notice that because of attaching the leads to the disordered region the recursion scheme eventually gives the transport properties of the **system plus leads**, i.e. in the sense of a two-terminal measurement. The d.c. conductivity obtained from Equation (4.19) for a system with leads is therefore strictly speaking **not** the conductivity of the disordered region. It should rather be understood as the two-terminal conductance multiplied by L^{2-d} [44].

4.3.1 Self-Energy due to the Leads

The effects of the leads can be described in an elegant way using the notation of self-energies. It can be shown [28] that the Green's function of a finite system connected to

N_L leads is given by

$$\left(E\delta_{ij} - H^0_{ij} - \Sigma^+_{ij}\right) G^+_{ij} = \delta_{ij} \ , \tag{4.22}$$

where H^0_{ij} is the Hamilton matrix of the isolated system, which is for example a disordered system described by the Anderson Hamiltonian (3.24). The matrix Σ^+_{ij} is called the self-energy due to the interaction of the system with the leads. If different leads are independent their effects are additive, i.e.

$$\mathbf{\Sigma}^+ = \sum_{i=1}^{N_L} \mathbf{\Sigma}^+_i = \sum_{i=1}^{N_L} \mathbf{t}\mathbf{G_0}\mathbf{t}^\dagger \ , \tag{4.23}$$

where $\mathbf{G_0}$ is the Green's function of a semi-infinite metallic wire. In a two terminal configuration, where the leads are just coupled to the first and the last slice, the self-energy due to the leads effects only the Green's functions of these two slices. Therefore,

$$\mathbf{G}^+_{ii} = \left[E\mathbf{I} - \mathbf{H}_{ii} - \mathbf{\Sigma}^+\right]^{-1} \quad (i = 1, N) \ . \tag{4.24}$$

The most important effect of the self-energy is that it already provides a small imaginary term in Equation (4.22), which makes the somewhat artificial choice of γ unnecessary. Physically, this is connected to the fact that elastic scattering processes cannot lead to an equilibration of the electrons, which is necessary to obtain a steady state current. In Equation (4.5) this was taken into account by choosing a finite γ. However, in the case of completely coherent transport one usually assumes all inelastic processes to occur in some electron reservoirs connected to the sample by the leads [29]. The imaginary part of $\mathbf{\Sigma}^+$ determines the "escape rate" at which electrons can get out of the sample through the leads and eventually reach the reservoirs [28]. Therefore, it already determines the rate of electrons being inelastically scattered and an additional imaginary term is unnecessary.

4.3.2 1D Semi-infinite Leads

It remains to derive an expression for the self-energy of a semi-infinite lead. Starting point is the expansion of the Green's function in terms of a complete set of eigenfunctions

$\phi_\alpha(\mathbf{r}) = \langle \mathbf{r}|\alpha\rangle$ [43],

$$\langle \mathbf{r}|\mathcal{G}^+|\mathbf{r}'\rangle = G^+(\mathbf{r},\mathbf{r}';E) = \sum_\alpha \frac{\phi_\alpha(\mathbf{r})\phi_\alpha^*(\mathbf{r}')}{E - E_\alpha + \imath\delta} \quad (\delta > 0)\ , \tag{4.25}$$

where

$$H_0\phi_\alpha(\mathbf{r}) = E_\alpha\phi_\alpha(\mathbf{r})\ . \tag{4.26}$$

For a purely 1D wire of length $L = (N-1)a$, which consists of N sites, the eigenfunctions are known to be

$$\phi_k(\mathbf{r}) = \frac{1}{\sqrt{2L}}\left[\exp(\imath kx) - \exp(-\imath kx)\right]\ , \tag{4.27a}$$

$$E_k = 2t\cos(ka)\ . \tag{4.27b}$$

Upon taking the limit $N \to \infty$ (while keeping L fixed), the wave vectors k form a continuum and the sum in Equation (4.25) can be replaced by an integral. The Green's function along the edge of the wire is then [28]

$$G_0^{1\mathrm{D}}(1,1;E) = \frac{1}{ta}\left[\chi \pm (\chi^2-1)^{1/2}\right]\ , \tag{4.28}$$

where $\chi \equiv (E + \imath\delta + 2t)/2t$ and the sign is chosen such that $\left|\chi \pm (\chi^2-1)^{1/2}\right| < 1$.

4.3.3 Semi-infinite Leads with finite Cross Section

For a wire with a finite cross section of size $M \times M$ or a finite width M the eigenfunctions are separable, e.g. in the former case

$$\Psi = \phi_\alpha^x\ \varphi_\beta^y\ \zeta_\nu^z\ . \tag{4.29}$$

Consequently, the eigenenergy E in 3D is just a sum of the respective eigenvalues,

$$E = E_\alpha + E_\beta + E_\nu = 2t\left[\cos(k_\alpha a) + \cos(k_\beta a) + \cos(k_\nu a)\right]\ . \tag{4.30}$$

Depending on the boundary conditions across each slice, k_β and k_ν take discrete values only. Therefore, k_α will also be discrete for a fixed energy. The number of possible values

for k_α determines the number of propagating channels at a given energy. This eventually leads to the conductance quantisation in a two terminal measurement, because each channel has a conductance of e^2/h and the total conductance is a sum of all the channel contributions [28]. Substituting these eigenfunctions in Equation (4.25) and performing the summation involving ϕ^x_α we are left with two additional summations,

$$G_0(\mathbf{q},\mathbf{q}';E) = \sum_\beta \sum_\nu \varphi^y_\beta(q_y)\varphi^{y*}_\beta(q'_y)\zeta^z_\nu(q_z)\zeta^{z*}_\nu(q'_z)G_0^{1\mathrm{D}}(1,1;E-E_\beta-E_\nu). \quad (4.31)$$

Here $\mathbf{q}$ and $\mathbf{q}'$ denote the position of sites along the edge of the wire, i.e. in the slice connected to the sample. The eigenfunctions φ^y_β, ζ^z_ν and the respective eigenenergies E_β, E_ν can be obtained analytically for hard wall and periodic boundary conditions. Thus, the sum can be easily evaluated to obtain the Green's function of the wire, which is then used as initial value for $\mathbf{R}_N$ in Equations (4.17). Additionally, another lead has to be attached at the end of the stack. For this purpose the lead is treated as a slice with the Hamiltonian $\mathbf{H}_{N+1N+1} = \mathbf{G}_0^{-1}$.

4.4 Finite-Size Scaling

A problem one is always faced with when using numerical methods investigating phase transitions, is the fact that for finite systems there can be no singularities induced by a transition and the divergences are always rounded off [45]. Fortunately, the phase transition can still be studied using finite-size scaling. Here we briefly review the main results taking the dimensionless conductance g of a cubic sample of size $L \times L \times L$ as an example. Notice that the same ideas can also be applied to the reduced localisation length ξ/L.

Near the MIT one expects the following one-parameter scaling law for the dimensionless conductance [37, 45]

$$g(L,\varepsilon,b) = \mathcal{F}\left(\frac{L}{b}, \chi(\varepsilon)b^{1/\nu}, \phi(\varepsilon)b^{-y}\right) ,$$

where b is the scale factor in the renormalisation group, χ is a relevant scaling variable, ϕ is a irrelevant scaling variable, $\nu > 0$ is the critical exponent and $y > 0$ is the irrelevant scaling exponent. The irrelevant scaling variable allows us to take account of *corrections to scaling* due to the finite size of the sample. The parameter $\varepsilon = |E - E_\mathrm{c}|/E_\mathrm{c}$ measures the distance from the the mobility edge E_c. The choice[2] $b = L$ leads to the standard scaling form

$$g(L, \varepsilon) = F(L^{1/\nu}\chi(\varepsilon), L^{-y}\phi(\varepsilon)) \tag{4.32}$$

with F being related to $\mathcal{F}$. For E close to E_c we expand F as a Taylor series up to order n_I and obtain a series of functions F_n. Each function F_n is then expanded up to order n_R,

$$g(L, \varepsilon) = \sum_{n=0}^{n_\mathrm{I}} \phi^n L^{-ny} F_n(\chi L^{1/\nu}) \;, \tag{4.33a}$$

$$F_n(\chi L^{1/\nu}) = \sum_{m=0}^{n_\mathrm{R}} a_{nm} \chi^m L^{m/\nu} \;. \tag{4.33b}$$

Additionally χ and ϕ are expanded in terms of the small parameter ε up to order m_R and m_I, respectively. This procedure gives

$$\chi(\varepsilon) = \sum_{n=1}^{m_\mathrm{R}} b_n \varepsilon^n, \quad \phi(\varepsilon) = \sum_{n=0}^{m_\mathrm{I}} c_n \varepsilon^n \;. \tag{4.34}$$

From Equation (4.32) and (4.33) on can see that finite system size results in a systematic shift of g with L, where the direction of the shift depends on the boundary conditions [45]. Consequently, the curves $g(L, \varepsilon)$ do not intersect at the critical point $\varepsilon = 0$ for different system sizes. The term F_0 on the other hand shows the expected behaviour.

Using a least square fit of the numerical data to Equations (4.33) and (4.34) allows to extract the critical parameters ν and E_c. With the fitting procedure one can also obtain the finite-size corrections and subtract them from the data to show the anticipated scaling behaviour. This kind of finite-size scaling analysis has been successfully applied to

[2] The apparent choice of b is strictly speaking connected to the iteration of the Renormalisation Group [45].

numerical calculations of the localisation length and the conductance within the Anderson model [3, 9].

Chapter 5

Coherent Transport near the MIT at $T = 0$

The zero temperature limit is usually employed in theoretical investigations of the Anderson MIT. In most cases the one-parameter scaling theory is then used to obtain the critical parameters. There are some discussions whether this scaling theory is generally applicable [9,10]. So far, one-parameter scaling has been demonstrated to an astonishing degree by numerical studies of the Anderson model [8]. However, most studies focused on scaling of the localisation length and the conductance at the disorder-driven MIT in the vicinity of the band centre [8–10].

Here we will also present calculations of the conductance and the density of states close to $E = 0$ which are in accordance with the known results. We will also show results for a disorder transition outside the band centre and investigate the influence of the metallic leads. At last we focus on the energy transition for fixed disorder strength.

5.1 Disorder Transition at $E = 0.5\,t$

In order to test our numerics and to have some reference point for our investigations of the influence of the leads we follow Ref. [9] and therefore fix $E = 0.5\,t$ in the vicinity of the band centre. We also impose hard wall boundary conditions in the transverse direction. For each combination of disorder strength W and system size L we generate an ensemble of 10000 samples. The systems under investigation are cubes of size $L \times L \times L$ and $L = 4, 6, 8, 10, 12$ and 14. For each sample we calculate the density of states $\rho(E, L)$ and the dimensionless two-terminal conductance g_2 using the RGFM explained in Section 4.2. To get the dimensionless conductance g_4 of the disordered region only, we have to subtract the contact resistance due to the leads. This gives

$$\frac{1}{g_4} = \frac{1}{g_2} - \frac{1}{N}\,. \tag{5.1}$$

Here $N = N(E)$ is the number of propagating channels at the Fermi energy E [46]. Finally we compute the average DOS $\langle \rho(E, L) \rangle$, the average conductance $\langle g_4(E, L) \rangle$ and the typical conductance $\langle \ln g_4(E, L) \rangle$.

The results for the different conductance averages are shown in Fig. 5.1 and 5.2 together with respective fits to the standard scaling form Equation (4.32). The expansion parameters and the results for the critical exponent and the critical disorder are given in Table 5.1. In Fig. 5.3 we show the same data as in Fig. 5.1 and 5.2 after the corrections

average	$W_{\min}/t$	$W_{\max}/t$	n_{R}	n_{I}	m_{R}	ν	W_{c}/t	y
$\langle g_4 \rangle$	15.0	18.0	2	0	2	1.55 ± 0.11	16.47 ± 0.06	–
$\langle \ln g_4 \rangle$	15.0	18.0	3	1	1	1.55 ± 0.18	16.8 ± 0.3	0.8 ± 1.0

Table 5.1: Best fit estimates of the critical exponent and the critical disorder for both averages of g_4 using Eq. (4.32). The system sizes used were $L = 8, 10, 12, 14$ and $L = 4, 6, 8, 10, 12, 14$ for $\langle g \rangle$ and $\langle \ln g \rangle$, respectively. For each combination of disorder strength W and system size L we generate an ensemble of 10000 samples.

to scaling have been subtracted indicating that the data points for different system sizes fall on a common curve with two branches as it is expected from the one-parameter

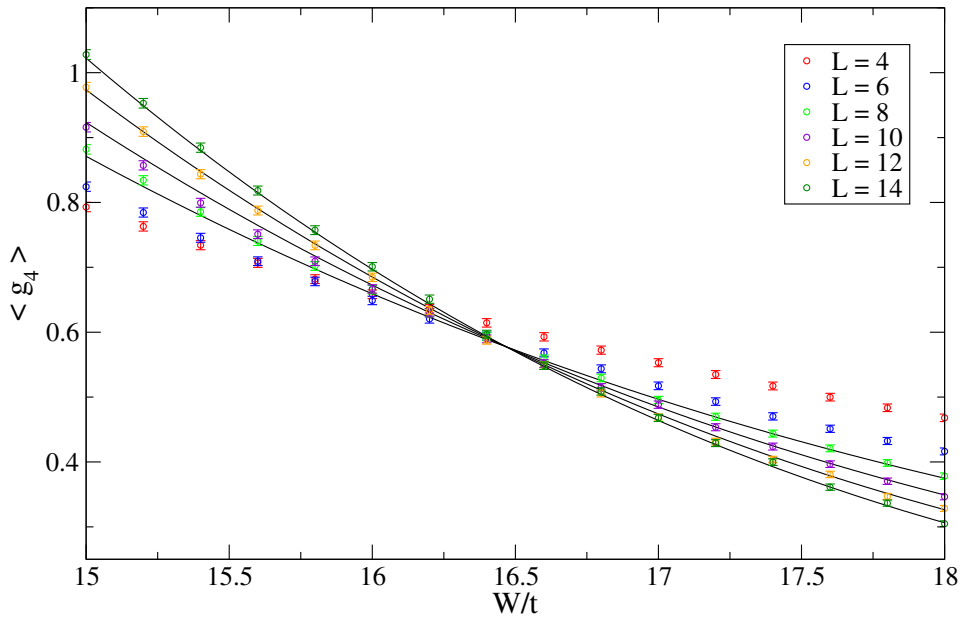

Figure 5.1: Average dimensionless conductance vs disorder strength for $E = 0.5\,t$. System sizes are given in the legend. Error bars obtained from ensemble average. Also shown are fits to Eq. (4.32) for $L = 8, 10, 12$ and 14.

scaling theory. The results for the conductance averages and also the critical values are in good agreement with Ref. [9] and transfer-matrix calculations [8, 9].

5.1.1 Disorder Dependence of the Density of States

The RGFM enables us to compute the DOS of the disordered system. Fig. 5.4 shows the average DOS for different system sizes. The DOS should be independent of L. However, one can see that there are still some fluctuations present. These can be reduced by using larger system sizes and increasing the number of samples. The reduction of the DOS with increasing disorder strength can be understood from a simple argument. The DOS is defined as the number of states $\triangle N$ in an energy interval $\triangle E$ divided by $\triangle E$. If the density of states ρ_c is constant for all energies its value is given by $\rho_c = N/B$, where B is the bandwidth. In the Anderson model with a box distribution for the on-site

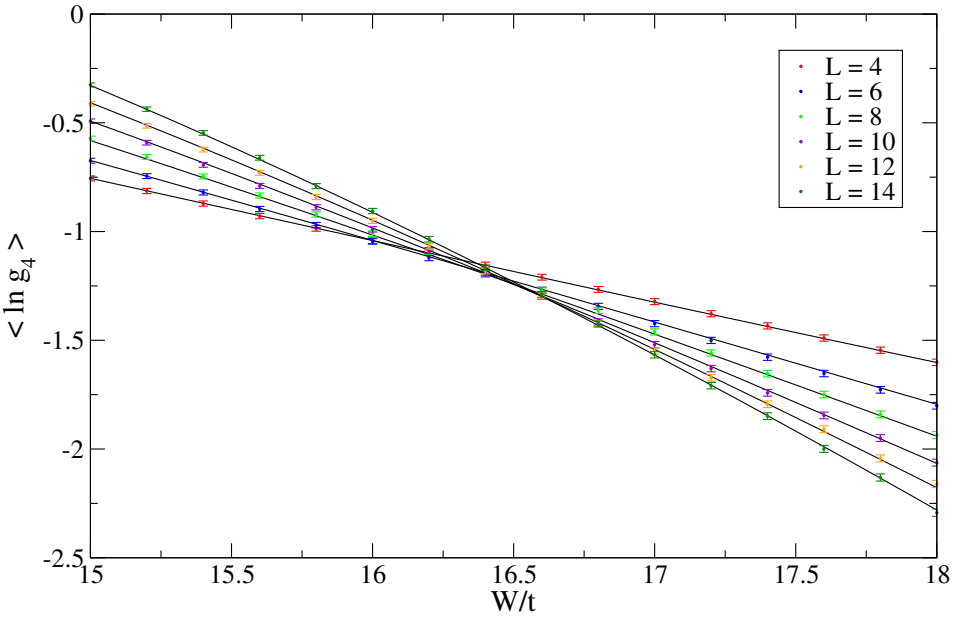

Figure 5.2: Typical dimensionless conductance vs disorder strength for $E = 0.5\,t$. System sizes are given in the legend. Error bars obtained from ensemble average. The solid lines are fits to Eq. (4.32).

energies the bandwidth increases linear with the disorder strength W and the respective band edge is called Lifshitz band edge. Although the DOS in the Anderson model is not constant, one can assume that for energies in the vicinity of the band centre the exact shape of the tails is not important. Therefore, we have

$$\rho_c(W) = \frac{N}{B + \alpha W} \,, \tag{5.2}$$

which shows a decrease of the DOS with W because the total number of states is fixed for a given system size. The parameter α allows for deviations due to the numerical generation of the random on-site energies. These deviations occur, because it is highly unlikely to obtain exactly the values $\pm W/2$ from such a random number generator.

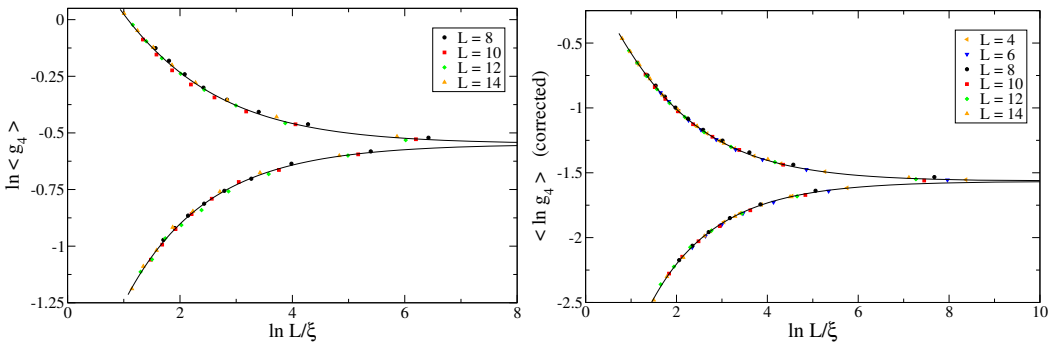

Figure 5.3: Same data as in Figs. 5.1 and 5.2 after corrections to scaling are subtracted and plotted vs L/ξ to show single-parameter scaling. Different colours indicate the system sizes given in the legend.

5.2 Influence of the Metallic Leads

As mentioned in the introduction most numerical studies of the conductance have been focused on the disorder transition in the vicinity of the band centre. However, the one-parameter scaling theory should be valid for any energy inside the band. Therefore we set $E = -5.0\,t$ and calculate the conductance averages as before. The results for the typical conductance are shown in Fig. 5.5a. Surprisingly, there is no evidence of scaling behaviour. The order of magnitude is also much smaller than in the case of $E = 0.5\,t$, although one expects the critical conductance to be universal.

The origin of this reduction can be understood from Fig. 5.6, which shows the density of states of a disordered and a clean system such as in the metallic leads. As MacKinnon already pointed out in his paper on the RGFM [13], a difference between the DOS in the leads and in the disordered region may lead to false results for the transport properties. Put to an extreme, if there are no states available at a certain energy in the leads, e.g. for $|E| \geq 6\,t$, there will be no transport regardless of the DOS and the conductance in the disordered system at that energy. The DOS of the latter system becomes always broadened by the disorder. Therefore it is not possible to investigate transport

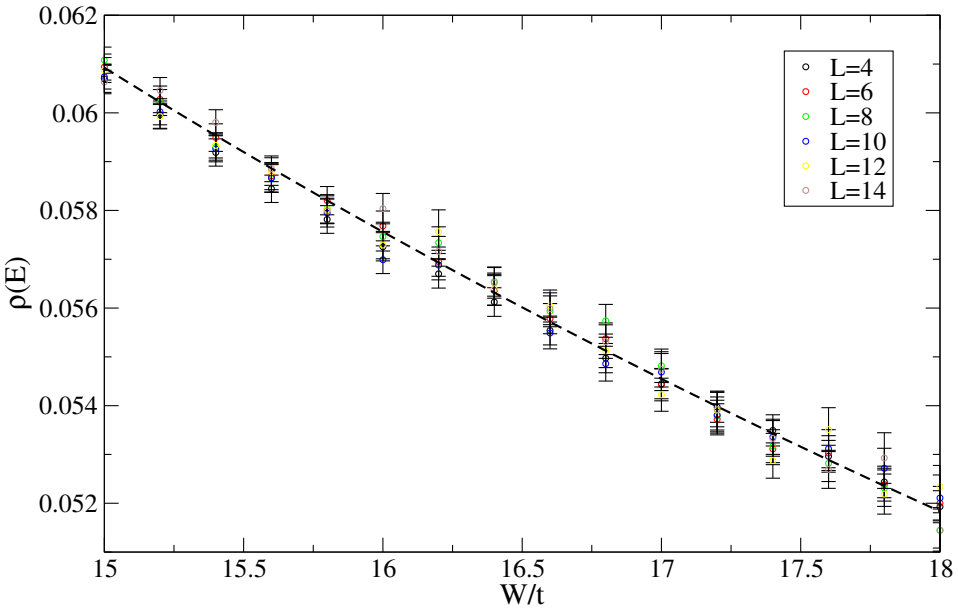

Figure 5.4: Density of states vs disorder strength for $E = 0.5\,t$ and $L = 4, 6, 8, 10, 12, 14$. Error bars obtained from ensemble average. The dashed line shows a fit to Eq. (5.2) for $L = 6$ to illustrate the reduction of ρ with increasing disorder strength.

properties at energies outside the ordered band using the standard System+Leads setup. Additionally, for energies $3\,t \lessapprox |E| < 6\,t$ the DOS of the clean system is smaller than the disorder broadened DOS. The transport properties, that crucially depend on the DOS, are consequently reduced. The problems can be overcome by shifting the energy of the disordered region while keeping the Fermi energy in the leads in the lead-band centre (or vice versa). This is equivalent to applying a gate voltage to the disordered region and sweeping it — a technique similar to MOSFET experiments. The results for the typical conductance using this method are shown in Fig. 5.5. One can see some indication of scaling behaviour and also the order of magnitude is found to be comparable to the $E = 0.5\ t$ case. Another possibility of avoiding the DOS mismatch is choosing a larger hopping parameter in the leads [47], which results in a larger bandwidth.

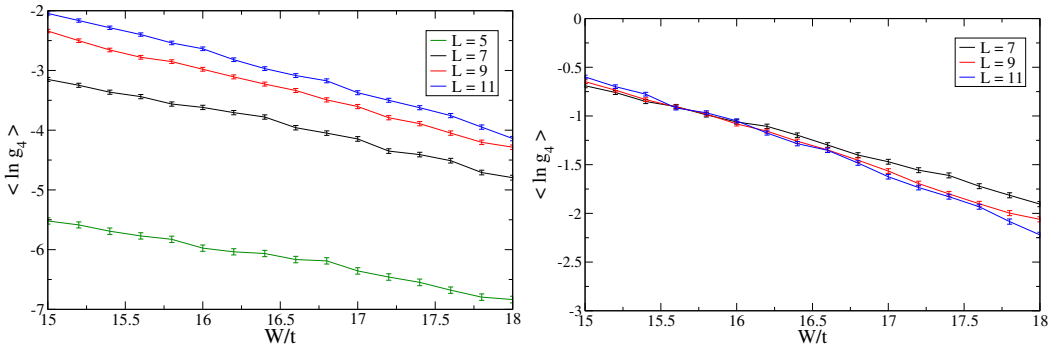

(a) typical conductance, no "energy shift"

(b) typical conductance, with "energy shift"

Figure 5.5: System size dependence of the typical conductance for fixed energy $E = -5.0\,t$. The legend next to the plots shows the system sizes involved. The left plot was calculated using the metallic leads "as they are", i.e. the band centre of the leads coincides with the band centre in the disordered region. In the right plot the band centre of the leads was "shifted" to the respective Fermi energy.

5.3 Energy Transition

Knowing the difficulties involving the metallic leads and using the "shifting technique" we set the disorder strength to $W = 12\,t$ and impose hard wall boundary conditions in the transverse direction [9]. Analogous to the disorder transition case we generate for each combination of Fermi energy and system size an ensemble of 10000 samples (except for $L = 19$ and $L = 21$, where 4000 and 2000 were generated) and examine the size-dependence of the average and the typical conductance, $\langle g_4 \rangle$ and $\langle \ln g_4 \rangle$, respectively.

5.3.1 Energy Dependence of the Density of States

Before looking at the scaling behaviour of the conductance we have to make sure that the "shifting technique" indeed gives the right DOS outside the ordered band. Additionally, we have to check the average DOS for being independent of the system-size.

In Fig. 5.7 we show the DOS obtained from RGFM calculations and from diago-

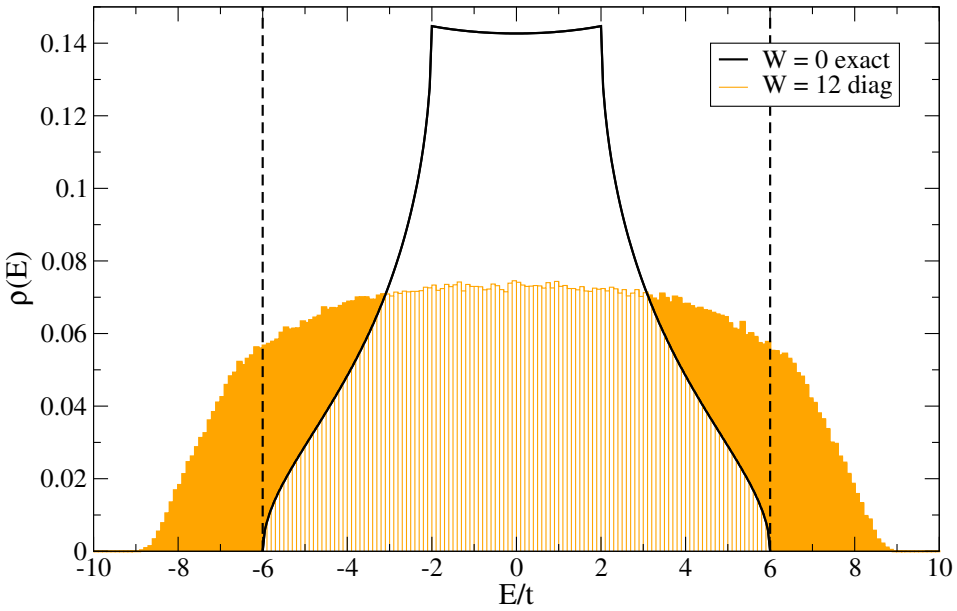

Figure 5.6: Density of states of a clean system (full black line) and a disordered system with $W = 12$ and $L = 21$, obtained from diagonalising Eq. (3.24). The dashed lines indicate the band edges of the ordered system.

nalising the Anderson Hamiltonian. In the latter case we generated 30 configurations and diagonalised the respective Hamiltonians using LAPACK. The DOS is obtained from a normalised histogram of all eigenvalues. In all cases $W = 12\,t$ and $L = 21$. The RGFM calculations agree very well with diagonalisation results, although there are - at least for the number of configurations used - still bumps present which are relics of the finiteness of the sample. Also shown is a smoothed DOS obtained from the diagonalisation data using a Bezier spline. We calculated the average DOS for different system sizes, which is shown in Fig. 5.8. One can see that for large energies the DOS is system size independent. Close to the band edge there are still fluctuations present because deep in the tails only a few states exist and therefore many samples are necessary to obtain a smooth DOS.

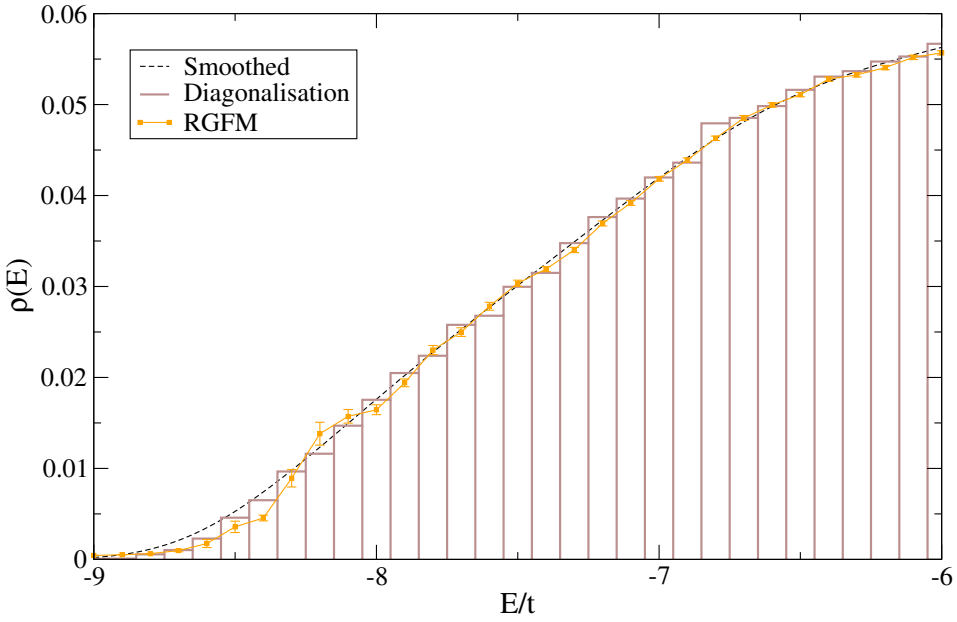

Figure 5.7: Density of states vs energy for $W = 12\,t$ obtained from the RGFM and also from diagonalising the Anderson Hamiltonian. The system size in both cases was $L = 21$.

5.3.2 Scaling Behaviour of the Conductance

The size-dependence of the average and the typical conductance is shown in Fig. 5.9. We find that for $E/t \leq -8.2$ the typical conductance is proportional to the system size L and the constant of proportionality is negative. This corresponds to an exponential decay of the conductance with increasing L and is characteristic for *insulating* behaviour (cf. Section 3.2.2). Moreover, it follows from Equation (3.27) that the constant of proportionality is the localisation length ξ. We find that ξ diverges at some energy, which indicates a phase transition. The energy dependence of ξ is shown in Fig. 5.10.

For E/t being larger than -8.05, $\langle g_4 \rangle$ is proportional to L. This indicates the *metallic* regime and the slope of $\langle g_4 \rangle$ vs L is related to the d.c. conductivity. We fit the data in the respective regimes to the standard scaling form (4.32). The results for the critical exponent and the mobility edge are given in Table 5.2. The obtained

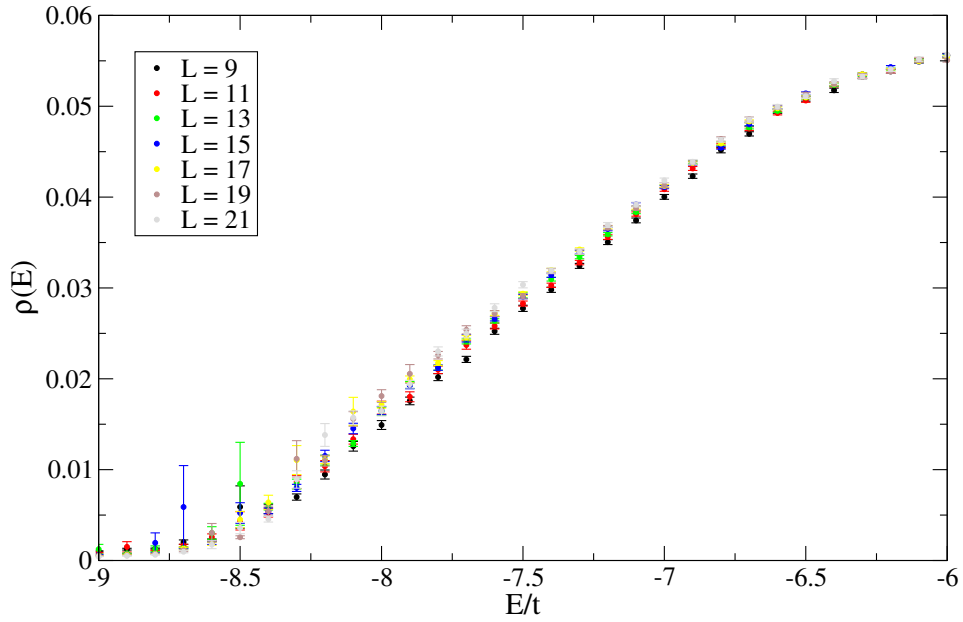

Figure 5.8: Density of states vs energy for different system sizes and $W = 12\,t$ calculated with the RGFM.

average	$E_{\min}/t$	$E_{\max}/t$	n_{R}	m_{R}	ν	E_{c}/t
$\langle g_4 \rangle$	-8.2	-7.4	3	2	1.60 ± 0.18	-8.14 ± 0.02
$\langle \ln g_4 \rangle$	-8.8	-7.85	3	2	1.58 ± 0.06	-8.185 ± 0.012

Table 5.2: Best fit estimates of the critical exponent and the mobility edge for both averages of g_4 using Eq. (4.32). The system sizes used were in both cases $L = 11, 13, 15, 17, 19, 21$.

values for both types of averages, $\langle g_4 \rangle$ and $\langle \ln g_4 \rangle$, are consistent. The average value of $\nu = 1.59 \pm 0.18$ is in accordance with results for conductance scaling at $E/t = 0.5$ and transfer-matrix calculations [8, 9].

5.3.3 Calculation of the D.C. Conductivity

In order to calculate the temperature dependence of the thermoelectric properties using the CTKG formalism, we need to obtain the d.c. conductivity from $\langle g_4(E, L) \rangle$. From

Equation (3.23) one expects the macroscopic conductivity to be the ratio of $\langle g_4(E,L)\rangle$ and L. There are, however, several complications. First, as it was shown in Section 3.1.2 the mechanism of weak localisation gives rise to corrections to the classical behaviour for $g \gg 1$. Second, it is a priori not known if Equation (3.23) still holds in the critical regime. And third, the expansion (4.33) does not yield a behaviour of the form $g \propto \varepsilon^{\nu}$.

In order to check our data for consistence with the anticipated power-law form for the conductivity $\sigma(E)$ in the critical regime, we assume the following scaling law for the conductance,

$$\langle g_4 \rangle = f(\chi^{\nu} L) \,, \tag{5.3}$$

which results from setting[1] $b = \chi^{-\nu}$ in Equation (4.4). The scaling function f is related to the general scaling form $\mathcal{F}$. Due to the large error bars of $\langle g_4 \rangle$ at the MIT, we neglect the irrelevant scaling parameter. However, using only system sizes $L \geq 11$ the corrections to scaling are expected to be small. Then we expand f as a Taylor series up to order n_{R} and χ in terms of the small parameter $\varepsilon = (E_{\mathrm{c}} - E)/E_{\mathrm{c}}$ up to order m_{R}. This procedure gives

$$f(\chi^{\nu} L) = \sum_{m=0}^{n_{\mathrm{R}}} a_m \, (\chi^{\nu} L)^m \qquad \text{and} \qquad \chi(\varepsilon) = \sum_{n=1}^{m_{\mathrm{R}}} b_n \varepsilon^n \,. \tag{5.4}$$

The best fit to our data is determined by minimising the χ^2 statistic. Using $n_{\mathrm{R}} = 3$ and $m_{\mathrm{R}} = 2$ we obtain for the critical values, $\nu = 1.58 \pm 0.18$ and $E_{\mathrm{c}}/t = -8.12 \pm 0.03$. These values are consistent with our previous fits. The $m = 1$ term $a_1 \chi^{\nu}$ in f corresponds to the conductivity close to the MIT. To estimate the quality of this procedure we calculate the conductivity from the slope of a linear fit to $\langle g_4 \rangle$ throughout the metallic regime, and also from the ratio $\langle g_4 \rangle / L$. The resulting conductivities are shown in Fig. 5.11. The power-law form is in good agreement with the conductivity obtained from the linear fit to $\langle g_4 \rangle = \sigma L + \mathrm{const.}$ for $E \leq -7\,t$. In this range it is also consistent with the ratio of $\langle g_4 \rangle$ and L for the largest system computed ($L = 21$). Deviations occur for energies close to the MIT and for $E > -7\,t$. In the critical regime one can argue that for finite

[1] cf. footnote on page 36

systems the conductance will always be larger than zero in the insulating regime because the localisation length becomes eventually larger than the system size. The difference between the ratio $\langle_4 g\rangle/L$ and σ from the linear fit is probably due to weak localisation. However, this should be investigated further.

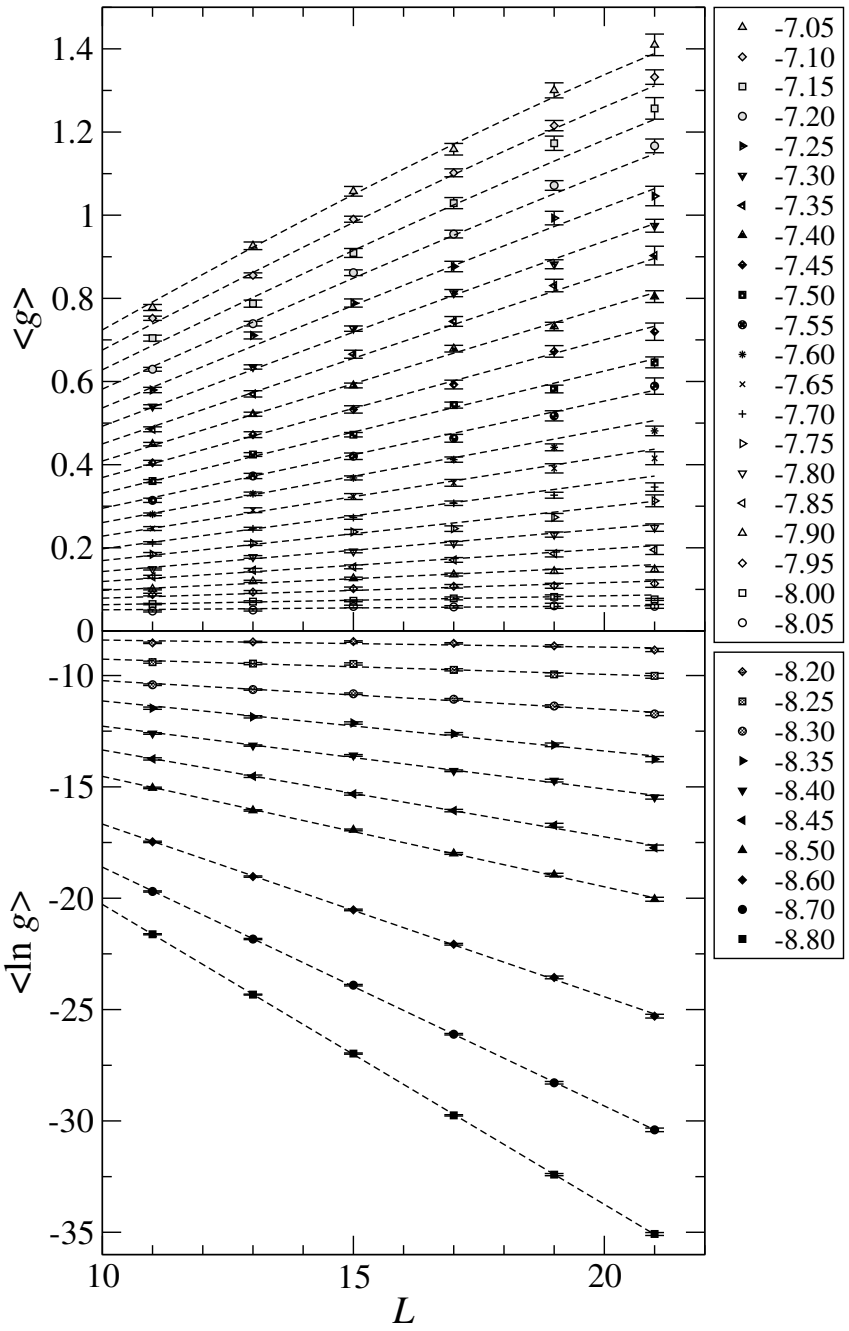

Figure 5.9: System size dependence of the 4-point conductance averages $\langle g_4 \rangle$ and $\langle \ln g_4 \rangle$ for $W = 12t$ and Fermi energies are given in the legend. Error bars obtained from ensemble average. The dashed lines indicate the fit results to Eq. (5.3) and a linear function to $\langle g \rangle$ and $\langle \ln g_4 \rangle$, respectively.

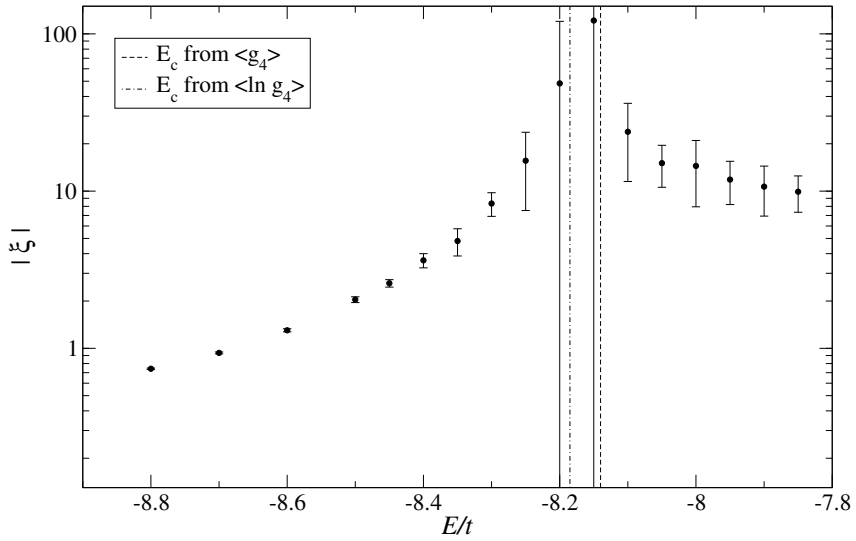

Figure 5.10: Localisation length vs energy obtained from a linear fit to $\langle \ln g_4 \rangle = -L/\xi + \text{const.}$

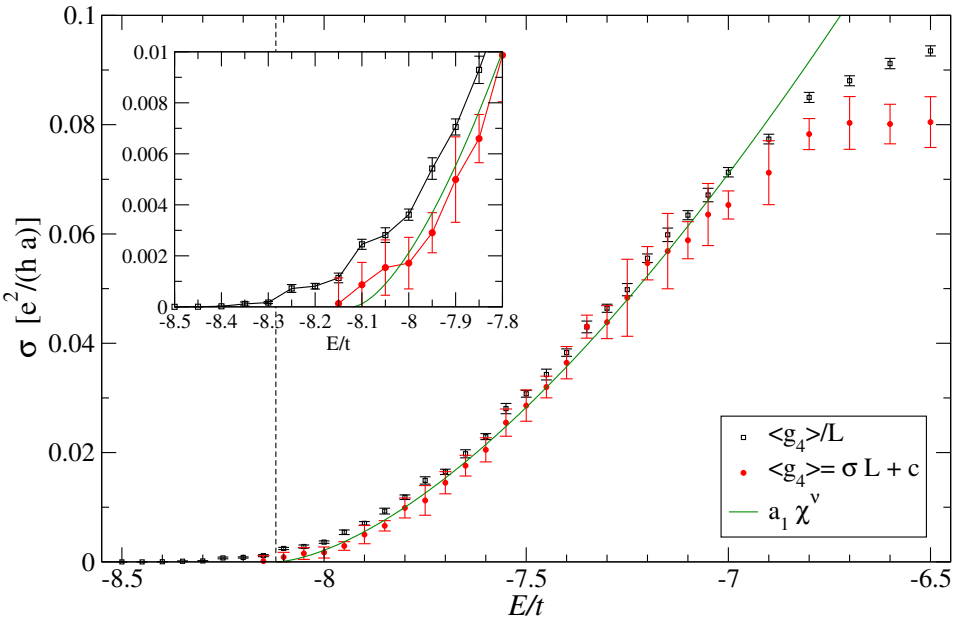

Figure 5.11: Conductivity σ vs energy computed from $\langle g_4 \rangle / L$ ($\square$), a linear fit with $\langle g_4 \rangle = \sigma L + \text{const.}$ ($\bullet$) and a scaling according to Eq. (5.3) (solid line). The dashed line indicates $E_c/t = -8.12$. Error bars of $\langle g_4 \rangle / L$ represent the error-of-mean obtained from an ensemble average.

Chapter 6

Coherent Thermoelectric Transport near the MIT at $T \neq 0$

Knowing the explicit form of the d.c. conductivity, one can calculate the temperature dependence of σ and other thermoelectric quantities within the the CTKG formalism as it was shown in Section 2.3. Using the anticipated power-law (3.28) for the d.c. conductivity in the thermodynamic limit and assuming a smooth density of states it is possible to derive expressions for the thermoelectric quantities at low and high temperatures from perturbative methods [5]. Villagonzalo et al. [5] have used the CTKG formalism and the assumptions made above to calculate the temperature dependence of σ, S, κ and L_0 numerically for a range of $T = 0, \ldots, 120K$. They were also able to show that all thermoelectric quantities follow single-parameter scaling laws, but yielding an unphysical dynamical exponent [4, 11]. Here we will give a brief summary of the main results of these expansions and using the same numerical method we will show the dependence of the thermoelectric transport properties on a *dimensionless* temperature parameter, which allows us to compare the results independently from the unit of energy. This is important for treating thermoelectric transport in amorphous alloys and in doped semiconductors on an equal footing. In the former case $t \approx 1\mathrm{eV}$, whereas for the latter materials $t \approx 1\mathrm{meV}$.

6.1 Low- and High Temperature Expansions

For $T = 0$ the derivative of the Fermi function $(-\partial f/\partial E)$ becomes a Dirac-delta function at $E = E_{\mathrm{F}}$ and the kinetic coefficients are solely determined by their values at the Fermi energy. Upon partial integration the integral in Equation (2.21) can be written in the general form [17]

$$\int_{-\infty}^{\infty} dE\; H(E)\; f(E,\mu,T)\;, \tag{6.1}$$

where f is the Fermi function and $H(E)$ is non-singular and not rapidly varying. For low temperatures the integral will be mainly determined by the form of $H(E)$ near the Fermi energy E_{F} and $H(E)$ can be replaced by its Taylor expansion about $E = E_{\mathrm{F}}$. From this procedure, which is known as the Sommerfeld expansion [17], one can obtain the first non-zero temperature corrections. In order to get results independent of the actual energy unit, e.g. independent of the hopping parameter in the the Anderson model (3.24), we define a dimensionless energy ε and temperature Θ, such that

$$E = \varepsilon t \qquad \text{and} \qquad k_{\mathrm{B}}T = \Theta t\;, \tag{6.2}$$

where t is the unit of energy. In the metallic regime the Sommerfeld expansion for low temperatures, i.e. $\Theta \ll |\varepsilon_{\mathrm{c}} - \varepsilon_{\mathrm{F}}|$, leads to

$$\sigma(\varepsilon_{\mathrm{F}},\Theta) = \sigma(\varepsilon_{\mathrm{F}}) + \frac{\pi^2}{6}\Theta^2\;\frac{d^2\sigma(\varepsilon)}{d\varepsilon^2}\bigg|_{\varepsilon=\varepsilon_{\mathrm{F}}}\;, \tag{6.3}$$

$$S(\varepsilon_{\mathrm{F}},\Theta) = -\frac{k_{\mathrm{B}}}{|e|}\frac{\pi^2\Theta}{3\sigma(\varepsilon_{\mathrm{F}})}\;\frac{d\sigma(\varepsilon)}{d\varepsilon}\bigg|_{\varepsilon=\varepsilon_{\mathrm{F}}}\;, \tag{6.4}$$

$$\kappa(\varepsilon_{\mathrm{F}},\Theta) = \frac{\pi^2 k_{\mathrm{B}}\Theta t}{3e^2}\left\{\sigma(\varepsilon_{\mathrm{F}}) - \frac{\pi^2\Theta^2}{3\sigma(\varepsilon_{\mathrm{F}})}\left[\frac{d\sigma(\varepsilon)}{d\varepsilon}\right]^2_{\varepsilon=\varepsilon_{\mathrm{F}}}\right\}, \tag{6.5}$$

$$L_0(\varepsilon_{\mathrm{F}},\Theta) = \frac{\pi^2}{3}\left\{1 - \frac{\pi^2\Theta^2}{3[\sigma(\varepsilon_{\mathrm{F}})]^2}\left[\frac{d\sigma(\varepsilon)}{d\varepsilon}\right]^2_{\varepsilon=\varepsilon_{\mathrm{F}}}\right\}\;. \tag{6.6}$$

Additionally, from Equations (3.28) and (6.4) one can deduce

$$S(\varepsilon_{\mathrm{F}},\Theta) = -\frac{k_{\mathrm{B}}}{|e|}\frac{\nu\pi^2\Theta}{3(\varepsilon_{\mathrm{F}} - \varepsilon_{\mathrm{c}})}\;. \tag{6.7}$$

This linear temperature dependence of S in the metallic regime is known as *Mott's law*.

On the other hand at high temperatures and close to the MIT, that is $|\varepsilon_{\mathrm{c}} - \mu(T)| \ll \Theta$, one can expand the Fermi function. This finally yields [48]

$$\sigma(\varepsilon_{\mathrm{F}}, \Theta) = \frac{\sigma_0 \nu \Theta^{\nu}}{|\varepsilon_{\mathrm{c}}|^{\nu}} \left[I_{\nu} - (\nu - 1) I_{\nu-1} \frac{\varepsilon_{\mathrm{c}} - \varepsilon_{\mathrm{F}}}{\Theta} \right] , \tag{6.8}$$

where $I_1 = \ln\ 2$, $I_{\nu} = (1 - 2^{1-\nu})\Gamma(\nu)\zeta(\nu)$ with $\Gamma(\nu)$ and $\zeta(\nu)$ the usual Gamma and Riemann zeta functions. Using the same procedure for the thermopower one gets

$$S(\varepsilon_{\mathrm{F}}, \Theta) = -\frac{k_{\mathrm{B}}}{|e|} \left[\frac{\nu + 1}{\nu} \frac{I_{\nu+1}}{I_{\nu}} + \frac{\varepsilon_{\mathrm{c}} - \varepsilon_{\mathrm{F}}}{\Theta} \right] . \tag{6.9}$$

Thus the thermopower at the MIT is basically a constant, whose value is fixed by the critical exponent.

The high temperature expansions for κ and L_0 eventually lead to the following expressions,

$$\kappa(\varepsilon_{\mathrm{F}}, \Theta) = \frac{k_{\mathrm{B}} \sigma_0 t}{e^2} \frac{\Theta^{\nu+1}}{|\varepsilon_{\mathrm{c}}|^{\nu}} \left\{ (\nu + 2) \left[I_{\nu+2} - (\nu + 1) I_{\nu+1} \frac{\varepsilon_{\mathrm{c}} - \varepsilon_{\mathrm{F}}}{\Theta} \right] - \frac{(\nu + 1)^2}{\nu} \frac{\left[I_{\nu+1} - \nu I_{\nu+1} \frac{\varepsilon_{\mathrm{c}} - \varepsilon_{\mathrm{F}}}{\Theta} \right]^2}{I_{\nu} - (\nu - 1) I_{\nu-1}} \frac{\varepsilon_{\mathrm{c}} - \varepsilon_{\mathrm{F}}}{\Theta} \right\} , \tag{6.10}$$

$$L_0(\varepsilon_{\mathrm{F}}, \Theta) = \frac{\nu + 2}{\nu} \frac{I_{\nu+2} - (\nu + 1) I_{\nu+1} \frac{\varepsilon_{\mathrm{c}} - \varepsilon_{\mathrm{F}}}{\Theta}}{I_{\nu} - (\nu - 1) I_{\nu-1} \frac{\varepsilon_{\mathrm{c}} - \varepsilon_{\mathrm{F}}}{\Theta}} - \left[\frac{\nu + 1}{\nu} \frac{I_{\nu+1} - \nu I_{\nu} \frac{\varepsilon_{\mathrm{c}} - \varepsilon_{\mathrm{F}}}{\Theta}}{I_{\nu} - (\nu - 1) I_{\nu-1} \frac{\varepsilon_{\mathrm{c}} - \varepsilon_{\mathrm{F}}}{\Theta}} \right]^2 . \tag{6.11}$$

At the MIT the high temperature expansions for σ, S, κ and L_0 correspond to exact calculations fixing $\mu(\Theta) = \varepsilon_{\mathrm{c}}$ at finite Θ and then taking the limit $\Theta \to 0$ [4].

6.2 Numerical Calculations

In Section 5.3.3 it was shown that the numerical results for the conductivity near the MIT are consistent with the power-law form given by Equation (3.28). We have also

seen that the DOS exhibits a smooth dependence on the energy. For the pure power-law case Villagonzalo et al. [5] have used the CTKG formalism to numerically compute the kinetic coefficients and thus the thermoelectric properties for the whole temperature range. They found good agreement of the numerical data and the expansions in the respective low and high temperature regimes. From Fig. 5.11 one expects qualitatively the same behaviour using the conductivity obtained from the conductance calculations. There are two complications, first, the conductance shows large fluctuations close to the MIT, which makes it difficult to evaluate the integral in Equation (2.21). And second, if the numerical results are interpolated using for example cubic splines, the temperature behaviour of the thermoelectric properties in the limit $T \to 0$ will not be determined by the critical exponent ν but by the order of the interpolation polynomial, e.g. $\nu \approx 3$ in case of a cubic spline.

The first problem might be overcome by calculating more samples, which is, however, computationally expensive and therefore out of the scope of this work. Consequently, we restrict our discussion of the influence of deviations from the power-law behaviour to the high-temperature regime. In this case we can use the obtained power-law (cf. 5.3.3) for energies close to the MIT ($E/t \leq -7.8$). Otherwise we interpolate σ obtained from the numerical data using a polynomial of order 3.

6.2.1 Thermoelectric Properties Near the Anderson MIT Assuming a Power-law Form for $\sigma(E)$

At first we calculate the temperature behaviour of the thermoelectric properties assuming a pure power-law form for the d.c. conductivity. We use $W = 12\,t$ and the following values for the critical exponent and the mobility edge,

$$\nu = 1.6 \qquad \text{and} \qquad E_\mathrm{c} = -7.8\,t\ .$$

Chemical Potential

In order to evaluate the integral in Equation (2.21) the explicit temperature dependence of the chemical potential μ is needed. It can be determined self-consistently from the following considerations. The number density for non-interacting system can be calculated from the density of states $\rho(E)$ using

$$n(\mu, \Theta) = \int_{-\infty}^{\infty} \rho(\varepsilon)\, f(\varepsilon, \mu, \Theta)\; t\; d\varepsilon \; . \tag{6.12}$$

This allows us to compute $n(\varepsilon_{\mathrm{F}})$ for $\mu(\Theta = 0) = \varepsilon_{\mathrm{F}}$ via

$$n(\varepsilon_{\mathrm{F}}) = \int_{-\infty}^{\varepsilon_{\mathrm{F}}} \rho(\varepsilon)\; t\; d\varepsilon \; . \tag{6.13}$$

Since the number density should be the same for any Θ, the temperature dependence of μ can be obtained from the condition $|n(\varepsilon_{\mathrm{F}}, 0) - n(\mu, \Theta)| = 0$.

For the calculations in this section the density of states $\rho(\varepsilon)$ was obtained from diagonalising the Anderson Hamiltonian (3.24) for a 3D cubic system of size $L = 21$ (cf. Section 5.3.1). The obtained DOS was then smoothed by fitting the data to a Bezier-spline. The resulting temperature behaviour of μ is shown in Fig. 6.1 for several Fermi energies. The temperature behaviour is similar for insulating, critical and metallic regimes. Furthermore, the difference from E_{F} is small in the considered temperature range. Therefore, the temperature dependence of μ is not expected to have a significant influence on the behaviour of the thermoelectric properties.

Temperature Dependence of Thermoelectric Properties

Knowing the explicit temperature dependence of μ it is straightforward to evaluate Equation (2.21) and to calculate the thermoelectric properties. The results for σ, S, κ and L_0 are shown together with the respective expansions in Figures 6.2-6.5. We see that the expansions are in good agreement with the numerical calculations for E_{F} close to

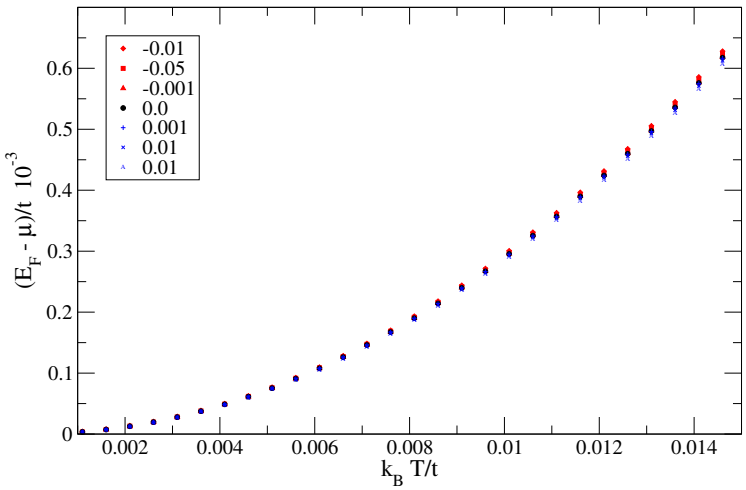

Figure 6.1: The temperature dependence of the chemical potential for several Fermi energies. The distance from the mobility edge $E_{\mathrm{F}} - E_{\mathrm{c}}$ is given in the legend.

E_{c}. The explicit temperature behaviour for all thermoelectric properties is discussed in detail in Ref. [48].

6.2.2 Thermoelectric Properties in the High Temperature Limit

The deviation of σ from the power-law form for energies with $E_{\mathrm{F}} - E_{\mathrm{c}} > 0.3\,t$ does not significantly influence the high temperature behaviour of the thermoelectric properties. This is demonstrated in Fig. 6.6. We show the results for the thermopower together with the low- and high-temperature expansions (6.4) and (6.9), respectively. Deviations from the pure power-law result accumulate above $k_{\mathrm{B}}T/t \approx 0.5$. At this temperature the integrand in Equation (2.21) has already a significant contribution from the pure numerical data. Nevertheless, the deviations of S from the expansions are small even for higher temperatures. This indicates a certain robustness of the results using a pure power-law.

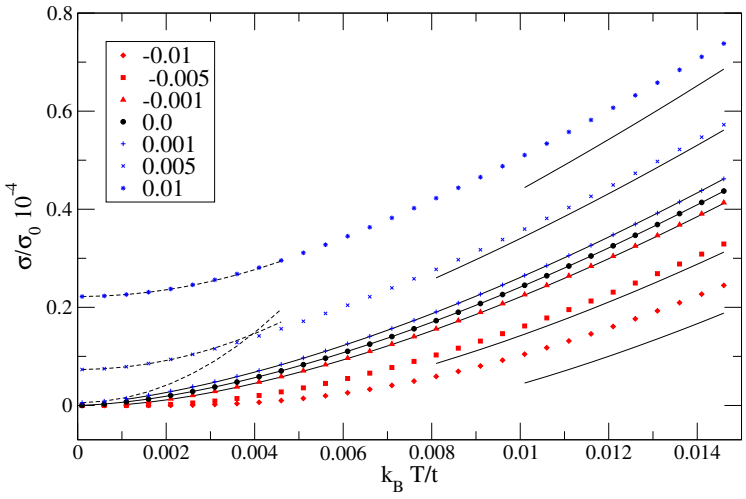

Figure 6.2: The temperature dependence of the d.c. conductivity. Blue symbols indicate *metallic*, black symbols *critical* and red symbols *insulating* behaviour. The distance from the mobility edge $E_{\rm F} - E_{\rm c}$ is given in the legend. Full lines are obtained from a high-temperature expansion (6.8). The dashed lines indicate $\sigma(T)$ using the Sommerfeld expansion (6.3).

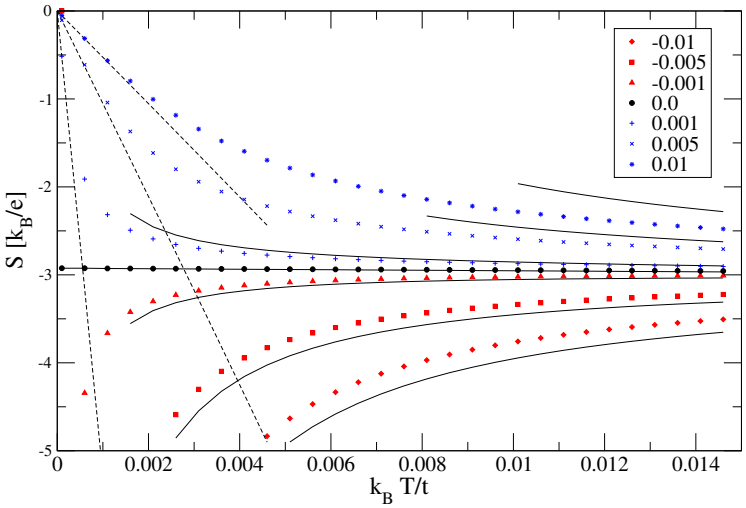

Figure 6.3: The temperature dependence of the thermopower. Blue symbols indicate *metallic*, black symbols *critical* and red symbols *insulating* behaviour. The distance from the mobility edge $E_{\rm F} - E_{\rm c}$ is given in the legend. Full lines are obtained from a high-temperature expansion (6.9). The dashed lines indicate $S(T)$ using the Sommerfeld expansion (6.4).

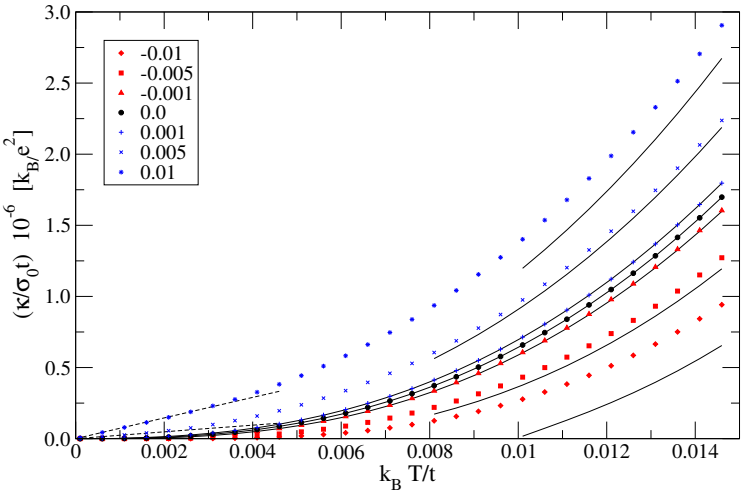

Figure 6.4: The temperature dependence of the thermal conductivity. Blue symbols indicate *metallic*, black symbols *critical* and red symbols *insulating* behaviour. The distance from the mobility edge $E_{\mathrm{F}} - E_{\mathrm{c}}$ is given in the legend. Full lines are obtained from a high-temperature expansion (6.10). The dashed lines indicate $\kappa(T)$ using the Sommerfeld expansion (6.5).

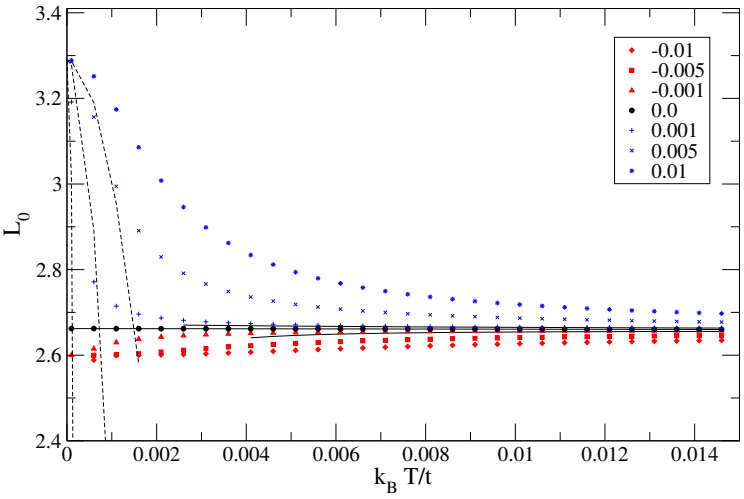

Figure 6.5: The temperature dependence of the Lorenz number. Blue symbols indicate *metallic*, black symbols *critical* and red symbols *insulating* behaviour. The distance from the mobility edge $E_{\mathrm{F}} - E_{\mathrm{c}}$ is given in the legend. Full lines are obtained from a high-temperature expansion (6.11). The dashed lines indicate $L_0(T)$ using the Sommerfeld expansion (6.6).

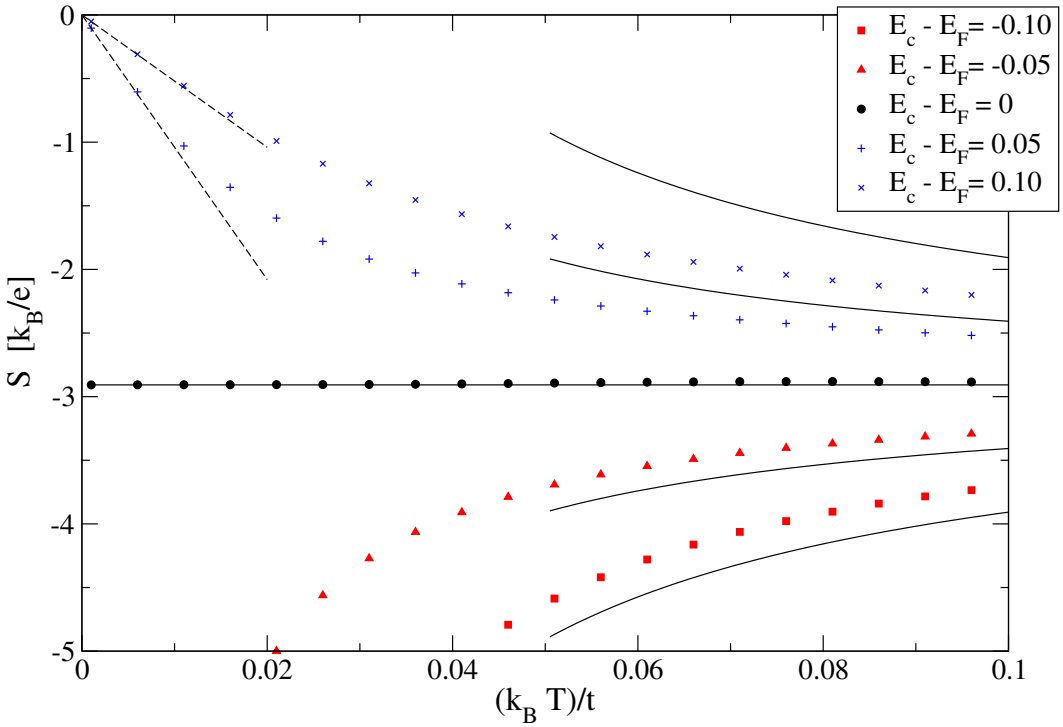

Figure 6.6: Thermopower S vs a dimensionless temperature parameter $k_{\mathrm{B}}T/t$. Blue symbols indicate *metallic*, black symbols *critical* and red symbols *insulating* behaviour. The distance from E_{c} is given in the legend. Full lines are obtained from a high-temperature expansion (6.9). The dashed lines indicate S using the Sommerfeld expansion (6.4). In both cases average values of ν and E_{c} from Table 5.2 were used.

Chapter 7

Incoherent Transport

It was shown in Section 3.1.1 that completely phase-coherent transport is only possible if the phase-relaxation length ℓ_Φ is larger than the system size L. Otherwise, if $\ell_\Phi \leq L$ the physics is governed by the interplay of localisation and dephasing. In this chapter we show how inelastic scattering can be introduced to the Landauer-Büttiker formalism, which allows to study incoherent transport. We also investigate if the same approach can be used to understand if the parameter γ in the Kubo formalism can be related to inelastic scattering.

7.1 Dissipation and Coupling to an Environment

A complete microscopic description of inelastic scattering is in general complicated to obtain, because scattering processes like electron-electron and electron-phonon interactions have to be considered explicitly. A different and rather general description is based on coupling the system to a reservoir with other degrees of freedom [29]. If one thinks of the system as being coupled to the reservoir through some leads, then the coupling can be characterised by a self-energy Σ^+ (cf. Section 4.3), which is in general not hermitian [28]. The eigenvalues of the effective Hamiltonian $\mathcal{H}_{\rm eff} = \mathcal{H} + \Sigma^+$ are therefore

complex,

$$\varepsilon'_\alpha = \varepsilon_\alpha - \triangle_\alpha - (\imath\frac{\gamma_\alpha}{2}) \; . \tag{7.1}$$

Here ε_α is the eigenvalue of the Hamiltonian $\mathcal{H}$, $\triangle_\alpha$ and γ_α are induced by the self-energy. The time dependence of the eigenstate associated with ε_α is then given by

$$\Psi_\alpha \propto \exp\left[-\imath(\varepsilon_\alpha - \triangle_\alpha)t/\hbar\right] \exp\left[-\gamma_\alpha t/\hbar\right] \; . \tag{7.2}$$

The average time (or lifetime) an electron remains in the state Ψ_α is connected to the imaginary part of the eigenenergy γ_α, which in turn is just the rate at which electrons can escape from the system [28]. In this sense the coupling of the system to an environment leads to dissipation, but notice that the nature of the dissipation mechanism does not enter these general considerations at all, so this has to be included separately, e.g. through a proper modelling of the reservoirs.

7.2 Incoherent Transport in 1D Chains

Starting with the setup given by Landauer, Büttiker [14] found that any additional lead coupled to the sample and connected to an electron reservoir can describe an inelastic scatterer. In his proposal the electron reservoir will absorb any injected electron and immediately emit a *new* electron with a random phase. This process yields a well defined phase-relaxation length.

7.2.1 Landauer-Büttiker Formalism

D'Amato and Pastawski [15] incorporated inelastic scattering into the Landauer formalism using the proposal of Büttiker. In their model, which is shown in Fig. 7.1, they chose the on-site energies E_l in the additional leads to coincide with the Fermi energy of the system and the hopping parameter for hopping from the sites into the leads to be γ. In this case attaching the leads is equivalent to adding an imaginary potential $-\imath\gamma$ to each on-site energy [15]. Additionally, a condition of current conservation has to be satisfied

in order to guarantee that no extra electrons are destroyed or created in the electron reservoirs [14, 15]. An inelastic scattering time τ_{in} can then be related to the "escape rate" γ such that $\tau_{in} = \hbar/(2\gamma)$ [15, 28]. Following Ref. [15] the current I_i through lead

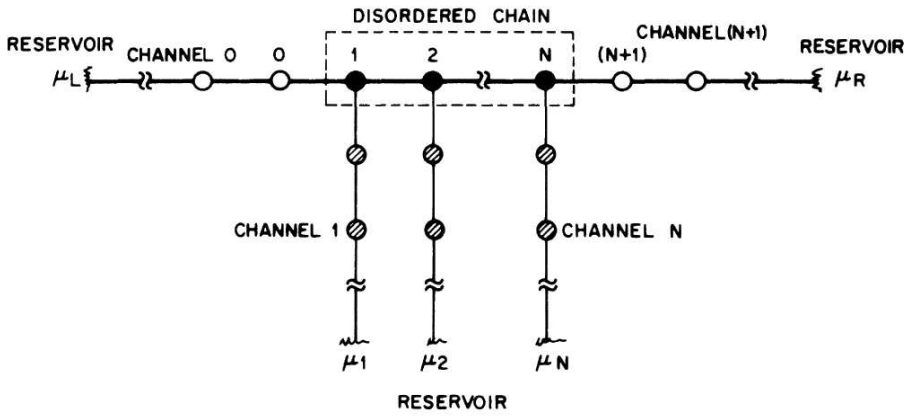

Figure 7.1: Illustration of the model proposed by D'Amato et al. [15].

i is given in terms of the (local) chemical potentials μ_i and the transmission probability T_{ij} from lead j to i,

$$I_i = \sum_{j=0}^{N+1} (\mu_j - \mu_i) T_{ij} \; . \tag{7.3}$$

If there is no net current flowing at each lead to the reservoirs the current through the sample is given by

$$I_R = \sum_{j=0}^{N+1} (\mu_j - \mu_R) T_{Rj} = (\mu_L - \mu_R) T_{RL} + \sum_{j=1}^{N} (\mu_j - \mu_R) T_{Rj} \; . \tag{7.4}$$

The chemical potentials μ_i are fixed by the condition of no net current, which can be derived from Equation (7.3) [15],

$$(1 - R_{ii})(\mu_i - \mu_R) - \sum_{\substack{j=1 \\ (j \neq i)}}^{N} (\mu_j - \mu_i) T_{ij} - (\mu_L - \mu_R) T_{iL} = 0 \quad \forall i = 1, 2, \ldots, N \; . \tag{7.5}$$

The reflection coefficients R_{ii} are given by current conservation,

$$R_{ii} = 1 - \sum_{\substack{j=0 \\ (j \neq i)}}^{N+1} T_{ji} \, . \tag{7.6}$$

This leads to an expression for determining μ_i

$$\mu_i - \mu_R = \left(\sum_{\substack{j=1 \\ (j \neq i)}}^{N} W_{ij}^{-1} \, T_{j\,L} \right) (\mu_L - \mu_R) \quad \forall i = 1, 2, \ldots, N \, , \tag{7.7}$$

with

$$W_{ij} = \begin{cases} 1 - R_{ii} & , i = j \\ -T_{ij} & , i \neq j \end{cases} \, . \tag{7.8}$$

The transmission probabilities can be related to the retarded Green's function $\mathcal{G}^+(E)$,

$$\begin{aligned} T_{R\,L} &= v_x^2 |G^+_{R\,L}|^2 \, , \\ T_{i\,L} &= 2\gamma v_x |G^+_{i\,L}|^2 \, , \quad T_{Ri} = 2\gamma v_x |G^+_{Ri}|^2 \, , \\ T_{ij} &= 4\gamma^2 |G^+_{ij}|^2 \quad \forall i = 1, 2, \ldots, N \, , \end{aligned} \tag{7.9}$$

where $v_x = \partial E(k)/\partial k = 2t \sin(ka)$ is proportional to the Fermi energy $v_F = v_x a/\hbar$. In analogy to the Landauer formula (4.2), the two-terminal conductance can be expressed in terms of the transmission probabilities,

$$\mathfrak{g}_2 = \frac{2e^2}{h} g_2 = \frac{2e^2}{h} \left(T_{R\,L} + \sum_{i,j=1}^{N} T_{Ri} W_{ij}^{-1} T_{j\,L} \right) \, . \tag{7.10}$$

This implies that the effective transmission probability consists of the probability of coherent tunnelling and of probabilities including phase randomisations at the lateral reservoirs. Finally, the four-terminal conductance can be obtained from Equation (4.1),

$$\mathfrak{g}_4 = \frac{2e^2}{h} g_4 = \frac{2e^2}{h} \frac{g_2}{1 - g_2} \, . \tag{7.11}$$

For an ordered chain an expression for the 4-terminal conductance $\mathfrak{g}_4$ in terms of the inelastic scattering length [1] $L_{\mathrm{in}} = a v_x/\gamma$ can be calculated analytically up to corrections

[1] As it is at this stage not known if this length is equal to the phase-relaxation length ℓ_Φ, we will denote the inelastic scattering length with L_{in}.

of order $a/L_{\rm in}$ [15],

$$\mathfrak{g}_4 = \frac{2e^2}{h}\frac{2L_{\rm in}}{L} = \frac{2e^2}{h}\frac{a}{L}\frac{v_x}{\gamma} \ . \tag{7.12}$$

This is the Drude formula for ballistic transport ($\ell \gg L$) and $L_{\rm in} < L$.

It is a priori not clear whether the choice of a site independent γ is physically plausible as the hopping rate of particles scattered into the reservoir should depend on the available and the free states both at one site and in the reservoir. This has been taken into account in Refs. [49,50], where the reservoirs were heat baths of independent harmonic oscillators and a site specific scattering time τ_j was calculated.

7.2.2 Kubo Formalism and RGFM

In Section 7.1 it was shown that the imaginary part of the complex energy γ plays the role of an inverse lifetime due to inelastic scattering. The expression (4.12) for the Kubo conductance, however, was derived assuming coherent transport only. In this case the wave function extends over the whole sample and the current density is constant. Therefore, one can spatially average the non-local conductivity $\sigma(\mathbf{r},\mathbf{r}')$ to get the macroscopic conductivity σ, which relates the spatially averaged current to the spatially averaged field [29].

In the following we consider a 1D chain consisting of $N+1$ sites and a length $L = Na$ with a being the lattice spacing. Explicitly including the self-energy of the additional leads we have in terms of the position operator (cf. Appendix A)

$$\sigma = -\frac{e^2 8}{hL}\mathrm{Tr}\left\{\mathrm{x}\,(\mathrm{Im}\,\mathrm{Z}^+)\,\mathrm{G}^-\mathrm{x}\,(\mathrm{Im}\,\mathrm{Z}^+)\,\mathrm{G}^+ + \frac{\imath}{2}\mathrm{x}\left[(\mathrm{Im}\,\mathrm{Z}^+)\,\mathrm{G}^- - (\mathrm{Im}\,\mathrm{Z}^+)\,\mathrm{G}^+\right]\mathrm{x}\right\} \tag{7.13}$$

with $Z^+ = (E+\imath\gamma)\mathbb{1} - \Sigma^+$. The self-energy Σ^+ due to the leads at both ends is given by [15]

$$\Sigma^+ = \left(\frac{E}{2} - \imath\frac{v_x}{2}\right)\left(|1\rangle\langle 1| + |N\rangle\langle N|\right) \ , \tag{7.14}$$

whereas the self-energy due to the additional leads gives just the imaginary part of the

complex energy [15]. The trace in (7.13) can be evaluated in a position basis to yield

$$\sigma = -\frac{e^2 4}{hL} \left\{ \sum_{\substack{i,j=0 \\ (i<j)}}^{N+1} (x_i - x_j)^2 \, (\gamma - \mathrm{Im}\,\Sigma^+)_{\mathrm{i\,i}} \, \mathrm{G}^-_{\mathrm{i\,j}} \, (\gamma - \mathrm{Im}\,\Sigma^+)_{\mathrm{j\,j}} \, \mathrm{G}^+_{\mathrm{j\,i}} \right\} . \tag{7.15}$$

Using (7.9) one can rewrite the last equation in terms of transmission probabilities

$$\begin{aligned} \sigma = -\frac{e^2}{hL} \Bigg\{ & \sum_{\substack{i,j=1 \\ (i<j)}}^{N} (x_i - x_j)^2 \, T_{i\,j} + (x_{N+1} - x_1)^2 \, T_{R\,L} \\ & + \sum_{i=1}^{N} (x_i - x_1)^2 \, T_{i\,L} + \sum_{i=1}^{N} (x_{N+1} - x_i)^2 \, T_{R\,i} \Bigg\} . \end{aligned} \tag{7.16}$$

Assuming a constant electric field $\mathcal{E}$ over the whole sample,

$$\mathcal{E} = \frac{U}{L} = \frac{\mu_L - \mu_R}{x_{N+1} - x_1} = \frac{\mu_i - \mu_j}{x_i - x_j} , \tag{7.17}$$

one can substitute $(x_i - x_j)$ by

$$x_i - x_j = \frac{\mu_i - \mu_j}{\mathcal{E}} . \tag{7.18}$$

In order to get the current through the sample, we have to multiply Equation (7.16) with the electric field $\mathcal{E}$ and after making the substitution (7.18) we obtain

$$\begin{aligned} I = \sigma\mathcal{E} = \frac{e^2}{hL} \Bigg\{ & \sum_{\substack{i,j=1 \\ (i<j)}}^{N} (x_j - x_i)(\mu_i - \mu_j) \, T_{j\,i} + (x_{N+1} - x_1)(\mu_L - \mu_R) \, T_{R\,L} \\ & + \sum_{i=1}^{N} (x_i - x_0)(\mu_L - \mu_i) \, T_{i\,L} + \sum_{i=1}^{N} (x_{N+1} - x_i)(\mu_i - \mu_R) \, T_{R\,i} \Bigg\} . \end{aligned} \tag{7.19}$$

Here, $I_{ji} = (\mu_i - \mu_j) \, T_{j\,i}$ is the current flowing from the reservoir at site i to the one at site j. The factor $(x_j - x_i) = (j - i)a$ is proportional to the number of "planes" between site i and j. The expression for I can therefore be interpreted as an average over all currents flowing in the sample. Notice that in the case of a completely coherent transport, when the current is flowing from the left to the right reservoir only ($\gamma = 0$), Equation (7.19) yields the same current as the Landauer formula.

7.2.3 Results for an Ordered Chain

To further investigate the differences between the "incoherent" Landauer-Büttiker formalism and the RGFM we numerically calculate as a start the 2- and 4-terminal conductance of a small ($L = 30$) one-dimensional system without any disorder. We also compute the length dependence of $\mathfrak{g}_4$ for different values of γ. In Fig. 7.2 the energy dependence of the 2-terminal conductance is shown for $\gamma = 0.001, 0.01$ and 0.5. The RGFM results are seen to be larger for all energies in the band and all values of γ. The 4-terminal conductance calculated by Equation (7.11) is shown in Fig. 7.3. Here, the RGFM data is also larger than the Landauer-Büttiker data.

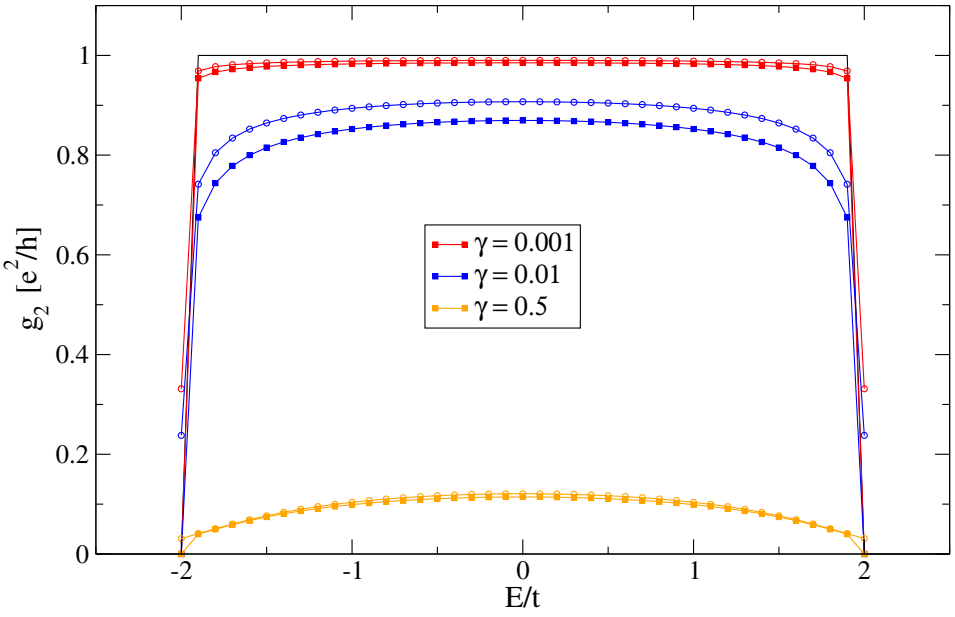

Figure 7.2: Two-terminal conductance $\mathfrak{g}_2$ vs energy computed from the Landauer-Büttiker formalism (filled symbols) and the RGFM (open symbols). The values of γ used are indicated in the legend.

From Equation (7.12) one expects that the dimensionless 4-terminal conductance $\mathfrak{g}_4$ is proportional to $1/\gamma$ with the constant of proportionality being v_x/L. In Fig. 7.4

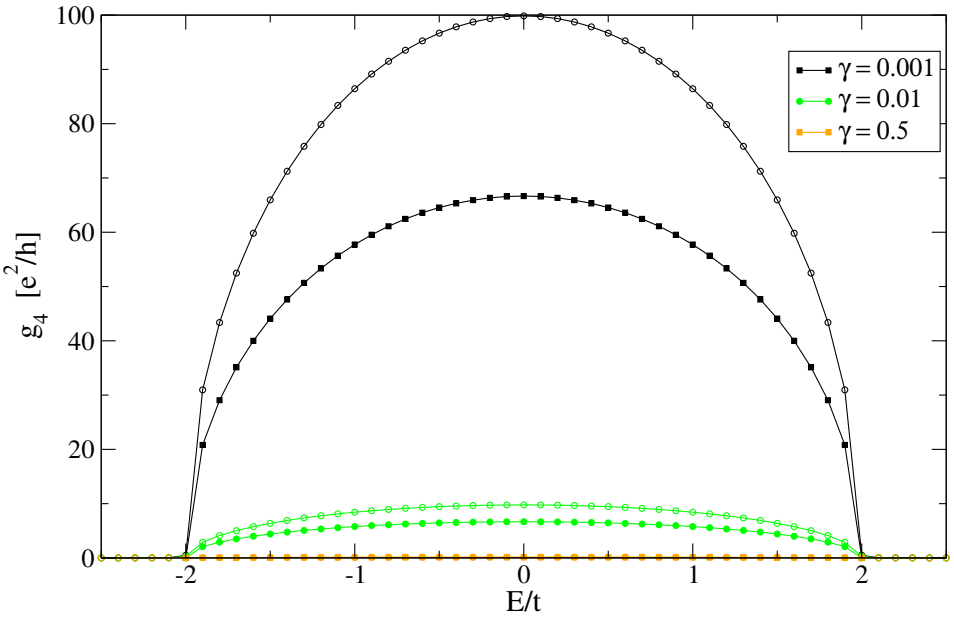

Figure 7.3: Four-terminal conductance $\mathfrak{g}_4$ vs energy obtained from Eq. (7.11). Filled symbols indicate Landauer-Büttiker calculations and open symbols denote RGFM results. The values of γ used are shown in the legend.

we show $\mathfrak{g}_4$ vs $1/\gamma$ calculated from both methods at $E = 0$. One can see that the Landauer-Büttiker results show the expected linear behaviour with the right slope, which is $2/L$ for the band centre. The RGFM results also show a linear dependence on $1/\gamma$ but with a slope larger than v_x/L.

Also the length dependence of $\mathfrak{g}_4$ calculated with the RGFM shows deviations from Equation (7.12) as it can be seen in Fig. 7.5. Especially for small systems the RGFM data show a strong system size dependence, whereas the Landauer-Büttiker results are constant for all L. Notice that for larger γ the Landauer-Büttiker calculation also yields a deviation from Equation (7.12), because then a/L_{in} is not a small parameter and corrections to the first order result (7.12) have to be included.

The comparison of the RGFM and the Landauer-Büttiker method in the case of incoherent transport showed that both methods are not yielding the same results. From

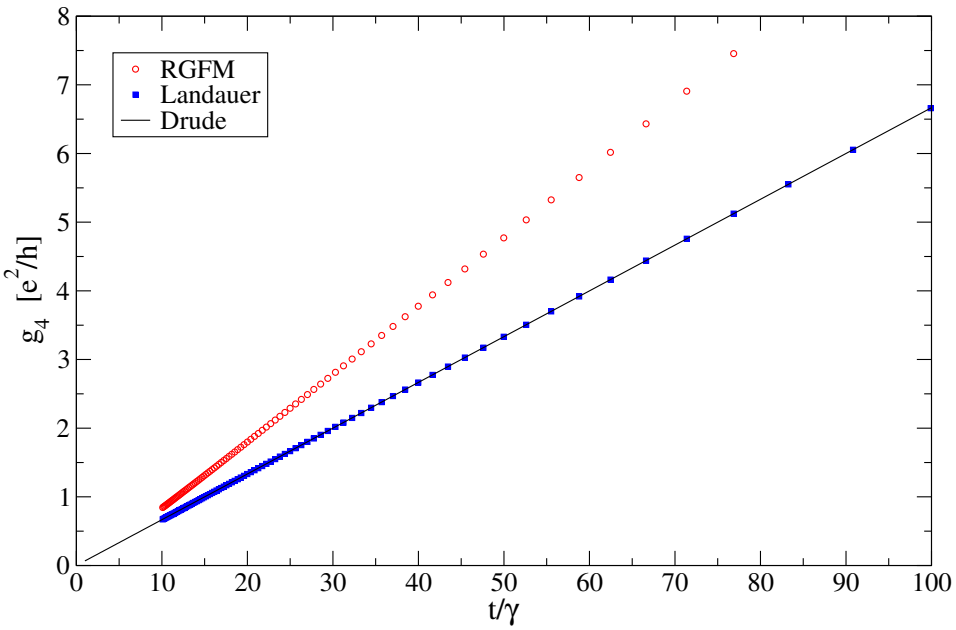

Figure 7.4: Four-terminal conductance g_4 vs $1/\gamma$ at $E = 0$ and $L = 30$. Blue squares indicate Landauer-Büttiker data and red circles denote RGFM results. The full line represents Eq. (7.12) with $v_x(E = 0) = 2$.

our analysis it is, however, difficult to identify the origin of the differences and to see how they have to be interpreted. The modified Landauer-Büttiker formalism provides a clear physical picture in terms of additional electron reservoirs coupled to heat baths. In contrast, in the Kubo formalism it is hard to justify the ad hoc introduction of the additional leads, because this eventually leads to an additional electric field, which is not accounted for in the formalism.

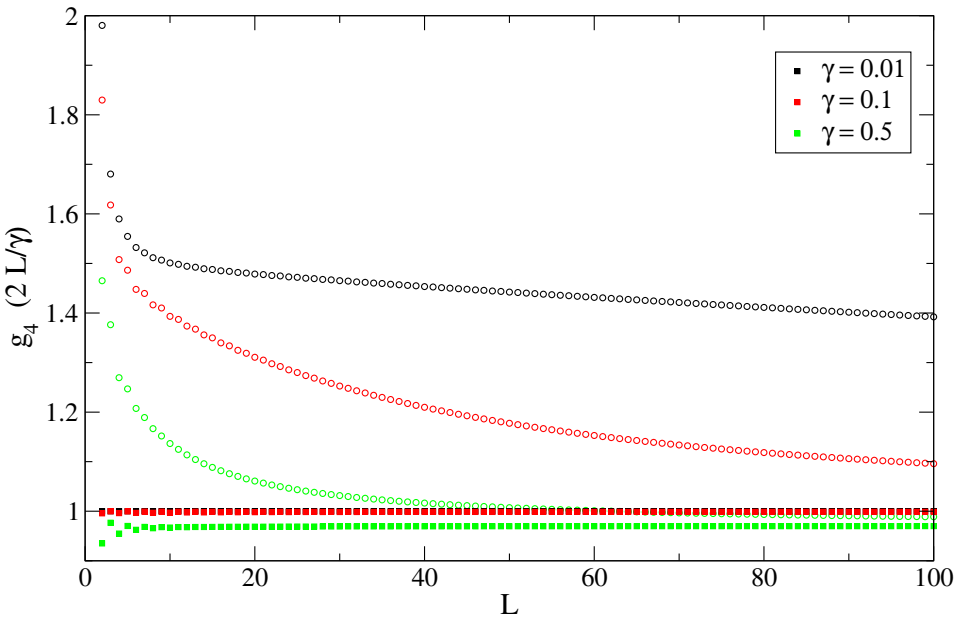

Figure 7.5: Four-terminal conductance $\mathfrak{g}_4$ vs length L of the system. The values of γ used are shown in the legend.

Chapter 8

Summary and Outlook

This thesis deals with thermoelectric transport in disordered systems. In particular, we investigated whether the scaling assumptions made in previous studies [5, 11] can be supported by numerical calculations. Therefore, we computed electronic properties at $T = 0$, namely the conductance and the density of states, of 3D disordered systems within the Anderson model of localisation. These properties were obtained from the recursive Green's function method in which semi-infinite metallic leads at both ends of the system were taken into account. In order to study the influence of dephasing on the electronic properties, we compared results for the conductance of a 1D clean system in the case of incoherent transport using the recursive Green's function method with an approach based on the Landauer-Büttiker formalism.

The basic definitions of the thermoelectric transport properties, electric and thermal conductivity, thermopower and Lorenz number, were given in Chapter 2. It was shown how they can be expressed in terms of the kinetic coefficients, which in turn can be obtained from the Chester-Thellung-Kubo-Greenwood formalism knowing the explicit energy dependence of the d.c. conductivity at $T = 0$. Additionally, some technological applications utilising thermoelectric effects were mentioned.

In Chapter 3 we gave an introduction to the key concepts of mesoscopic physics. We introduced the Anderson model of localisation, which is the basis for our investigations of disordered systems. We explained the occurrence of the Anderson metal-insulator transition in 3D systems using the one-parameter scaling theory and discussed some consequences of this hypothesis.

The recursive Green's function method which we used to calculate the conductance of disordered systems was introduced in Chapter 4. We gave the basic recursion formulae for computing the conductance, the density of states and the localisation length. We showed how semi-infinite leads can be incorporated into the formalism using the concept of self-energy. Finally, we explained the idea of finite size scaling.

In Chapter 5 we demonstrated how the difference in the density of states between the disordered region and the metallic leads has a significant influence on the results for the electronic properties at energies outside the band centre. This poses a big problem for the investigation of the energy transition. We showed that by shifting the energy levels in the disordered region the mismatch can be reduced. In this case the average conductance and the typical conductance were found to be consistent with the one-parameter scaling theory at the energy transition. Using finite size scaling analysis of the system size and energy dependence of both conductance averages we obtained an average critical exponent $\nu = 1.59 \pm 0.18$, which is in accordance with results for conductance scaling at $E/t = 0.5$ and transfer-matrix calculations [8, 9]. However, a thorough investigation of the influence of the leads is still lacking. It would also be interesting to see if these effects can be related to studies of 1D multichannel systems with impurities [51].

We calculated the d.c. conductivity from the system size dependence of the average conductance and found it consistent with a power-law form at the MIT. This strongly supports previous analytical and numerical calculations of thermoelectric properties reviewed in Chapter 6.

Finally, in Chapter 7 we investigated the case of incoherent transport. Therefore, we used an approach based on the Landauer-Büttiker formalism with additional electron reservoirs coupled to the system. We compared numerical results of the conductance of a 1D clean wire to calculations obtained from the Kubo formula for the same setup. It turned out that both methods are not equivalent. Whether they describe completely different physical situations or refer to different regimes of the same process is still to be shown. Further investigation of this question would not only be valuable for the calculation of incoherent transport, but also for a deeper understanding of the relationship between the Landauer-Büttiker formalism and the Kubo formula.

In summary, we found that the one-parameter scaling theory at the energy transition can be supported by numerical calculations. Our results are therefore promising with regard to a fully numerical calculation of thermoelectric properties of disordered systems without making further assumptions.

Appendix A

Kubo-Conductivity in Position Basis

Some definitions and useful relations:

$$\left(z^{\pm}\mathbb{1} - \mathcal{H} - \Sigma^{\pm}\right)\mathcal{G}^{\pm} \equiv \left(Z^{\pm} - \mathcal{H}\right)\mathcal{G}^{\pm} = \mathbb{1} \tag{A.1}$$

This leads to

$$\mathcal{H}\mathcal{G}^{\pm} = Z^{\pm}\mathcal{G}^{\pm} - \mathbb{1} \quad \text{and} \quad \mathcal{G}^{\pm}\mathcal{H} = \mathcal{G}^{\pm}Z^{\pm} - \mathbb{1} \tag{A.2}$$

$$\mathrm{Im}\,\mathcal{G}^{+} = -\mathrm{Im}\,\mathrm{Z}^{+}\;\mathcal{G}^{+}\mathcal{G}^{-} = \frac{1}{2\imath}(\mathcal{G}^{+} - \mathcal{G}^{-}) \tag{A.3}$$

The d.c. conductivity in the linear response regime is given by the Kubo formula (4.12)

$$\sigma = \frac{2e^2\hbar}{\pi L m^2}\mathrm{Tr}\,\left[\mathrm{p}\,\mathrm{Im}\,\mathcal{G}^{+}\,\mathrm{p}\,\mathrm{Im}\,\mathcal{G}^{+}\right] \tag{A.4}$$

$$= -\frac{2e^2\hbar}{4\pi L m^2}\mathrm{Tr}\,\left[\mathrm{p}\,(\mathcal{G}^{+} - \mathcal{G}^{-})\,\mathrm{p}\,(\mathcal{G}^{+} - \mathcal{G}^{-})\right]$$

$$= -\frac{2e^2\hbar}{4\pi L m^2}\mathrm{Tr}\,\left[\mathrm{p}\,\mathcal{G}^{+}\,\mathrm{p}\,\mathcal{G}^{+} + \mathrm{p}\,\mathcal{G}^{-}\,\mathrm{p}\,\mathcal{G}^{-} - \mathrm{p}\,\mathcal{G}^{-}\,\mathrm{p}\,\mathcal{G}^{+} - \mathrm{p}\,\mathcal{G}^{+}\,\mathrm{p}\,\mathcal{G}^{-}\right] \tag{A.5}$$

Using $p = \frac{m}{\hbar}\imath[\mathcal{H}, x]$ yields

$$\mathrm{Tr}\,\mathrm{p}\,\mathcal{G}^{\pm}\,\mathrm{p}\,\mathcal{G}^{\pm} = -\frac{m^2}{\hbar^2}\mathrm{Tr}\,\{\quad x\mathcal{H}\mathcal{G}^{\pm}x\mathcal{H}\mathcal{G}^{\pm} + \mathcal{H}x\mathcal{G}^{\pm}\mathcal{H}x\mathcal{G}^{\pm} - \mathcal{H}x\mathcal{G}^{\pm}x\mathcal{H}\mathcal{G}^{\pm} - x\mathcal{H}\mathcal{G}^{\pm}\mathcal{H}x\mathcal{G}^{\pm}\}$$

$$= -\frac{m^2}{\hbar^2}\mathrm{Tr}\,\{\quad x\mathcal{H}\mathcal{G}^{\pm}x\mathcal{H}\mathcal{G}^{\pm} + x\mathcal{G}^{\pm}\mathcal{H}x\mathcal{G}^{\pm}\mathcal{H} - 2x\mathcal{G}^{\pm}\mathcal{H}\mathcal{G}^{\pm}\mathcal{H}\} \tag{A.6}$$

$$
\begin{aligned}
&= -\frac{m^2}{\hbar^2}\mathrm{Tr}\,\{ \quad x(Z^{\pm}\mathcal{G}^{\pm}-\mathbb{1})x(Z^{\pm}\mathcal{G}^{\pm}-\mathbb{1}) + x(\mathcal{G}^{\pm}Z^{\pm}-\mathbb{1})x(\mathcal{G}^{\pm}Z^{\pm}-\mathbb{1}) \\
&\qquad\qquad - 2x\mathcal{G}^{\pm}x\big(Z^{\pm}(\mathcal{G}^{\pm}Z^{\pm}-\mathbb{1})-\mathcal{H}\big)\big\} \\
&= -\frac{m^2}{\hbar^2}\mathrm{Tr}\,\{ \quad xZ^{\pm}\mathcal{G}^{\pm}xZ^{\pm}\mathcal{G}^{\pm} - xZ^{\pm}\mathcal{G}^{\pm}x + x^2 - x^2Z^{\pm}\mathcal{G}^{\pm} \\
&\qquad\qquad + x\mathcal{G}^{\pm}Z^{\pm}x\mathcal{G}^{\pm}Z^{\pm} - x\mathcal{G}^{\pm}Z^{\pm}x + x^2 - x^2\mathcal{G}^{\pm}Z^{\pm} \\
&\qquad\qquad - 2x\mathcal{G}^{\pm}xZ^{\pm}\mathcal{G}^{\pm}Z^{\pm} + 2x\mathcal{G}^{\pm}xZ^{\pm} + 2x\mathcal{G}^{\pm}x\mathcal{H}\big\} \\
&= -\frac{m^2}{\hbar^2}\mathrm{Tr}\,\{ \quad x^2 - x^2Z^{\pm}\mathcal{G}^{\pm} - x^2\mathcal{G}^{\pm}Z^{\pm} + 2x\mathcal{G}^{\pm}x\mathcal{H}\big\}
\end{aligned}
\tag{A.7}
$$

$$
\begin{aligned}
\mathrm{Tr}\,\mathrm{p}\,\mathcal{G}^{-}\,\mathrm{p}\,\mathcal{G}^{+} &= -\frac{m^2}{\hbar^2}\mathrm{Tr}\,\{ \quad (x\mathcal{H}\mathcal{G}^{-}-\mathcal{H}x\mathcal{G}^{-})(x\mathcal{H}\mathcal{G}^{+}-\mathcal{H}x\mathcal{G}^{+})\big\} \\
&= -\frac{m^2}{\hbar^2}\mathrm{Tr}\,\{ \quad x\mathcal{H}\mathcal{G}^{-}x\mathcal{H}\mathcal{G}^{+} + \mathcal{H}x\mathcal{G}^{-}\mathcal{H}x\mathcal{G}^{+} - x\mathcal{H}\mathcal{G}^{-}\mathcal{H}x\mathcal{G}^{+} - \mathcal{H}x\mathcal{G}^{-}x\mathcal{H}\mathcal{G}^{+}\big\} \\
&= -\frac{m^2}{\hbar^2}\mathrm{Tr}\,\{ \quad x\mathcal{H}\mathcal{G}^{-}x\mathcal{H}\mathcal{G}^{+} + x\mathcal{G}^{-}\mathcal{H}x\mathcal{G}^{+}\mathcal{H} - x\mathcal{G}^{+}x\mathcal{H}\mathcal{G}^{-}\mathcal{H} - x\mathcal{G}^{-}x\mathcal{H}\mathcal{G}^{+}\mathcal{H}\big\}
\end{aligned}
\tag{A.8}
$$

$$
\begin{aligned}
\mathrm{Tr}\,\mathrm{p}\,\mathcal{G}^{-}\,\mathrm{p}\,\mathcal{G}^{+} &= -\frac{m^2}{\hbar^2}\mathrm{Tr}\,\{ \quad x(Z^{-}\mathcal{G}^{-}-\mathbb{1})x(Z^{+}\mathcal{G}^{+}-\mathbb{1}) + x(\mathcal{G}^{-}Z^{-}-\mathbb{1})x(\mathcal{G}^{+}Z^{+}-\mathbb{1}) \\
&\qquad\qquad - x\mathcal{G}^{-}x\big(Z^{+}(\mathcal{G}^{+}Z^{+}-\mathbb{1})-\mathcal{H}\big) - x\mathcal{G}^{+}x\big(Z^{-}(\mathcal{G}^{-}Z^{-}-\mathbb{1})-\mathcal{H}\big)\big\} \\
&= -\frac{m^2}{\hbar^2}\mathrm{Tr}\,\{ \quad xZ^{-}\mathcal{G}^{-}xZ^{+}\mathcal{G}^{+} - xZ^{-}\mathcal{G}^{-}x + x^2 - x^2Z^{+}\mathcal{G}^{+} \\
&\qquad\qquad + x\mathcal{G}^{-}Z^{-}x\mathcal{G}^{+}Z^{+} - x\mathcal{G}^{-}Z^{-}x + x^2 - x^2\mathcal{G}^{+}Z^{+} \\
&\qquad\qquad - x\mathcal{G}^{-}xZ^{+}\mathcal{G}^{+}Z^{+} + x\mathcal{G}^{-}xZ^{+} + x\mathcal{G}^{-}x\mathcal{H} \\
&\qquad\qquad - x\mathcal{G}^{+}xZ^{-}\mathcal{G}^{-}Z^{-} + x\mathcal{G}^{+}xZ^{-} + x\mathcal{G}^{+}x\mathcal{H}\big\} \\
&= -\frac{m^2}{\hbar^2}\mathrm{Tr}\,\{ \quad (xZ^{-}\mathcal{G}^{-}xZ^{+}\mathcal{G}^{+} - x\mathcal{G}^{+}xZ^{-}\mathcal{G}^{-}Z^{-}) \\
&\qquad\qquad + (x\mathcal{G}^{-}Z^{-}x\mathcal{G}^{+}Z^{+} - x\mathcal{G}^{-}xZ^{+}\mathcal{G}^{+}Z^{+}) \\
&\qquad\qquad - xZ^{-}\mathcal{G}^{-}x - x^2Z^{+}\mathcal{G}^{+} - x\mathcal{G}^{-}Z^{-}x - x^2\mathcal{G}^{+}Z^{+} \\
&\qquad\qquad + x\mathcal{G}^{-}xZ^{+} + x\mathcal{G}^{-}x\mathcal{H} + x\mathcal{G}^{+}xZ^{-} + x\mathcal{G}^{+}x\mathcal{H} + 2x^2\big\}
\end{aligned}
$$

$$
\begin{aligned}
&= -\frac{m^2}{\hbar^2}\mathrm{Tr}\ \{ \qquad xZ^-\mathcal{G}^-x(Z^+ - Z^-)\mathcal{G}^+ + x\mathcal{G}^-(Z^- - Z^+)x\mathcal{G}^+Z^+ \\
&\qquad\qquad -xZ^-\mathcal{G}^-x - x^2Z^+\mathcal{G}^+ - x\mathcal{G}^-Z^-x - x^2\mathcal{G}^+Z^+ \\
&\qquad\qquad + x\mathcal{G}^-xZ^+ + x\mathcal{G}^-x\mathcal{H} + x\mathcal{G}^+xZ^- + x\mathcal{G}^+x\mathcal{H} + 2x^2\} \\
&= -\frac{m^2}{\hbar^2}\mathrm{Tr}\ \{ \qquad x(Z^- - Z^+)\mathcal{G}^-x(Z^+ - Z^-)\mathcal{G}^+ \\
&\qquad\qquad -xZ^-\mathcal{G}^-x - x^2Z^+\mathcal{G}^+ - x\mathcal{G}^-Z^-x - x^2\mathcal{G}^+Z^+ \\
&\qquad\qquad + x\mathcal{G}^-xZ^+ + x\mathcal{G}^-x\mathcal{H} + x\mathcal{G}^+xZ^- + x\mathcal{G}^+x\mathcal{H} + 2x^2\}
\end{aligned}
\tag{A.9}
$$

$$
\begin{aligned}
&\mathrm{Tr}\ \left\{p\mathcal{G}^+p\mathcal{G}^+ + p\mathcal{G}^-p\mathcal{G}^- - p\mathcal{G}^-p\mathcal{G}^+ - p\mathcal{G}^+p\mathcal{G}^-\right\} \\
&\quad = -\frac{m^2}{\hbar^2}\mathrm{Tr}\ \left\{-2\mathrm{x}(\mathrm{Z}^- - \mathrm{Z}^+)\mathcal{G}^-\mathrm{x}(\mathrm{Z}^+ - \mathrm{Z}^-)\mathcal{G}^+ + 2\mathrm{x}(\mathrm{Z}^- - \mathrm{Z}^+)\mathcal{G}^-\mathrm{x} + 2\mathrm{x}(\mathrm{Z}^+ - \mathrm{Z}^-)\mathcal{G}^+\mathrm{x}\right\} \\
&\quad = -\frac{m^2}{\hbar^2}\mathrm{Tr}\ \left\{-8\mathrm{x}(\mathrm{Im}\,\mathrm{Z}^+)\mathcal{G}^-\mathrm{x}(\mathrm{Im}\,\mathrm{Z}^+)\mathcal{G}^+ + 4\imath\mathrm{x}\left[(\mathrm{Im}\,\mathrm{Z}^+)\mathcal{G}^+ - (\mathrm{Im}\,\mathrm{Z}^+)\mathcal{G}^-\right]\mathrm{x}\right\}
\end{aligned}
\tag{A.10}
$$

This finally gives

$$
\sigma = -\frac{8\,e^2}{h\,L}\mathrm{Tr}\ \left\{\mathrm{x}(\mathrm{Im}\,\mathrm{Z}^+)\mathcal{G}^-\mathrm{x}(\mathrm{Im}\,\mathrm{Z}^+)\mathcal{G}^+ + \frac{\imath}{2}\mathrm{x}\left[(\mathrm{Im}\,\mathrm{Z}^+)\mathcal{G}^- - (\mathrm{Im}\,\mathrm{Z}^+)\mathcal{G}^+\right]\mathrm{x}\right\} \tag{A.11}
$$

Transformation of Z^+ to position basis yields

$$
(\mathrm{Im}\,\mathrm{Z}^+)_{\mathrm{ij}} = \gamma\delta_{\mathrm{ij}} - \Sigma^{(2)}_{\mathrm{ii}}\delta_{\mathrm{ij}} \quad \text{with} \quad \Sigma^{(2)}_{\mathrm{ii}} = \Sigma_{\mathrm{L}}\delta_{\mathrm{i1}} + \Sigma_{\mathrm{R}}\delta_{\mathrm{iN}} \tag{A.12}
$$

Now we evaluate the trace by considering states in the disordered region,

$$
\begin{aligned}
&\mathrm{Tr}\ \left\{x(\mathrm{Im}\,\mathrm{Z}^+)\mathcal{G}^-\mathrm{x}(\mathrm{Im}\,\mathrm{Z}^+)\mathcal{G}^+\right\} \\
&\quad = \sum_{i,j,\alpha,\beta,\mu,\nu=0}^{N+1} \langle i|x|\alpha\rangle\langle\alpha|(\mathrm{Im}\,\mathrm{Z}^+)|\beta\rangle\langle\beta|\mathcal{G}^-|\mu\rangle\langle\mu|\mathrm{x}|\nu\rangle\langle\nu|(\mathrm{Im}\,\mathrm{Z}^+)|\mathrm{j}\rangle\langle\mathrm{j}|\mathcal{G}^+|\mathrm{i}\rangle \\
&\quad = \sum_{i,j,\beta,\mu=0}^{N+1} x_i(\mathrm{Im}\,\mathrm{Z}^+)_{\mathrm{i}\beta}\mathcal{G}^-_{\beta\mu}\mathrm{x}_\mu(\mathrm{Im}\,\mathrm{Z}^+)_{\mu\mathrm{j}}\mathcal{G}^+_{\mathrm{ji}} \\
&\quad = \sum_{\substack{i,j=0 \\ (i<j)}}^{N+1} x_i(\gamma - \Sigma^{(2)})_{ii}G^-_{ij}x_j(\gamma - \Sigma^{(2)})_{jj}G^+_{ji}
\end{aligned}
\tag{A.13}
$$

$$\mathrm{Tr}\left\{\frac{\imath}{2}x(\mathrm{Im\,Z^{+}})\mathrm{G^{-}x}\right\}$$
$$= \sum_{i,j,\alpha,\beta=0}^{N+1} \frac{\imath}{2}\langle i|x|\alpha\rangle\langle\alpha|(ImZ^{+})|\beta\rangle\langle\beta|G^{-}|j\rangle\langle j|x|i\rangle = \sum_{i=0}^{N+1}\frac{\imath}{2}x_i(\gamma-\Sigma^{(2)})_{ii}G^{-}_{ii}x_i \tag{A.14}$$

The conductivity in position basis is consequently given by

$$\sigma = -\frac{8\,e^2}{h\,L}\left\{\sum_{i,j=0}^{N+1} x_i(\gamma-\Sigma^{(2)})_{ii}G^{-}_{ij}x_j(\gamma-\Sigma^{(2)})_{jj}G^{+}_{ji} - \sum_{i=0}^{N+1}x_i(\gamma-\Sigma^{(2)})_{ii}G^{+}_{ii}G^{-}_{ii}x_i\right\} \tag{A.15}$$

The last expression can be recast into a spatially invariant form,

$$\begin{aligned}
\sigma &= \frac{4\,e^2}{h\,L}\sum_{i,j=0}^{N+1}(x_i-x_j)(\gamma-\Sigma^{(2)})_{ii}G^{-}_{ij}(\gamma-\Sigma^{(2)})_{jj}G^{+}_{ji}\\
&= \frac{4\,e^2}{h\,L}\sum_{i,j=0}^{N+1}\Big\{(x_i-x_j)^2\gamma^2G^{-}_{ij}G^{+}_{ji} + (x_i-x_j)^2\Sigma^{(2)}_{ii}G^{-}_{ij}\Sigma^{(2)}_{jj}G^{+}_{ji}\\
&\qquad -(x_i-x_j)^2\gamma G^{-}_{ij}\Sigma^{(2)}_{jj}G^{+}_{ji} - (x_i-x_j)^2\Sigma^{(2)}_{ii}G^{-}_{ij}\gamma G^{+}_{ji}\Big\}\\
&= \frac{4\,e^2}{h\,L}\left\{\sum_{\substack{i,j=1\\(i<j)}}^{N}(x_i-x_j)^2\gamma^2G^{-}_{i\,j}G^{+}_{j\,i} + (x_0-x_{N+1})^2\Sigma_LG^{-}_{1\,N+1}\Sigma_RG^{+}_{N+1\,1}\right.\\
&\qquad \left. -\sum_{i=1}^{N}(x_i-x_{N+1})^2\gamma G^{-}_{i\,N+1}\Sigma_RG^{+}_{N+1\,i} - \sum_{j=1}^{N}(x_1-x_j)^2\Sigma_LG^{-}_{1\,j}\gamma G^{+}_{j\,0}\right\}
\end{aligned} \tag{A.16}$$

Appendix B

Recursion Formulæ

B.1 Density of States

The density of states is defined as

$$\rho^{(N)}(E) = -\frac{1}{\pi N M^2}\mathrm{Im}\left\{\sum_{\mathrm{i}=1}^{\mathrm{N}}\mathrm{Tr}\,\mathbf{G}_{\mathrm{ii}}^{+(\mathrm{N})}\right\} = -\frac{1}{\pi \mathrm{N M}^2}\mathrm{Im}\,\mathrm{s}_{\rho}^{(\mathrm{N})}\ . \tag{B.1}$$

Adding an additional slice results in the following expression,

$$\begin{aligned}
s^{(N+1)} &= \mathrm{Im}\sum_{\mathrm{i}=1}^{\mathrm{N+1}}\mathrm{Tr}\,\mathbf{G}_{\mathrm{ii}}^{+(\mathrm{N+1})} \\
&= \mathrm{Im}\sum_{\mathrm{i}=1}^{\mathrm{N}}\left\{\mathrm{Tr}\,\left[\mathbf{G}_{\mathrm{ii}}^{+(\mathrm{N})} + \mathbf{G}_{\mathrm{iN}}^{+(\mathrm{N})}\mathbf{t}_{\mathrm{N}}\mathbf{G}_{\mathrm{N+1N+1}}^{+(\mathrm{N+1})}\mathbf{t}_{\mathrm{N}}^{\dagger}\mathbf{G}_{\mathrm{Ni}}^{+(\mathrm{N})}\right]\right\} + \mathrm{Im}\,\mathrm{Tr}\,\mathbf{G}_{\mathrm{N+1N+1}}^{+(\mathrm{N+1})} \\
&= \mathrm{Im}\sum_{\mathrm{i}=1}^{\mathrm{N}}\mathrm{Tr}\,\mathbf{G}_{\mathrm{ii}}^{+(\mathrm{N})} + \mathrm{Im}\,\mathrm{Tr}\,\mathbf{G}_{\mathrm{N+1N+1}}^{+(\mathrm{N+1})} + \mathrm{Im}\,\mathrm{Tr}\sum_{\mathrm{i}=1}^{\mathrm{N}}\mathbf{t}_{\mathrm{N}}^{\dagger}\mathbf{G}_{\mathrm{Ni}}^{+(\mathrm{N})}\mathbf{G}_{\mathrm{iN}}^{+(\mathrm{N})}\mathbf{t}_{\mathrm{N}}\mathbf{G}_{\mathrm{N+1N+1}}^{+(\mathrm{N+1})} \\
&= s_{\rho}^{(N)} + \mathrm{Im}\,\mathrm{Tr}\left\{\mathbf{G}_{\mathrm{N+1N+1}}^{(+\mathrm{N+1})}\left[\mathbf{I} + \mathbf{t}_{\mathrm{N}}^{\dagger}\sum_{\mathrm{i}=1}^{\mathrm{N}}\mathbf{G}_{\mathrm{Ni}}^{+(\mathrm{N})}\mathbf{G}_{\mathrm{iN}}^{+(\mathrm{N})}\mathbf{t}_{\mathrm{N}}\right]\right\} \\
&= s_{\rho}^{(N)} + \mathrm{Im}\,\mathrm{Tr}\left\{\mathbf{G}_{\mathrm{N+1N+1}}^{+(\mathrm{N+1})}\left[\mathbf{I} + \mathbf{F}_{\mathrm{N}}\right]\right\}\ .
\end{aligned} \tag{B.2}$$

In the last equation we have used the auxiliary matrix

$$\mathbf{F}_N = \mathbf{t}_N^{\dagger}\sum_{i=1}^{N}\left[\mathbf{G}_{Ni}^{+(N)}\mathbf{G}_{iN}^{+(N)}\right]\mathbf{t}_N\ . \tag{B.3}$$

The recursion relation for this quantity is

$$\begin{aligned}
\mathbf{F}_{N+1} &= \mathbf{t}^{\dagger}_{N+1} \sum_{i=1}^{N+1} \left[\mathbf{G}^{+(N+1)}_{N+1i} \mathbf{G}^{+(N+1)}_{iN+1} \right] \mathbf{t}_{N+1} \\
&= \mathbf{t}^{\dagger}_{N+1} \sum_{i=1}^{N} \left[\mathbf{G}^{+(N+1)}_{N+1i} \mathbf{G}^{+(N+1)}_{iN+1} + \mathbf{G}^{+(N+1)}_{N+1N+1} \mathbf{G}^{+(N+1)}_{N+1N+1} \right] \mathbf{t}_{N+1} \\
&= \mathbf{t}^{\dagger}_{N+1} \sum_{i=1}^{N} \left[\mathbf{G}^{+(N+1)}_{N+1N+1} \mathbf{t}^{\dagger}_{N} \mathbf{G}^{+(N)}_{Ni} \mathbf{G}^{+(N)}_{iN} \mathbf{t}_{N} \mathbf{G}^{+(N+1)}_{N+1N+1} + \mathbf{G}^{+(N+1)}_{N+1N+1} \mathbf{G}^{+(N+1)}_{N+1N+1} \right] \mathbf{t}_{N+1} \\
&= \mathbf{t}^{\dagger}_{N+1} \mathbf{G}^{+(N+1)}_{N+1N+1} \left[\mathbf{F}_{N} + \mathbf{I} \right] \mathbf{G}^{+(N+1)}_{N+1N+1} \mathbf{t}_{N+1}
\end{aligned} \tag{B.4}$$

B.2 D.C. Conductivity

$$\begin{aligned}
\sigma^{(N)} &= \frac{e^2 4}{hNM^2} \mathrm{Tr} \left\{ \gamma^2 \sum_{\mathrm{i,j}}^{\mathrm{N}} \mathbf{G}^{+(\mathrm{N})}_{\mathrm{i\,j}} \, \mathrm{x_j} \, \mathbf{G}^{-(\mathrm{N})}_{\mathrm{ji}} \, \mathrm{x_i} - \imath \frac{\gamma}{2} \sum_{\mathrm{i}}^{\mathrm{N}} (\mathbf{G}^{+(\mathrm{N})}_{\mathrm{i\,i}} - \mathbf{G}^{-(\mathrm{N})}_{\mathrm{i\,i}}) \, \mathrm{x_i^2} \right\} \\
&= \frac{e^2 4}{hNM^2} s^{(N)}_{\sigma}
\end{aligned} \tag{B.5}$$

$$\begin{aligned}
s^{(N+1)}_{\sigma} &= \mathrm{Tr} \left\{ \gamma^2 \sum_{\mathrm{i,j}}^{\mathrm{N+1}} \mathbf{G}^{+(\mathrm{N+1})}_{\mathrm{i\,j}} \, \mathrm{x_j} \, \mathbf{G}^{-(\mathrm{N+1})}_{\mathrm{ji}} \, \mathrm{x_i} - \imath \frac{\gamma}{2} \sum_{\mathrm{i}}^{\mathrm{N+1}} (\mathbf{G}^{+(\mathrm{N+1})}_{\mathrm{i\,i}} - \mathbf{G}^{-(\mathrm{N+1})}_{\mathrm{i\,i}}) \, \mathrm{x_i^2} \right\} \\
&= \mathrm{Tr} \left\{ \gamma^2 \sum_{\mathrm{i,j}}^{\mathrm{N+1}} \left[\mathbf{G}^{+(\mathrm{N})}_{\mathrm{i\,j}} + \mathbf{G}^{+(\mathrm{N})}_{\mathrm{i\,N}} \mathbf{t}_{\mathrm{N}} \mathbf{G}^{+(\mathrm{N+1})}_{\mathrm{N+1\,N+1}} \mathbf{t}^{\dagger}_{\mathrm{N}} \mathbf{G}^{+(\mathrm{N})}_{\mathrm{N\,j}} \right] \mathrm{x_j} \times \right. \\
&\qquad \left[\mathbf{G}^{-(N)}_{j\,i} + \mathbf{G}^{-(N)}_{j\,N} \mathbf{t}_{N} \mathbf{G}^{-(N+1)}_{N+1\,N+1} \mathbf{t}^{\dagger}_{N} \mathbf{G}^{-(N)}_{N\,i} \right] x_i \\
&\quad - \imath\gamma \frac{1}{2} \sum_{i}^{N+1} \left[\mathbf{G}^{+(N)}_{i\,i} + \mathbf{G}^{+(N)}_{i\,N} \mathbf{t}_{N} \mathbf{G}^{+(N+1)}_{N+1\,N+1} \mathbf{t}^{\dagger}_{N} \mathbf{G}^{+(N)}_{N\,i} \right. \\
&\qquad \left. \left. - \mathbf{G}^{-(N)}_{i\,i} - \mathbf{G}^{-(N)}_{i\,N} \mathbf{t}_{N} \mathbf{G}^{-(N+1)}_{N+1\,N+1} \mathbf{t}^{\dagger}_{N} \mathbf{G}^{-(N)}_{N\,i} \right] x_i^2 \right\}
\end{aligned}$$

For notational convenience we introduce the following auxiliary matrix

$$\mathbf{a}^{+}_{ij} = \mathbf{G}^{+(N)}_{i\,N} \mathbf{t}_{N} \mathbf{G}^{+(N+1)}_{N+1\,N+1} \mathbf{t}^{\dagger}_{N} \mathbf{G}^{+(N)}_{N\,j} \, . \tag{B.6}$$

To simplify the derivation we consider the new slice to be at $x_{N+1} = 0$ and take account for this afterwards. Substituting for $\mathbf{a}^{+}_{ij}$ then gives

$$
\begin{aligned}
s_\sigma^{(N+1)} &= \mathrm{Tr}\left\{\gamma^2 \sum_{\mathrm{i,j}}^{\mathrm{N+1}} \Big[\mathbf{G}^{+(\mathrm{N})}_{\mathrm{ij}} \mathrm{x_j} \mathbf{G}^{-(\mathrm{N})}_{\mathrm{ji}} \mathrm{x_i} + \mathbf{G}^{+(\mathrm{N})}_{\mathrm{ij}} \mathrm{x_j} \mathbf{a}^{-}_{\mathrm{ji}} \mathrm{x_i} + \mathbf{a}^{+}_{\mathrm{ij}} \mathrm{x_j} \mathbf{G}^{-(\mathrm{N})}_{\mathrm{ji}} \mathrm{x_i} \right. \right. \\
&\qquad \left. \left. + \mathbf{a}^{+}_{ij} x_j \mathbf{a}^{-}_{ji} x_i \Big] - \imath\gamma \frac{1}{2} \left[\sum_i^N \left(\mathbf{G}^{+(N)}_{ii} - \mathbf{G}^{-(N)}_{ii} \right) x_i^2 + \left(\mathbf{a}^{+}_{ii} - \mathbf{a}^{-}_{ii} \right) x_i^2 + (\ldots) x_{N+1}^2 \right] \right\} \\
&= \mathrm{Tr}\left\{\gamma^2 \sum_{\mathrm{i,j}}^{\mathrm{N}} \Big[\mathbf{G}^{+(\mathrm{N})}_{\mathrm{ij}} \mathrm{x_j} \mathbf{G}^{-(\mathrm{N})}_{\mathrm{ji}} \mathrm{x_i} + \mathbf{G}^{+(\mathrm{N})}_{\mathrm{ij}} \mathrm{x_j} \mathbf{a}^{-}_{\mathrm{ji}} \mathrm{x_i} + \mathbf{a}^{+}_{\mathrm{ij}} \mathrm{x_j} \mathbf{G}^{-(\mathrm{N})}_{\mathrm{ji}} \mathrm{x_i} \right. \right. \\
&\qquad \left. \left. + \mathbf{a}^{+}_{ij} x_j \mathbf{a}^{-}_{ji} x_i \Big] - \imath\gamma \frac{1}{2} \left[\sum_i^N \left(\mathbf{G}^{+(N)}_{ii} - \mathbf{G}^{-(N)}_{ii} \right) x_i^2 + \left(\mathbf{a}^{+}_{ii} - \mathbf{a}^{-}_{ii} \right) x_i^2 \right] \right\} \\
&= s_\sigma^{(N)} + \mathrm{Tr}\left\{\gamma^2 \sum_{\mathrm{i,j}}^{\mathrm{N}} \Big[\mathbf{G}^{+(\mathrm{N})}_{\mathrm{ij}} \mathrm{x_j} \mathbf{G}^{-(\mathrm{N})}_{\mathrm{jN}} \mathbf{t}_{\mathrm{N}} \mathbf{G}^{-(\mathrm{N+1})}_{\mathrm{N+1\,N+1}} \mathbf{t}^{\dagger}_{\mathrm{N}} \mathbf{G}^{-(\mathrm{N})}_{\mathrm{Ni}} \mathrm{x_i} \right. \right. \\
&\qquad + \mathbf{G}^{+(N)}_{iN} \mathbf{t}_N \mathbf{G}^{+(N+1)}_{N+1\,N+1} \mathbf{t}^{\dagger}_N \mathbf{G}^{+(N)}_{Nj} x_j \mathbf{G}^{-(N)}_{ji} x_i \\
&\qquad + \mathbf{G}^{+(N)}_{iN} \mathbf{t}_N \mathbf{G}^{+(N+1)}_{N+1\,N+1} \mathbf{t}^{\dagger}_N \mathbf{G}^{+(N)}_{Nj} x_j \mathbf{G}^{-(N)}_{jN} \mathbf{t}_N \mathbf{G}^{-(N+1)}_{N+1\,N+1} \mathbf{t}^{\dagger}_N \mathbf{G}^{-(N)}_{Ni} x_i \Big] \\
&\qquad \left. \left. - \imath\gamma \frac{1}{2} \sum_i^N \left[\mathbf{G}^{+(N)}_{iN} \mathbf{t}_N \mathbf{G}^{+(N+1)}_{N+1\,N+1} \mathbf{t}^{\dagger}_N \mathbf{G}^{+(N)}_{Ni} - \mathbf{G}^{-(N)}_{iN} \mathbf{t}_N \mathbf{G}^{-(N+1)}_{N+1\,N+1} \mathbf{t}^{\dagger}_N \mathbf{G}^{-(N)}_{Ni} \right] x_i^2 \right\} \\
&= s_\sigma^{(N)} + \mathrm{Tr}\left\{ \mathrm{Re}\left[\gamma \mathbf{t}^{\dagger}_{\mathrm{N}} \sum_{\mathrm{i,j}}^{\mathrm{N}} \Big(2\gamma \mathbf{G}^{+(\mathrm{N})}_{\mathrm{Nj}} \mathrm{x_j} \mathbf{G}^{-(\mathrm{N})}_{\mathrm{ji}} \mathrm{x_i} \mathbf{G}^{+(\mathrm{N})}_{\mathrm{iN}} \right. \right. \right. \\
&\qquad \left. \left. \left. - \imath\delta_{ij} \mathbf{G}^{+(N)}_{Nj} \mathbf{G}^{+(N)}_{iN} x_j x_i \Big) \mathbf{t}_N \mathbf{G}^{+(N+1)}_{N+1N+1} \right] + \gamma \mathbf{t}^{\dagger}_N \left[\sum_{i=1}^N \mathbf{G}^{+(N)}_{Ni} x_i \mathbf{G}^{-(N)}_{iN} \right] \mathbf{t}_N \times \right. \\
&\qquad \left. \left(\mathbf{G}^{-(N+1)}_{N+1N+1} \right) \gamma \mathbf{t}^{\dagger}_N \left[\sum_{i=1}^N \mathbf{G}^{-(N)}_{Ni} x_i \mathbf{G}^{+(N)}_{iN} \right] \mathbf{t}_N \mathbf{G}^{+(N+1)}_{N+1N+1} \right\} \\
&= s_\sigma^{(N)} + \mathrm{Tr}\left\{ \mathrm{Re}\left(\mathbf{B}_{\mathrm{N}} \mathbf{G}^{+(\mathrm{N+1})}_{\mathrm{N+1N+1}} \right) + \mathbf{C}^{+}_{\mathrm{N}} \mathbf{G}^{-(\mathrm{N+1})}_{\mathrm{N+1N+1}} \mathbf{C}^{-}_{\mathrm{N}} \mathbf{G}^{+(\mathrm{N+1})}_{\mathrm{N+1N+1}} \right\} \qquad \text{(B.7)}
\end{aligned}
$$

In the last Equation we introduced the following matrices,

$$
\mathbf{B}_N = \gamma \mathbf{t}^{\dagger}_N \left[\sum_{ij}^N \mathbf{G}^{+(N)}_{Nj} x_j (2\gamma \mathbf{G}^{-(N)}_{ji} - \imath \mathbf{I} \delta_{ij}) x_i \mathbf{G}^{+(N)}_{iN} \right] \mathbf{t}_N \ , \qquad \text{(B.8)}
$$

$$\mathbf{C}_N^+ = \gamma \mathbf{t}_N^\dagger \left[\sum_{i=1}^{N} \mathbf{G}_{Ni}^{+(N)} x_i \mathbf{G}_{iN}^{-(N)} \right] \mathbf{t}_N = (\mathbf{C}_N^+)^\dagger \,, \tag{B.9}$$

$$\mathbf{C}_N^- = \gamma \mathbf{t}_N^\dagger \left[\sum_{i=1}^{N} \mathbf{G}_{Ni}^{-(N)} x_i \mathbf{G}_{iN}^{+(N)} \right] \mathbf{t}_N = (\mathbf{C}_N^-)^\dagger \,. \tag{B.10}$$

The recursion relations for these can be found as follows

$$\begin{aligned}
\mathbf{C}_{N+1}^+ &= \gamma \mathbf{t}_{N+1}^\dagger \left[\sum_{i=1}^{N+1} \mathbf{G}_{N+1i}^{+(N+1)} x_i \mathbf{G}_{iN+1}^{-(N+1)} \right] \mathbf{t}_{N+1} \\
&= \gamma \mathbf{t}_{N+1}^\dagger \left[\sum_{i=1}^{N} \mathbf{G}_{N+1N+1}^{+(N+1)} \mathbf{t}_N^\dagger \mathbf{G}_{N\,i}^{+(N)} x_i \mathbf{G}_{iN}^{-(N)} \mathbf{t}_N \mathbf{G}_{N+1N+1}^{-(N+1)} \right] \mathbf{t}_{N+1} \\
&\qquad + (\ldots)\, x_{N+1}
\end{aligned}$$

$$\mathbf{C}_{N+1}^+ = \mathbf{t}_{N+1}^\dagger \mathbf{G}_{N+1N+1}^{(N+1)} \mathbf{C}_N^+ \mathbf{G}_{N+1N+1}^{-(N+1)} \mathbf{t}_{N+1} \tag{B.11}$$

$$\mathbf{C}_{N+1}^- = \mathbf{t}_{N+1}^\dagger \mathbf{G}_{N+1N+1}^{-(N+1)} \mathbf{C}_N^- \mathbf{G}_{N+1N+1}^{+(N+1)} \mathbf{t}_{N+1} \tag{B.12}$$

$$\begin{aligned}
\mathbf{B}_{N+1} &= \gamma \mathbf{t}_{N+1}^\dagger \left[\sum_{ij}^{N+1} \mathbf{G}_{N+1j}^{+(N+1)} x_j \left(2\gamma \mathbf{G}_{ji}^{-(N+1)} - \imath \mathbf{I} \delta_{ij} \right) x_i \mathbf{G}_{iN+1}^{+(N+1)} \right] \mathbf{t}_{N+1} \\
&= \gamma \mathbf{t}_{N+1}^\dagger \left\{ \sum_{ij}^{N+1} \mathbf{G}_{N+1N+1}^{+(N+1)} \mathbf{t}_N^\dagger \mathbf{G}_{N\,j}^{+(N)} x_j \left[2\gamma \left(\mathbf{G}_{ji}^{-(N)} + \mathbf{G}_{j\,N}^{-(N)} \mathbf{t}_N \mathbf{G}_{N+1\,N+1}^{-(N+1)} \mathbf{t}_N^\dagger \mathbf{G}_{N\,i}^{-(N)} \right) \right. \right. \\
&\qquad \left. \left. - \imath \mathbf{I} \delta_{ij} \right] x_i \mathbf{G}_{iN}^{-(N)} \mathbf{t}_N \mathbf{G}_{N+1N+1}^{-(N+1)} \right\} \mathbf{t}_{N+1} \\
&= \gamma \mathbf{t}_{N+1}^\dagger \mathbf{G}_{N+1N+1}^{+(N+1)} \mathbf{t}_N^\dagger \left\{ \sum_{ij}^{N} \mathbf{G}_{N\,j}^{+(N)} x_j \left(2\gamma \mathbf{G}_{ji}^{-(N)} - \imath \mathbf{I} \delta_{ij} \right) x_i \mathbf{G}_{iN}^{+(N)} \right. \\
&\qquad \left. + \mathbf{G}_{N\,j}^{+(N)} x_j \mathbf{G}_{j\,N}^{-(N)} \mathbf{t}_N \mathbf{G}_{N+1\,N+1}^{-(N+1)} \mathbf{t}_N^\dagger \mathbf{G}_{N\,i}^{-(N)} x_i \mathbf{G}_{iN}^{+(N)} \right\} \mathbf{t}_N \mathbf{G}_{N+1N+1}^{+(N+1)} \mathbf{t}_{N+1} \\
&= \mathbf{t}_{N+1}^\dagger \mathbf{G}_{N+1N+1}^{+(N+1)} \left\{ \mathbf{B}_N + 2\gamma^2 \mathbf{t}_N^\dagger \left[\sum_{i=1}^{N} \mathbf{G}_{Ni}^{+(N)} x_i \mathbf{G}_{iN}^{-(N)} \right] \mathbf{t}_N \times \right. \\
&\qquad \left. \left(\mathbf{G}_{N+1N+1}^{+(N+1)} \right) \mathbf{t}_N^\dagger \left[\sum_{i=1}^{N} \mathbf{G}_{Ni}^{-(N)} x_i \mathbf{G}_{iN}^{+(N)} \right] \mathbf{t}_N \right\} \mathbf{G}_{N+1N+1}^{+(N+1)} \mathbf{t}_{N+1} \\
&= \mathbf{t}_{N+1}^\dagger \mathbf{G}_{N+1N+1}^{+(N+1)} \left[\mathbf{B}_N + 2\mathbf{C}_N^+ \mathbf{G}_{N+1N+1}^{-(N+1)} \mathbf{C}_N^- \right] \mathbf{G}_{N+1N+1}^{+(N+1)} \mathbf{t}_{N+1}
\end{aligned} \tag{B.13}$$

Bibliography

[1] P. W. Anderson. Absence of diffusion in certain random lattices. *Phys. Rev.*, 109:1492–1505, 1958.

[2] B. Kramer and A. MacKinnon. Localization: theory and experiment. *Rep. Prog. Phys.*, 56:1469–1564, 1993.

[3] R. A. Römer and M. Schreiber. *The Anderson Transition and its Ramifications — Localisation, Quantum Interference, and Interactions*, chapter Numerical investigations of scaling at the Anderson transition, pages 3–19. Springer, Berlin, 2003.

[4] J. E. Enderby and A. C. Barnes. Electron transport at the Anderson transition. *Phys. Rev. B*, 49:5062, 1994.

[5] C. Villagonzalo, R. A. Römer, and M. Schreiber. Thermoelectric transport properties in disordered systems near the Anderson transition. *Eur. Phys. J. B*, 12:179–189, 1999. ArXiv: cond-mat/9904362.

[6] E. Abrahams, P. W. Anderson, D. C. Licciardello, and T. V. Ramakrishnan. Scaling theory of localization: absence of quantum diffusion in two dimensions. *Phys. Rev. Lett.*, 42:673–676, 1979.

[7] P. A. Lee and T. V. Ramakrishnan. Disordered electronic systems. *Rev. Mod. Phys.*, 57:287–337, 1985.

[8] K. Slevin and T. Ohtsuki. Corrections to scaling at the Anderson transition. *Phys. Rev. Lett.*, 82:382–385, 1999. ArXiv: cond-mat/9812065.

[9] K. Slevin, P. Markoš, and T. Ohtsuki. Reconciling conductance fluctuations and the scaling theory of localization. *Phys. Rev. Lett.*, 86:3594–3597, 2001.

[10] D. Braun, E. Hofstetter, G. Montambaux, and A. MacKinnon. Boundary conditions, the critiical conductance distribution, and one-parameter scaling. *Phys. Rev. B*, 64:155107, 2001.

[11] C. Villagonzalo, R. A. Römer, and M. Schreiber. Transport properties near the Anderson transition. *Ann. Phys. (Leipzig)*, 8:SI 269–SI 272, 1999. ArXiv: cond-mat/9908218.

[12] A. MacKinnon. The conductivity of the one-dimensional disordered anderson model: a new numerical method. *J. Phys.: Condens. Matter*, 13:L1031–L1034, 1980.

[13] A. MacKinnon. The calculation of transport properties and density of states of disordered solids. *Z. Phys. B*, 59:385–390, 1985.

[14] M. Büttiker. Role of quantum coherence in series resistors. *Phys. Rev. B*, 33:3020, 1986.

[15] J.L. D'Amato and H.M. Pastawski. Conductance of a disordered linear chain including inelastic scattering events. *Phys. Rev. B*, 41:7411, 1990.

[16] M. Lakner and H. v. Löhneysen. Thermoelectric power of a disordered metal near the metal-insulator transition. *Phys. Rev. Lett.*, 70:3475, 1993.

[17] N. W. Ashcroft and N. D. Mermin. *Solid State Physics*. Saunders College, New York, 1976.

[18] G. V. Chester and A. Thellung. The law of Wiedemann and Franz. *Proc. Phys. Soc.*, 77:1005–1013, 1961.

[19] K. Schröder. *Electronic, magnetic, and thermal properties of solid materials*. Marcel Dekker Inc, New York, 1978.

[20] G.S. Nolas and G.A. Slack. *American Scientist*, 89:136, 2001.

[21] G. Mahan, B. Sales, and J. Sharp. Thermoelectric materials: New approaches to an old problem. *Physics Today*, pages 42–47, 1997. March.

[22] H. B. Callen. *Thermodynamics and an Introduction to Thermostatistics*. John Wiley & Sons, New York, 1985.

[23] R. Kubo. Statistical-mechanical theory of irreversible processes. i. General theory and simple applications to magnetic and conduction problems. *J. Phys. Soc. Japan*, 12:570–586, 1957.

[24] D. A. Greenwood. The Boltzmann equation in the theory of electrical conduction in metals. *Proc. Phys. Soc.*, 71:585–596, 1958.

[25] R. Kubo, M. Yokota, and S. Nakajima. Statistical-mechanical theory of irreversible processes. ii. Response to thermal disturbance. *J. Phys. Soc. Japan*, 12:1203–1211, 1957.

[26] G. D. Mahan. *Many Particle Physics*. Kluwer Academic/Plenum, New York, 2000.

[27] Y. Imry. *Introduction to mesoscopic physics*. Oxford University Press, New York, 2002.

[28] S. Datta. *Electronic, magnetic, and thermal properties of solid materials*. Cambridge University Press, Cambridge, 2003.

[29] T. Dittrich, P. Hänggi, G.-L. Ingold, B. Kramer, G. Schön, and W. Zwerger. *Quantum Transport and Dissipation*. Wiley-VCH, Berlin, 1998.

[30] T. Ohtsuki, K. Slevin, and T. Kawarabayashi. Review on recent progress on numerical studies of the Anderson transition. *Ann. Phys. (Leipzig)*, 8:655–664, 1999. ArXiv: cond-mat/9911213.

[31] T. Ando. Numerical study of symmetry effects on localization in two dimensions. *Phys. Rev. B*, 40:5325, 1989.

[32] I. Goldsheid, S. Molcanov, and L. Pastur. *Funct. Anal. Appl.*, 11:1, 1977.

[33] D. J. Thouless. In G. Toulouse and R. Balian, editors, *Ill-condensed Matter*, page 1, Amsterdam, 1979. North-Holland.

[34] L.A. Pastur and A. Figotin. *Spectra of Random and Almost-Periodic Operators*. Springer, Berlin, 1992.

[35] R. A. Römer and H. Schulz-Baldes. Weak disorder expansion for localization lengths of quasi-1d systems. *Europhys. Lett.*, 68:247, 2004.

[36] S. Waffenschmidt, C. Pfleiderer, and H. v. Löhneysen. Critical behavior of the conductivity of Si:P at the metal-insulator transition under uniaxial stress. *Phys. Rev. Lett.*, 83:3005–3008, 1999. ArXiv: cond-mat/9905297.

[37] F. Wegner. Electrons in disordered systems. scaling near the mobility edge. *Z. Phys. B*, 25:327–337, 1976.

[38] D. Belitz and T. R. Kirkpatrick. The Anderson-Mott transition. *Rev. Mod. Phys.*, 66:261–380, 1994.

[39] R. Landauer. Spatial variation of currents and fields du to localised scatterers in metallic conduction. *IBM J. Res. Dev.*, 1:223, 1957.

[40] R. Landauer. Electrical resistance of disordered one-dimensional lattices. *Phil. Mag.*, 21:863–867, 1970.

[41] R. Landauer. *Z. Phys. B*, 21:247, 1975.

[42] H. U. Baranger and A. D. Stone. *Phys. Rev. B*, 40:8169, 1989.

[43] E. N. Economou. *Green's Functions in Quantum Physics*. Springer-Verlag, Berlin, 1990.

[44] Branislav K. Nikolić. Deconstructing kubo formula usage: Exact conductance of a mesoscopic system from weak to strong disorder limit. *Phys. Rev. B*, 64:165303, 2001.

[45] J. L. Cardy. *Scaling and Renormalization in Statistical Physics*. Cambridge University Press, Cambridge, 1996.

[46] M. Büttiker. Absence of backscattering in the quantum hall effect in multiprobe conductors. *Phys. Rev. B*, 38:9375, 1988.

[47] Branislav K. Nikolić. Statistical properties of eigenstates in three-dimensional mesoscopic systems with off-diagonal or diagonal disorder. *Phys. Rev. B*, 64:14203, 2001.

[48] C. Villagonzalo. *Thermoelectric Transport at the Metal-Insulator Transition in Disordered Systems*. PhD thesis, Chemnitz University of Technology, 2001.

[49] M.J. MacLennan, Y. Lee, and S. Datta. Voltage drop in mesoscopic systems: A numerical study using a quantum kinetic equation. *Phys. Rev. B*, 43:13846, 1991.

[50] R. Hey and M. Schreiber. Temperature dependent dc transport in polyaniline chains. *Phys. Rev. B*, 56:1854, 1997.

[51] D. Boese, M. Lischka, and L.E. Reichl. Scaling behaviour in a quantum wire with scatteres. *Phys. Rev. B*, 62:16933, 2000.